University of Southampton

Faculty of Natural and Environmental Sciences

Lithium-oxygen batteries: The significance of the electrolyte and the use of soluble catalysts

James Thaddeus Frith

Thesis for the degree of Doctor of Philosophy

September 2015

UNIVERSITY OF SOUTHAMPTON

ABSTRACT

FACULTY OF NATURAL AND ENVIRONMENTAL SCIENCES

Chemistry

Doctor of Philosophy

Lithium-oxygen batteries: The significance of the electrolyte and the use of soluble catalysts

by James Thaddeus Frith

Research has been carried out into lithium-oxygen cells over the last 20 years in an effort to develop the next generation of energy storage devices. Due to the high theoretical specific capacity of lithium peroxide, $1165\,mAh \cdot g^{-1}_{Li_2O_2}$, lithium-oxygen cells promise to deliver high specific energy devices. However, their development has been hampered by several issues, including degradation reactions primarily initiated by the reactive superoxide radical, an intermediate reduction product of oxygen. Another issue is the slow kinetics of both the oxygen reduction reaction (ORR) and the oxygen evolution reaction (OER).

In this work the use of *in situ* SERS spectroscopy as a method for monitoring the degradation of electrolytes has been investigated. It was demonstrated that it was possible to monitor the formation of superoxide in two ionic liquids. As the experiment progressed it was possible to monitor the formation of breakdown products resulting from degradation reactions in one ionic liquid, while in the second ionic liquid it was possible to observe the formation of lithium peroxide, the desired discharge product.

The use of soluble redox catalyst for both the ORR and OER offers many advantages in lithium-oxygen cells. This is primarily a result of the nature of the lithium peroxide discharge product. As it is both insoluble and insulating, it forms a deposit on the electrode surface that limits the cell performance. In this work we have demonstrated techniques that can be used to assess the performance of potential soluble redox catalysts. Based on their standard potentials and their Gibbs free energy of reaction ethyl viologen was identified as being a suitable redox catalyst of the ORR, while cobalt terpyridine (CoTerpy) was identified as being a suitable catalyst of both the ORR and the OER. However, experimental results showed that while ethyl viologen was an efficient mediator of the ORR CoTerpy was not able to mediate the ORR or the OER.

Contents

Declaration ..... **VII**

Acknowledgements ..... **IX**

Abbreviations ..... **XI**

Chapter 1 : Introduction, Background and Aims **1**

1.1 Introduction 3

1.2 Fundamentals of Electrochemical Cells 4

1.3 Charge and Discharge 6

1.4 Cell Capacity 10

1.5 Li-ion Cells 12

1.6 Non-Aqueous Lithium-Oxygen Cells 17

1.6.1 Electrolyte 20

1.6.2 Oxygen Reduction Reaction 39

1.6.3 Oxygen Evolution Reaction 48

1.6.4 Oxygen Selective Membranes 56

1.7 Aims 59

1.8 References 60

Chapter 2 : Experimental Procedures & Techniques **69**

2.1 Solvent and Electrolyte Preparation 71

2.2 Cell Construction 72

2.2.1 Two Compartment Glass 'U' Cells 72

2.2.2 Swagelok Cells utilising a Stacked Cell Geometry 74

2.3 Electrochemical Techniques 77

2.3.1 Cyclic Voltammetry 77

2.3.2 Galvanostatic Cycling 83

2.4 References 88

Chapter 3 : An Investigation of Electrolyte Stability through the use of *In Situ* Raman Spectroscopy 91

3.1 Introduction 93

3.2 Experimental 97

3.2.1 Chemical Reagents 97

3.2.2 Instrumentation 97

3.2.3 Cell Design 98

3.3 Results and Discussion 100

3.3.1 SERS Investigation of Oxygen Reduction in 1-Ethyl-3-Methylimidazolium Bis(Trifluoromethanylsulfonyl)imide 100

3.3.2 SERS Investigation of Oxygen Reduction in 1-Butyl-1-Methylpyrrolidinium Bis(Trifluoromethylsulfonyl)imide 104

3.4 Conclusions and Further Work 111

3.5 References 113

3.6 Related Publications 117

Chapter 4 : Ethyl Viologen as a Homogeneous Catalyst for the Oxygen Reduction Reaction 119

4.1 Introduction 121

4.2 Experimental 126

4.2.1 Electrochemical Techniques 126

4.2.2 Chemical Reagents 126

4.2.3 Synthesis of Chemical Reagents 126

4.2.4 Instrumentation 126

4.2.5 Cell Design 126

4.3 Results and Discussion 129

4.3.1 Electrochemical Investigation of Ethyl Viologen Ditriflate 129

4.3.2 Investigating the Stability of Ethyl Viologen Ditriflate 139

4.3.3 Investigations into the Galvanostatic Cycling Behaviour of Ethyl Viologen Ditriflate 147

4.4 Conclusions and Further Work 157

4.5 References 159

4.6 Related Publications 161

Chapter 5 : The Electrochemcial Behaviour of the Cobalt Bis(Terpyridine) Complex 163

5.1 Introduction 165

5.2 Experimental 169

5.2.1 Electrochemical Techniques 169

5.2.2 Scanning Electron Microscopy and Energy-Dispersive X-Ray Spectroscopy 169

5.2.3 Chemical Reagents 170

5.2.4 Synthesis of Chemical Reagents 171

5.2.5 Instrumentation 171

5.3 Results and Discussion 172

5.3.1 Understanding the Effect of Electrolyte Composition on Soluble Catalysts 172

5.3.2 Voltammetric Characterisation of Cobalt Bis(Terpyridine) in Li-O_2 Cells 179

5.3.3 Galvanostatic Cycling of Cobalt Bis(Terpyridine) in Swagelok Cells 187

5.3.4 SEM and EDX Analysis of Galvanostatically Cycled Electrodes 193

5.4 Conclusions 197

5.5 References 199

Appendix A ..... **i**

Appendix B ..... **ix**

Academic Thesis: Declaration Of Authorship

I, James Thaddeus Frith

declare that this thesis and the work presented in it are my own and has been generated by me as the result of my own original research.

Lithium-oxygen batteries: The importance of the electrolyte and the use of soluble catalysts

I confirm that:

1. This work was done wholly or mainly while in candidature for a research degree at this University;
2. Where any part of this thesis has previously been submitted for a degree or any other qualification at this University or any other institution, this has been clearly stated;
3. Where I have consulted the published work of others, this is always clearly attributed;
4. Where I have quoted from the work of others, the source is always given. With the exception of such quotations, this thesis is entirely my own work;
5. I have acknowledged all main sources of help;
6. Where the thesis is based on work done by myself jointly with others, I have made clear exactly what was done by others and what I have contributed myself;
7. Either none of this work has been published before submission, or parts of this work have been published as:

   M. J. Lacey, J. T. Frith, and J. R. Owen, *Electrochem. Commun.*, **26**, 74–76, (2013).

   J. T. Frith, A. E. Russell, N. Garcia-Araez, and J. R. Owen, *Electrochem. Commun.*, **46**, 33–35, (2014).

   L. Yang, J. T. Frith, N. Garcia-Araez, and J. R. Owen, *Chem. Commun.*, **51**, 1705–1708, (2014).

Signed: .....

Date: .....

Acknowledgements

I would like to thank my supervisor, Professor John Owen, for his encouragement and guidance during my studies and in particular for providing me with the opportunity to study an area I had a great interest in. I would also like to thank Dr Nuria Garcia-Araez who has helped me out immensely during my studies. I would also like to thank Professor Phil Bartlett and Professor Andrea Russell for providing useful scientific discussions.

The past and present members of the Owen/Garcia-Araez Group and the Southampton Electrochemistry Group have always been a great help in the lab and have provided good times at the pub, so thank you all. In particular I would like to thank Dr Matthew Roberts for his help and encouragement during my undergraduate project which set me on the path I am now on.

I would like to thank all the participating members of the LABOHR project for the enlightening project meetings and the good food and drink. I would also like to thank the EU-FP7 for providing some of my funding.

A big thanks to all my friends from university and from home for providing a break from the world of chemistry. In particular Tom, Oscar and Turner for a couple of brilliant surf trips.

Last, and by no means least, I'd like to say thank you to my family and Charlotte for being so supportive.

Abbreviations

ICE	Internal combustion engine
SHE	Standard hydrogen electrode
SEI	Solid electrolyte interface
EC	Ethylene carbonate
PC	Propylene carbonate
PAN	Polyacrylonitrile
LiTFSI	Lithium bis(trifluoromethylsulfonyl)imide
FT-IR	Fourier-transform infra-red spectroscopy
^{13}C MAS NMR	Carbon 13 magic-angle spinning nuclear magnetic resonance
SERS	Surface enhanced Raman scattering
DEMS	Differential electrochemical mass spectroscopy
DME	Dimethyl ether
DOL	1,3-dioxolane
TEGDME	Tetraethylene glycol dimethyl ether
DEGDME	Diethylene glycol dimethyl ether
XRD	X-ray diffraction
Pyr_{14}TFSI	1-butyl-1-methylpyrrolidinium bis(trifluoromethylsulfonyl)imide
C_2mimTFSI	1-ethyl-3-methylimidiazolium bis(trifluoromethylsulfonyl)imide
TPFPB	Tris(pentafluorophenyl) borane
DMSO	Dimethyl sulfoxide
TMS	Tetramethylene sulfoxide
DMF	Dimethylformamide
VC	Vinyl carbonate
ORR	Oxygen reduction reaction

OER	Oxygen evolution reaction
FTBA	Perfluorotributylamine
TTF	Tetrathiafulevene
EELS	Electron energy loss spectroscopy
RTIL	Room temperature ionic liquid
PTFE	Polytetrafluoroethylene
OCV	Open circuit voltage
PEM	Polymer electrolyte membrane
GC	Glassy carbon
CNT	Carbon nanotube
CoTerpy	Cobalt (II) bis(2,2':6,2"-terpyridine)
SEM	Scanning electron microscope
EDX	Energy dispersive X-ray (spectroscopy)
CV	Cyclic voltammetry
NHE	Normal hydrogen electrode

Chapter 1 : Introduction, Background and Aims

1.1 Introduction

The industrial revolution and human activity over the following century has led to global climate change.[1] This has largely been ascribed to increasing levels of greenhouse gasses in the atmosphere. CO_2 has been identified as one of the major gasses contributing to climate change and, amongst other causes, is released when burning fossil fuels in internal combustion engines (ICEs).[2] In an effort to reduce global greenhouse gas emissions large amounts of research are being carried out to develop electric vehicles and their power sources as they are considered to be more environmentally friendly modes of transport than ICE powered vehicles.

This work investigates the fundamentals of lithium-oxygen batteries, an energy storage system that shows promise as a possible power source for electric vehicles.[3]

1.2 Fundamentals of Electrochemical Cells

An electrochemical cell is a device in which the flow of electrons is used to control the reactions occurring at two electrodes. During discharge a chemical species is oxidised at the anode giving up its electrons to the external circuit. At the cathode a chemical species is reduced by electrons from the external circuit. To allow for the flow of electroactive species between the electrodes a conductive medium must be present, this is known as the electrolyte and normally consists of a salt dissolved in a solvent. The electrolyte also serves the purpose of separating the electrodes and preventing a short circuit while maintaining ionic conductivity (Diagram 1.1).[4]

The components of the cell are crucial to its correct functioning. The anode and the cathode electrode materials must both be stable when in contact with the electrolyte and be good electronic conductors. The electrolyte must be a good ionic conductor, a conductor of charged ions, but a poor electronic conductor, conductor of electrons, so as to avoid creating a short circuit.

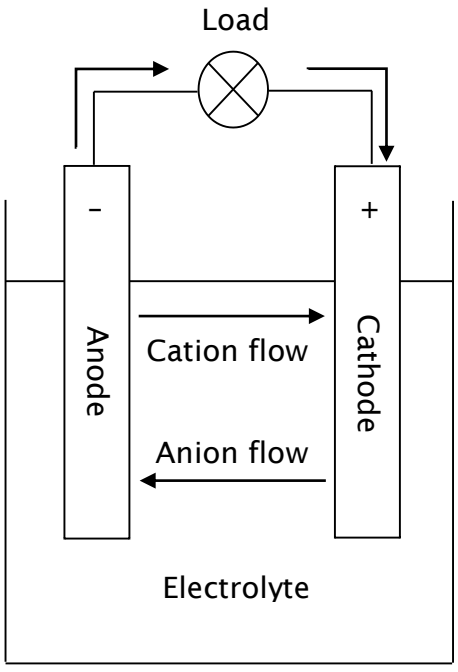

Diagram 1.1. A typical electrochemical cell during discharge.

The electrolyte must also be stable over the voltage range being used within the cell. Many electrochemical cells use aqueous electrolytes (water based electrolytes) including lead-acid batteries and alkaline batteries. However, these electrolytes have a small voltage range normally no more than $2\,V$. Non-aqueous batteries, such as Li-ion batteries, use water free electrolytes (non-aqueous electrolytes), this allows cells to operate over a wider potential window and keeps them free of the corrosive action of water.

1.3 Charge and Discharge

The most common devices currently used for powering portable electronics and electric vehicles are batteries, and capacitors. A battery is an electrochemical cell that undergoes a controlled redox reaction. This redox reaction converts stored chemical energy into electrical energy. In these cells electrical energy is generated by the flow of electrons, through an external circuit, from the anode to the cathode.

Capacitors are devices that store charge on parallel plates with opposing polarities. Often the charge is stored as the electrochemical double layer, this results in the total capacitance of the device being related to the surface area of the electrodes. As a result the total charge stored in a capacitor, according to Equation 1.1, is extremely small in comparison to the charge stored in a battery of a similar volume or mass. The response time of the device is however extremely fast in comparison to a battery as there are no electrochemical reactions occurring.

$$q = C \times V$$

Equation 1.1

Where:

q = charge (As)

C = capacitance ($As \cdot V^{-1}$)

V = Voltage over which device operates (V)

During the charge and discharge of batteries electrochemical reactions occur at both the anode and the cathode.

During discharge

Negative electrode: $Reduced\ species \rightarrow Oxidised\ species + electron$

Positive electrode: $Oxidised\ species + electron \rightarrow Reduced\ species$

During charge

Negative electrode: $Oxidised\ species + electron \rightarrow Reduced\ species$

Positive electrode: $Reduced\ species \rightarrow Oxidised\ species + electron$

As this shows the type of reaction at each electrode, oxidation or reduction, is reversed as you go from discharge to charge. Due to this, the labelling of the electrodes as anode and cathode is not recommended as they are dependent on whether the cell is being discharged or charged. When referring to batteries the use of positive and negative electrodes is more appropriate.[5] These terms refer to the electrochemical potential of the reaction happening at the electrodes relative to each other.

The potential of the reaction at an electrode can be determined from the Gibbs free energy of the reaction.[6]

$$\Delta G^0_{reaction} = -nFE^0$$

Equation 1.2

Where:

$\Delta G^0_{reaction}$ = Standard Gibbs free energy of the reaction ($kJ \cdot mol^{-1}$)

n = number of moles of electrons

F = Faradays constant ($96487\ C \cdot mol^{-1}$),

E^0 = Standard potential of the reaction (V)

In a battery the cell potential is then determined as the difference between the potential of the two electrodes:

$$E_{cell} = E_{+ve} - E_{-ve}$$

Equation 1.3

Where:

E_{cell} = cell potential (V)

E_{+ve} = potential at the positive electrode ($V\ vs\ SHE$)

E_{-ve} = potential at the negative electrode ($V\ vs\ SHE$)

It is important to note at this point that not all battery cells can be charged after discharge. Cells that can only be discharged once are referred to as primary cells, while cells that can be recharged and cycled multiple times are known as secondary cells. Some commonly used secondary batteries along with their electrode components, cell reactions during charge and discharge and cell potentials are shown in Table 1.1.

Various secondary batteries and their characteristics

Battery system	Cathode	Electrolyte/reaction	Anode	Nominal voltage (V)
Lead acid	PbO_2	H_2SO_4 aqueous solution $Pb + SO_4^{2-} \rightleftharpoons PbSO_4 + 2e^-$ (anode) $PbO_2 + 4H^+ + SO_4^{2-} + 2e^- \rightleftharpoons PbSO_4 + 2H_2O$ (cathode) $PbO_2 + 2H_2SO_4 + Pb \underset{\text{charge}}{\overset{\text{discharge}}{\rightleftharpoons}} 2PbSO_4 + 2H_2O$ (total reaction)	Pb	2
Ni–Cd	NiOOH	KOH aqueous solution $Cd + 2OH^- \rightleftharpoons Cd(OH)_2 + 2e^-$ (anode) $2NiOOH + 2H_2O + 2e^- \rightleftharpoons 2Ni(OH)_2 + 2OH^-$ (cathode) $2NiOOH + Cd + 2H_2O \underset{\text{charge}}{\overset{\text{discharge}}{\rightleftharpoons}} Ni(OH)_2 + Cd(OH)_2$ (total reaction)	Cd	1.2
Ni–MH	NiOOH	KOH aqueous solution $H_2 + 2OH^- \rightleftharpoons 2H_2O + 2e^-$ (anode) $2NiOOH + 2H_2O + 2e^- \rightleftharpoons 2Ni(OH)_2 + 2OH^-$ (cathode) $2NiOOH + H_2 \underset{\text{charge}}{\overset{\text{discharge}}{\rightleftharpoons}} 2Ni(OH)_2$ (total reaction)	Hydrogen adsorbed alloy	1.2
Lithium ion	CoO_2	Organic electrolyte + Li salt $Li(C) \rightleftharpoons Li^+ + e^-$ (anode) $Li^+ + e^- + CoO_2 \rightleftharpoons LiCoO_2$ (cathode) $Li(C) + CoO_2 \underset{\text{charge}}{\overset{\text{discharge}}{\rightleftharpoons}} LiCoO_2$ (total reaction)	C + Li	3.7

Table 1.1. Common secondary battery systems. The reactions occurring at each electrode as well as the global reaction are shown. The forward arrows denote the reaction occurring during discharge while the reverse arrows denote the reaction occurring during charging. It should be noted that the reactions labelled 'anode' refers to the reactions occurring at the negative electrode during discharge and the reactions labelled 'cathode' refers to the reactions occurring at the positive electrode during discharge. **Reprinted from "Materials Science and Engineering: R: Reports, 33/4, Masataka Wakihara, Recent developments in lithium ion batteries, 109-134." Copyright 2001, with permission from Elsevier.**[7]

1.4 Cell Capacity

One of the most important features of a portable energy storage device is its capacity. The capacity is a measure of the electrochemical charge stored within a cell. The capacity of a cell is intrinsically linked with the charge passed during an electrochemical reaction and the mass of the cell or specified cell components.

In electrochemistry the charge passed during a reaction is measured in units of coulombs, C (Equation 1.4);[6] however in battery science the charge is commonly expressed in the technical units of mAh. To convert from coulombs, C or As, to mAh you first divide by 3600 (the number of seconds in one hour) then multiply by 1000 (the conversion from A to mA). This can be simplified to dividing by 3.6.

$$q = nFm$$

Equation 1.4

Where:

q = capacity (As)

n = number of electrons

F = Faradays constant ($96485\ C \cdot mol^{-1}$)

m = number of moles of reactant (mol).

From the total charge passed it is then possible to calculate the specific capacity, $mAh \cdot g^{-1}$, by dividing by the mass of specified cell components. In battery science when comparing different systems it is normally the specific gravimetric capacity of a material that is of interest. This is calculated based on the mass of one mole of the active material.

$$Q_T = \frac{q}{M}$$

Equation 1.5

Where:

Q_T = specific capacity ($mAh \cdot g^{-1}$)

q = capacity (mAh)

M = molecular mass (g)

The specific energy, S_E ($Wh \cdot kg^{-1}$), of a battery is also very important as it defines the energy available in the cell for a given mass:

$$S_E = E_{cell} \times Q_T$$

Equation 1.6

Batteries based on lithium metal have risen to prominence over the last quarter of a century as lithium is the most electropositive metal at $-3.04\ V\ vs\ SHE$ (standard hydrogen electrode) and also extremely light at $6.94\ g \cdot mol^{-1}$. The combination of these two factors gives lithium metal a high specific energy, $293\ Wh \cdot kg^{-1}$. This high specific energy means that a lot of energy can be accessed from a relatively small amount of material. It is this property that has been the driving force behind the revolution in portable electronics.

As well as the specific energy of battery systems the energy density is also important as this defines the energy stored in a given volume, in units of $Wh \cdot L^{-1}$.

1.5 Li-ion Cells

Li-ion batteries have arguably been one of the greatest technological developments in power sources in the 20th century as they offer both high specific energies and capacities. This has fed in to the development of portable electronics such as laptops and smartphones.

With the exception of primary cells commercial Li-ion cell do not use lithium metal as an anode material.[8] This is due to safety problems associated with its use, in particular the formation of dendrites.[9] Instead Li-ion cells consist of two insertion electrodes. In general the active material in the negative electrode is graphite, although the use of silicon as the active material is a growing area.[10]

The active material in the positive electrode generally consists of a lithiated transition metal oxide or lithiated transition metal phosphate.[11] Figure 1.1 shows various negative and positive electrode materials that are used in or are under investigation for use in Li-ion cells.

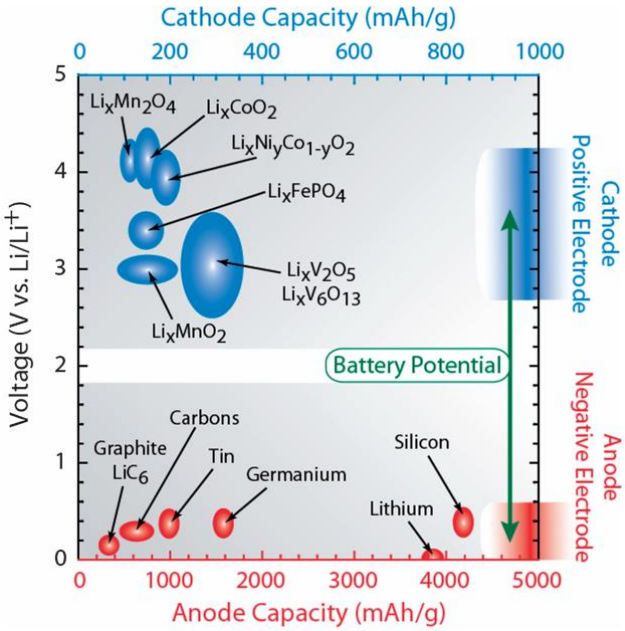

Figure 1.1. Diagram showing the potential and capacity of different negative (anode) and positive (cathode) electrode materials used in Li-ion cells. **Reproduced from Ref [12] with permission of The Royal Society of Chemistry.**

Li-ion cells are generally constructed in the discharged state with a lithiated positive electrode and de-lithiated negative electrode. During the charge process lithium ions de-intercalate from the positive electrode and migrate through the electrolyte to the negative electrode. During discharge this process is reversed. An example of a Li-ion cell with a $LiCoO_2$ positive electrode and a graphite negative electrode is shown in Diagram 1.2.

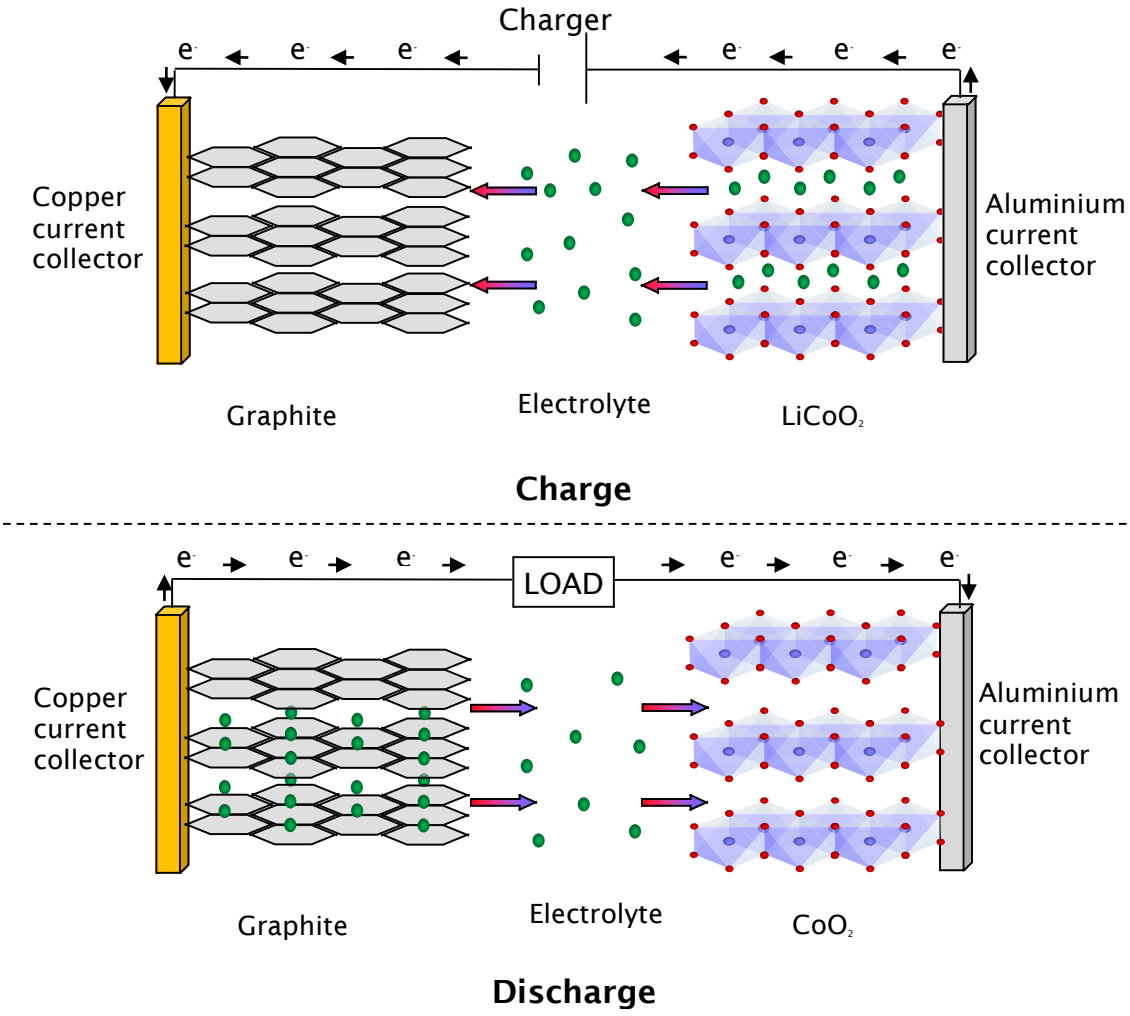

Diagram 1.2. A Li-ion cell with a $LiCoO_2$ positive electrode and graphite negative electrode. (●) Li ions (Li^+).

As well as the active material both electrodes require a binder and the positive electrode also requires the addition of conductive material such as carbon. The addition of carbon to the positive electrode is necessary as the active materials used tend to have low electronic conductivities.[13] It should be noted that a conductive material is also required when using silicon as the active material in the negative electrode. The use of a binder is necessary as it affords the electrodes a degree of mechanical strength but more importantly it helps to keep the active material and the conductive additives in good electronic contact.

There are a variety of different electrolytes that can be used in Li-ion cells. In general electrolytes are composed of a solvent formed of at least one of the following organic groups; carbonates, esters or ethers.[14, 15] To this a lithium salt is added in order to provide ionic conductivity, often lithium hexafluorophosphate ($LiPF_6$) or lithium bis(oxalato)borate (LiBOB) are used.

The lifetime of a Li-ion cell is intrinsically related to the composition of the electrolyte. This is a result of the formation of the SEI (solid electrolyte interface).[16] The SEI is a stable lithium ion conducting layer that forms on the negative electrode and is the result of the breakdown of the electrolyte solvent and its salt. This may at first seem counter intuitive, however the electronically insulating nature of this layer hinders the further degradation of the electrolyte.

The flammable nature of commonly used electrolyte solvents in Li-ion cells such as ethylene carbonate (EC) and propylene carbonate (PC) has raised concerns over their use.[17] As a result the use of alternative solvents is desirable to alleviate the public's fears. This presents problems as often the replacement solvents do not form a stable SEI. To try to overcome this problem electrolyte additives are often used.[18] These additives are molecules that will either be electrochemically reduced at the electrode surface prior to the reduction of the electrolyte or molecules that

will scavenge radicals during the reduction of the electrolyte and then help to form a stable SEI.

Despite the high specific energies and capacities of Li-ion cells, as the processing power of smartphones and laptops increases their energy demands result in shorter operating times of the cells. This results in a situation where an increasing volume of a device is given over to the battery with only marginal improvements to the amount of time the device can be powered for. A similar situation is seen in the electric vehicle market where it is not possible to match the performance of an ICE through the use of current Li-ion batteries, unless a significant proportion of the internal volume is given over to a battery pack. The use of large volumes of batteries also adds unwanted weight.

To meet increasing portable power demands new battery technologies are being researched. These new systems will provide increased power density, energy density or both. As a result a battery system of the same volume or mass of current Li-ion systems will provide increased driving range for electric vehicles or increased battery life for portable electronics. Figure 1.2 illustrates how the increased specific energies of various battery chemistries would affect the driving range of an electric vehicle. It should be noted that an increased specific energy results in a greater driving range while an increased specific power leads to greater acceleration.

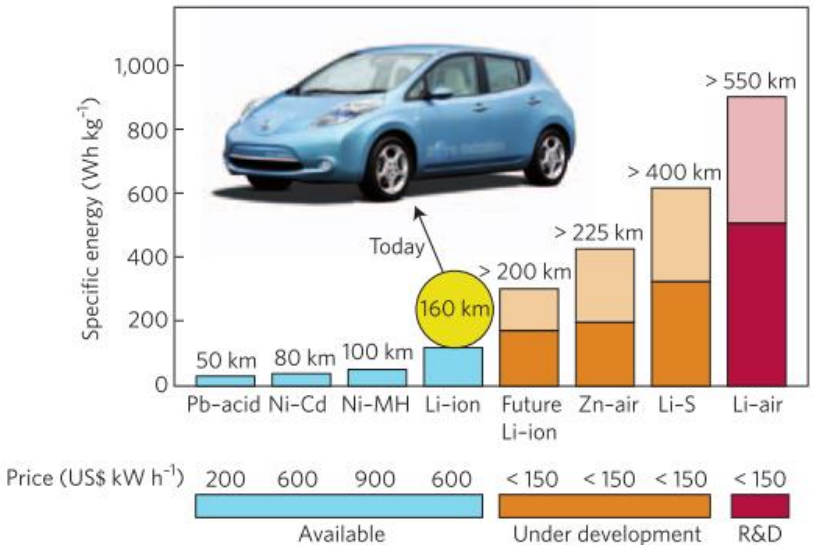

Figure 1.2. Practical specific energies of various commercial and research battery chemistries. **Reprinted by permission from Macmillan Publishers Ltd: Nature Materials, P. G. Bruce, S. A. Freunberger, L. J. Hardwick, and J.-M. Tarascon, *Nat. Mater.*, 11, 19–29, (2011)., copyright 2011.**[19]

1.6 Non-Aqueous Lithium-Oxygen Cells

Research into metal-oxygen power systems is a well-established field of electrochemistry dating back to the 1970's. These systems have the advantage that they only require half of the active material to be stored in the cell, as the active material for the positive electrode, oxygen, can be accessed from the environment. As a result metal-oxygen cells possess higher theoretical specific energies than typical Li-ion battery systems (Figure 1.2). As these metal-oxygen systems are designed around the idea of accessing oxygen from the air they are often referred to as metal-air batteries.

Early research into these metal-oxygen systems focused on the use of metal anodes in aqueous electrolytes, this limited the metals available for use based on their stability to water (or rather their lack of stability in contact with water). The Zn-air system in particular has been the focus of a large amount of research, and is one of the most widely commercialized metal-oxygen systems, commonly found in hearing aids.

During this period of research, in the 1970's, the lithium metal anode was investigated as a possible anode for use in aqueous systems by Littauer *et al.*.[20, 21] In this work it was suggested that during anodic polarization a passivating layer of Li_2O was formed that at least partially protected the lithium from further reactions with water.[20] The driving force behind this work was the high specific capacity offered by a lithium metal anode, approximately $3{,}800\ mAh \cdot g^{-1}$ using Equation 1.7.

$$Q = \frac{nF}{M}$$

Equation 1.7

Where:

Q = the specific capacity ($mAh \cdot g^{-1}$)

n = number of moles of electrons

F = Faradays constant ($96487\ As \cdot mol^{-1}$)

M = the molecular mass ($g \cdot mol^{-1}$)

However as previously mentioned due to the instability of the passivating layer and the reactivity of lithium with water this was soon ruled out as a viable option.[20] The idea of the lithium metal anode was then widely forgotten as focus shifted to the Li-ion cell that would go on to become one of the defining inventions of the 20th century.

Although thoughts of using lithium metal as a stand-alone negative electrode in commercial cells had been widely forgotten lithium metal was still being used as a counter electrode in Li-ion cell research. It was through this application that Abraham and Jiang accidently stumbled across the Li-O_2 cell. The accidental exposure of a cell, containing a lithium metal counter electrode and carbon composite working electrode, to a small amount of oxygen resulted in a capacity far in excess of that which had been expected.[22]

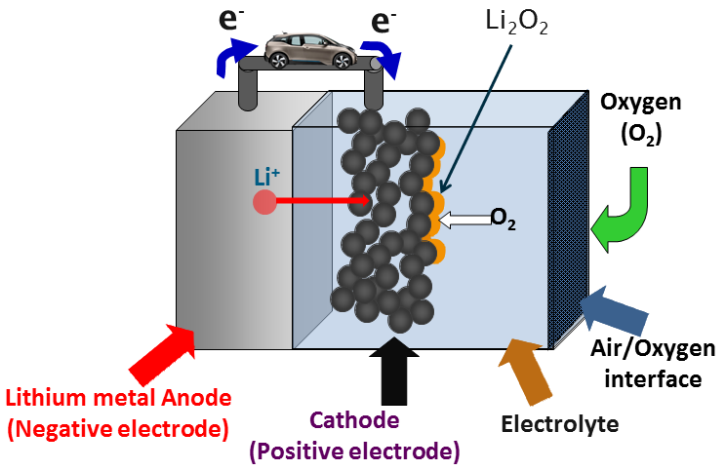

Figure 1.3. Schematic of a lithium-oxygen cell during discharge.

It was discovered that this excess capacity was the result of the reduction of oxygen as shown in Reaction 1.1:

$$O_2 + 2Li^+ + 2e^- \rightarrow Li_2O_2$$

Reaction 1.1

This reaction may proceed *via* a mixture of two routes, as shown in the schemes below. Scheme 1.1 represents an electrochemical step followed by a chemical disproportionation, while Scheme 1.2 represents two consecutive electrochemical steps.

$$O_2 + e^- + Li^+ \rightarrow LiO_2 \qquad step\ 1 \quad Electrochemical$$

$$2LiO_2 \rightarrow Li_2O_2 + O_2 \qquad step\ 2 \quad Chemical$$

Scheme 1.1

$$O_2 + e^- + Li^+ \rightarrow LiO_2 \qquad step\ 1 \quad Electrochemical$$

$$LiO_2 + e^- + Li^+ \rightarrow Li_2O_2 \qquad step\ 2 \quad Electrochemical$$

Scheme 1.2

The realisation of this cell chemistry has since opened up a new field of research, the end goal of which is to produce high performance batteries for electric vehicles that will allow for journeys in excess of 300 miles on a single charge.[23, 24]

1.6.1 Electrolyte

In Abraham and Jiang's initial work a polymer electrolyte consisting of polyacrylonitrile (PAN) plasticised with propylene carbonate (PC)/ethylene carbonate (EC) and lithium hexafluorophosphate ($LiPF_6$) was used (the structure of solvent molecules mentioned in this section can be found in Table 1.2).[22]
The capacities obtained in this cell, $1400\ mAh \cdot g^{-1}$, were far in excess of the capacities that could be achieved in a Li-ion cell.[22] Although it should be noted that the capacities quoted for lithium-oxygen cells are generally quoted with respect to the mass of carbon in the electrode, this makes comparison with lithium-ion batteries difficult. This is due to the capacities of lithium ion batteries being quoted with respect to the mass of active material present.
Through the use of *ex situ* Raman spectroscopy lithium peroxide (Li_2O_2) was found to be the primary discharge product.[22] However, as will be discussed later, the identification of lithium peroxide as the primary discharge product in carbonate electrolytes was something of a red herring.
Due to the design of this early Li-O_2 cell, with an air electrode (Figure 1.4) open to the surrounding environment, solvent evaporation became an important concern. To address this issue Abraham, Jiang and Carroll started exploring alternative polymer electrolytes.[25] This work introduced the use of lithium bis(trifluoromethsulfonyl)imide (LiTFSI) as a possible salt for use in Li-O_2 cells. The advantage of using LiTFSI over $LiPF_6$, a commonly used lithium salt in Li-ion cells, is that it does not react with water (HF is evolved when $LiPF_6$ reacts with water

under certain conditions). It should be noted that LiTFSI is not used in Li-ion cells as it reacts with the aluminium that is used as a current collector.

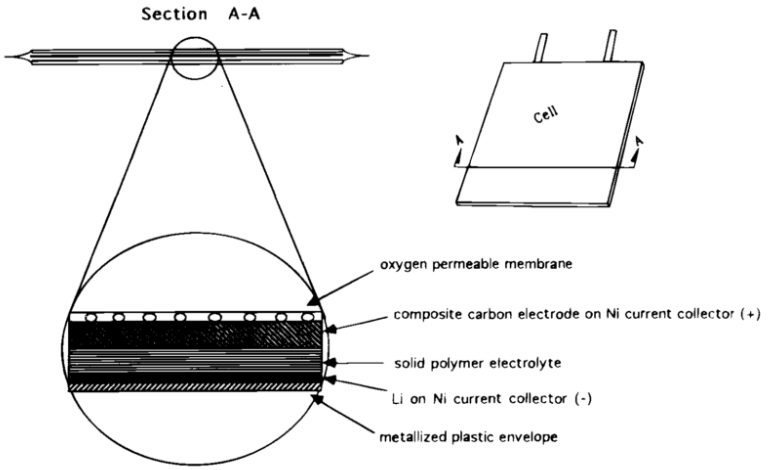

Figure 1.4. Schematic representation of a Li-O_2 plastic battery as shown by Abraham and Jiang. **Reprinted with permission from "K. M. Abraham and Z. Jiang, *J. Electrochem. Soc.*, 143, 1–5, (1996)". Copyright 1996, The Electrochemical Society.**[22]

The use of PC as an electrolyte in this first cell was likely to have been based on the wide spread use of carbonate based electrolytes in Li-ion cells.[26] Despite the differing chemistries of Li-O_2 and Li-ion cells, the use of these non-aqueous electrolytes would have seemed appropriate at the time, and as a result this initial summary of the work carried out in carbonate based electrolytes will focus on how their performance was initially perceived.

In 2002 Read again looked into electrolyte formulation.[27] Through the use of liquid electrolytes, containing carbonates, Read found that capacities ranging from $200 - 1000\, mAh \cdot g^{-1}$ could be achieved depending on the current density applied. Through gas consumption analysis Read also calculated that lithium oxide (Li_2O) should be formed alongside Li_2O_2 as discharge products in Li-O_2 cells.[27]

Read then followed this publication up with an in-depth study into the effects of oxygen solubility, diffusion coefficient and (external) partial pressure as well as

electrolyte viscosity on cell performance.[28] The aim of this study was the optimization of the electrolyte, with the conclusion being that the solubility of oxygen and its diffusion coefficient in a particular electrolyte plays a large role in the discharge capacity of a lithium-oxygen cell. The solubility was also found to be influenced by the partial pressure of oxygen in the environment surrounding the cell.[28] This is useful when attempting to achieve high capacities in a lab based environment, however, for practical operation a lithium-oxygen cell would access the oxygen it requires from the air. This would make increasing the partial pressure of oxygen more difficult without using an external device that would itself require power or an oxygen storage tank.

In 2006 Ogasawara *et al*. showed that a carbon cathode preloaded with Li_2O_2 could be charged up to give off oxygen and lithium ions in a carbonate based electrolyte.[29] At the same time it was shown that the cell could be cycled for 50 cycles and retain over $50\,\%$ of its initial capacity. This paper seemed to alleviate previous fears of cycle stability and the reversibility on charge of the insoluble and insulating discharge product Li_2O_2.

Due to the poor mechanical properties of cells containing liquid electrolytes, and the higher risk of electrolyte leakage associated with Li-O_2 cells Mohamed *et al.* looked into the use of epoxidised natural rubber based gel polymer electrolytes.[30] Both EC and PC were tested as possible plasticizers, with the best conductivity results found when using PC. The use of these gel polymers allowed the cells to be discharged at a relatively high current for lithium-oxygen cells, $0.3\ mA \cdot cm^{-2}$. This was approximately $3\times$ the current density used by Abraham *et al.,*[25] however it is not clear if the use of these natural rubber based polymers offered a significant advantage over those used by Abraham as the capacity of the cell was significantly smaller.

Abraham *et al.* then went on to report an improved solid state cell that utilised a glass ceramic membrane to prevent incursion of water on to the lithium anode side of the cell, combined with a PC plasticized polymer.[31] It was hoped that through the use of this membrane the rechargeability of the cell could be improved compared to their previous work.[22]

This was indeed shown to be the case with a cell with a $50\ \%$ loading of carbon in the cathode having a discharge capacity of $11.34\ mAh$ and a charge capacity of $11.40\ mAh$, although the cell required an operating temperature of $95\ ^{\circ}C$.[31] The extra capacity on charge compared to discharge was repeatedly observed, but not commented on.

These initial studies of Li-O_2 cells using traditional Li-ion solvents in their electrolytes showed great promise and put a working Li-O_2 cell almost within grasp. However the long term cycling of the cell still remained an issue. At the turn of the decade several groups published articles that threw in to question much of the work that had previously been published on Li-O_2 cells.

Mizuno *et al.*, Freunberger *et al.,* McCloskey *et al.* and Veith *et al.* all recognised that the high capacities previously seen in carbonate based solvents could not be due solely to the reduction of oxygen to give lithium peroxide.[32–35]

Through the use of FTIR Mizuno *et al.* found that lithium carbonate (Li_2CO_3) was the dominant discharge product in their cells when using carbonate based electrolytes.[32] The formation of Li_2CO_3 rather than Li_2O_2 was ascribed to the breakdown of the carbonate electrolyte by the intermediate discharge product, superoxide.[32]

Freunberger *et al.* used a range of techniques, including FTIR, ^{13}C MAS NMR, SERS and DEMS, to further investigate the mechanism behind the degradation reaction seen when using carbonate based electrolytes.[33] Along with lithium carbonate

they identified several other products of the degradation reaction, as well as proposing a possible reaction pathway (Scheme 1.3).[33]

They then went on to show that it was possible to charge (oxidise) these breakdown products. By charging electrodes that were pre-filled with the breakdown products that had been identified during discharge, they were able to illustrate the wide variety of different charging potentials. It was suggested that the different charging potentials of the various breakdown products could account for the wildly varying charging potentials seen in earlier works.[33]

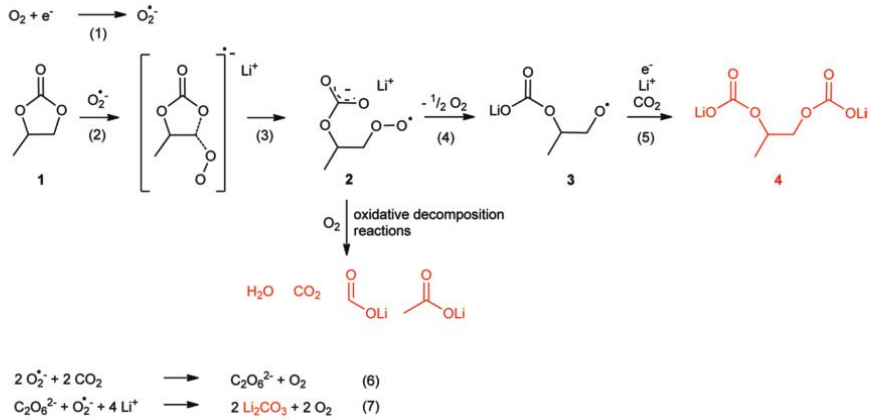

Scheme 1.3. Proposed reaction scheme for the degradation of PC by superoxide. **Reprinted with permission from "Reactions in the rechargeable lithium-O2 battery with alkyl carbonate electrolytes". Copyright 2011 American Chemical Society.**[33]

As the breakdown products identified by Freunberger *et al.* could all be oxidised, it suggested that the cell failures previously seen in cells using carbonate based electrolytes was a result of the consumption of the electrolyte.

Using a similar set of techniques McCloskey *et al.* and Veith *et al.* also examined the reactions of superoxide in carbonate based electrolytes, finding similar results to that of Freunberger *et al.*.[34, 35] However as well as investigating the stability of carbonate based electrolytes McCloskey *et al.* also looked into the use of dimethoxyethane (monoglyme, DME),[34] an alternative ether based solvent which had been suggested for use in lithium-oxygen cells by Freunberger *et al.*.[33]

Their results showed that DME appeared to exhibit a much greater stability to oxygen reduction products,[34] a suggestion that was echoed by Veith *et al.*.[35] The consumption of the electrolyte on discharge helps to explain both the limited cycle life as well as the poor capacity retention seen in early research. In hindsight the degradation of the electrolyte through reaction with superoxide should have been expected as ring opening reactions of carbonates with other strong nucleophiles such as OH^- had previously been reported.[36]

Despite the realisation that carbonate based electrolytes were not stable in Li-O_2 cells the theory behind their operation was still viable. If suitable electrolytes could be found, such as ethers, a working Li-O_2 cell could still operate as predicted. However it would no longer be possible to suggest that a cell was operating as expected based on capacity measurements alone. Instead cycling data would need to be combined with spectroscopic analysis to provide evidence that no/minimal degradation reactions were occurring. Results previously reported in carbonate based electrolytes could also no longer be considered reliable in terms of cell performance, however the techniques used could still be applied to new electrolytes.

The use of ether electrolytes in Li-O_2 cells was not a new concept and it had first been explored by Read in 2006.[37] Read's study focused on how the capacity of the cell and the rate at which it could be charged or discharged was affected by the solubility of oxygen, viscosity of the solvent and conductivity of the electrolyte. It was found that when using a solvent mixture of 1,3-dioxilane (DOL) and DME oxygen solubility played an important role in determining the capacity of the cell for low oxygen concentrations.[37] However as the oxygen concentration was increased the viscosity of the electrolyte played the largest role in determining the capacity of the cell.[37] In this work spectroscopic determination of the

discharge product was not provided, however it was assumed to be lithium peroxide.

In 2009 Xu *et al.* applied knowledge they had gained from investigating electrolytes for primary Li-O_2 cells to secondary Li-O_2 cells.[38] In this work they investigated several different ethers including DME.[39] This work took a similar approach to that used by Read [37] however they also looked into the contact angle between the electrolyte and the cathode, which is related to the polarity of the solvent. They found that the contact angle played a large role in the capacity of the cell as it helped to determine the number of tri-phase regions on the electrode surface.[39] The tri-phase region is an area where the electrolyte, electrode and oxygen meet and therefore the area where oxygen is reduced as shown by Diagram 1.3.

When using an air electrode that is half-flooded (in the ideal case), it can be seen that the number of these tri-phase regions would play an important role in determining the capacity of the cell as if the insoluble and insulating Li_2O_2 forms at these points it will 'clog' the electrode. Therefore it was postulated that if it was possible to increase the number of these regions you could increase the cell capacity.

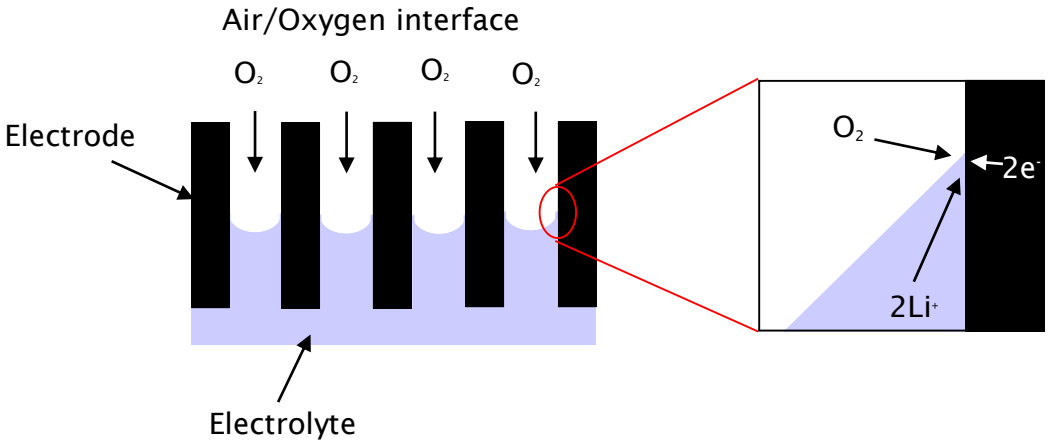

Diagram 1.3. Depiction of a tri-phase region at the interface of the porous cathode, electrolyte and gas phase in a lithium-oxygen cell.

O'laoire *et al.* investigated the use of a longer chain ether, tetraethylene glycol dimethyl ether (tetraglyme, TEGDME).[40] The advantage of TEGDME over DME and diethylene glycol dimethyl ether (diglyme, DEGDME) being that it is less volatile and would therefore result in less evaporation during the operation of a cell that's exposed to the environment.

They found that they could achieve excellent cycling behaviour, with an identical capacity seen on both discharge and charge, although this did require the cell to be charged up to $4.5\ V$.[40] To accompany the electrochemical results they also carried out XRD analysis on both a discharged and charged cathode, this provided evidence that the primary discharge product appeared to be Li_2O_2 which could then be reversibly oxidised.[40]

Since the realisation that superoxide readily attacks carbonate based solvents determining the stability of solvents has become crucial to avoid repeating previous mistakes and discrediting the area of Li-O_2 research. To this end Xu *et al.* published a comprehensive report in 2012 that looked into the stability of several ethers and compared their performance to carbonate based electrolytes and the ionic liquid $Pyr_{14}TFSI$.[41]

Their results showed that when using ethers as the electrolyte solvent lithium peroxide was formed as the predominant discharge product.[41] They also reported the presence of the unwanted discharge product Li_2CO_3 in all of the solvents they examined.[41] This was put down to superoxide reacting with the ether based solvents.

However a paper published in parallel by Wang *et al.* brings into question the assumption that it was a reaction between the ether based solvent and superoxide that caused Li_2CO_3 formation.[42] Wang *et al.* found that by exposing DME to oxygen over a period of 20 h a colour change was observed in the

solvent. It was proposed that this was due to autoxidation (Scheme 1.4),[42] a process that is commonly seen in organic chemistry.

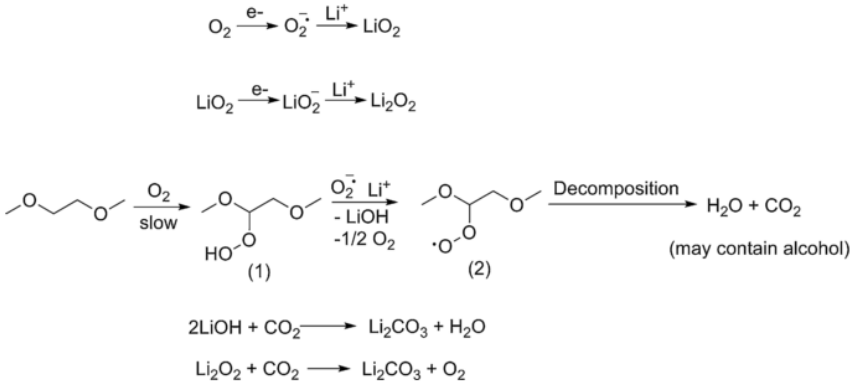

Scheme 1.4. Proposed route of degredation of DME in the presence of oxygen. DME must first form hydroperoxides with oxygen, these then react with superoxide formed during discharge of the cell which in turn leads to decomposition of the electrolyte. **Reprinted from "Electrochimica Acta, 64, H. Wang and K. Xie, Investigation of oxygen reduction chemistry in ether and carbonate based electrolytes for Li–O2 batteries, 29-34," Copyright 2012, with permission from Elsevier.**[42]

Black *et al.* investigated the stability of TEGDME to the highly reactive intermediate discharge product, superoxide.[43] Through the addition of potassium superoxide to an electrolyte of $LiPF_6$, TEGDME, they showed that no breakdown products were detected using both ^{1}H and ^{13}C NMR.[43] However, when adding the binder PvDF (poly(vinylidene difluoride)) to a TEGDME electrolyte containing potassium superoxide, in the presence of manganese dioxide (MnO_2), lithium hydroxide was detected.[43] The cause of this was the breakdown of PvDF in the presence of superoxide, to form hydrogen peroxide, which in turn reacted with MnO_2 to form water and subsequently lithium hydroxide.[43]

Schwenke *et al.* then went on to use a similar technique to Black *et al.,* using a barrage of analytical techniques to investigate the stability of ethers of various chain lengths.[44] The ethers investigated included DME, DEGDME, triglyme and TEGDME, that were either used as received or dried further. The stability of these ethers were investigated by the addition of potassium superoxide (KO_2) to the

solvent. Through the use of ^{1}H NMR (nuclear magnetic imaging) they managed to detect the formation of varying amounts of potassium formate and potassium acetate (products from the reaction of superoxide with ethers).[44]

The formation of these breakdown products was most evident when using tetraglyme and triglyme that were used as received, with only trace amounts detected in monoglyme and diglyme.[44] Distilled tetraglyme was also investigated, in the distilled solvent no breakdown products were detected.[44] This was confirmed through the use of FTIR (Fourier-Transition Infra-Red) spectroscopy as illustrated in Figure 1.5.

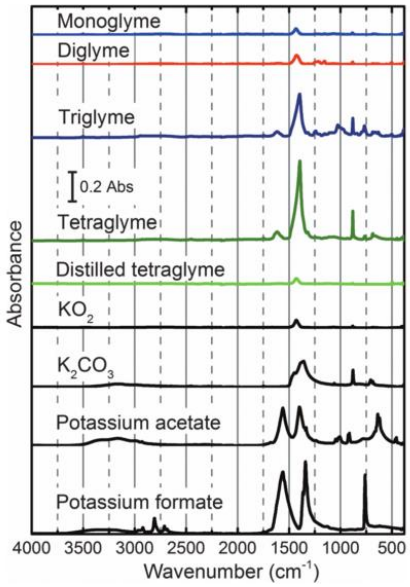

Figure 1.5. FTIR spectra of various ether based solvents after the addition of KO_2. Reference spectra of KO_2 and various possible breakdown products of superoxide and the ethers are also included. **Reproduced from Ref [44] with permission of The Royal Society of Chemistry.**

When used in a Li-O_2 cell the un-distilled tetraglyme resulted in a capacity of almost twice that of the distilled solvent.[44] These results indicate that the breakdown seen in ethers, particularly with longer chain lengths, is largely due to the impurities present.[44] This can therefore be avoided by distilling the ether or if this is not possible using shorter chain ethers such as monoglyme or diglyme.

As well as ethers, ionic liquids have also been suggested as alternative electrolytes for use in Li-O_2 cells. They were first suggested as a possible solvent by Kuboki *et al.* in 2005.[45] This was prior to the realisation of the unstable nature of organic carbonate solvents and was driven by the highly tuneable nature of ionic liquids as well as the need for Li-O_2 cells to operate free from water. It was believed that the hydrophobic nature of certain ionic liquids would help prevent some of the problems associated with water incursion.[45]

Ionic liquids also offer additional advantages in safety as they are non-flammable. This is an important issue if the public are to feel safe driving electric vehicles. Ionic liquids also have associated drawbacks such as low rate capabilities due to the high viscocity of the solvent and resulting low diffusion coefficients of dissolved species.[46]

Kuboki *et al.* identified 1-ethyl-3-methylimdiazolium bis(trifluoromethyl sulfonyl)imide (C_2mimTFSI) as being almost immiscible with water and therefore a potential candidate for use in Li-O_2 cells. Through the use of this ionic liquid a Li-O_2 cell was able to operate in ambient conditions for 56 days before the anode succumbed to water damage.[45]

This success was somewhat over shadowed by a previous study, unrelated to Li-O_2 research, that found that the C_2mim^+ cation was unstable in the presence of superoxide.[47] It should also be mentioned at this point that the primary discharge product, in Kuboki *et al.*'s work, was found to be Li_2CO_3.[45] This was presumably in part from oxygen reduction in the presence of carbon dioxide as shown by Scheme 1.5 and also possibly due to degradation reactions between superoxide and the solvent.

Despite the known breakdown that results from C_2mim^+ reacting with O_2^-, Allen *et al.* published a further study in 2011 into its use as an electrolyte in Li-O_2 cells.[48] The article focused on the possible mechanisms seen on charge and discharge in

Li-O_2 cells, but did not touch on the possible degradation of the ionic liquid cation by superoxide.

$$2Li_2O_2 + 2CO_2 \rightarrow 2LiCO_3 + O_2$$

Scheme 1.5

Although C_2mimTFSI had been shown to be unstable to superoxide, due to the highly tuneable nature of ionic liquids it is possible to use alternative cations that are stable. Searching through ionic liquid literature it is easy to find cations that have been identified as being stable to superoxide. One such cation is 1-butyl-1-methylpyrrolidiunium (Pyr_{14}^+).[48]

In 2011 De Giorgio *et al.* looked into the applicability of several pyrrolidinium based ionic liquids, including Pyr_{14}TFSI, for use in Li-O_2 cells.[49] They found that in the absence of lithium ions it was possible to achieve stable oxygen cycling in Pyr_{14}TFSI and $Pyr_{1(2O1)}$TFSI, using cyclic voltammetry.[49] The addition of lithium ions was then shown to give electrochemical results similar to those obtained in other solvents, such as TEGDME, that led to the passivation of the electrode by Li_2O_2.[49] It was also found that the passivation of the electrode surface could be dampened through the use of the additive tris(pentafluorophenyl) borane (TPFPB) which binds to the reduced form of oxygen resulting in an increased solubility of the discharge products.[49]

A further, more detailed, study into some of the ionic liquids looked at by De Giorgio as well as several alternative ionic liquids was published in 2012 by Monaco *et al.*.[50] In this report Monaco *et al.* examined the performance of a range of ionic liquids at both 30 °C and 60 °C. This study revealed that the diffusion coefficient of oxygen in the various ionic liquids decreased as the viscosity of the solvent increased.[50] It was also shown that the concentration of oxygen in the

electrolyte did not vary significantly with temperature, while the diffusion coefficient almost doubled from 30 ˚C to 60 ˚C.[50]

In 2012 Allen *et al*. followed up their previous study in to C_2mimTFSI with a study that also looked into the use of Pyr_{14}TFSI, amongst other solvents, as an electrolyte for Li-O_2 cells.[51] They suggested that the primary discharge product was Li_2O_2 but did not provide any spectroscopic data to support this claim.

More recently Acetonitrile (MeCN) has been used as a solvent in Li-O_2 cells.[52] Although it is not practical for use in a working Li-O_2 cell due to its reactivity with lithium metal, it has previously been shown to be stable to attack by the superoxide anion a result that has been more recently confirmed.[53, 54] It was due to the known stability of MeCN that Peng *et al.* used it for their study.[55] Through the use of *in situ* SERS (surface enhanced Raman scattering) on a Au electrode they identified the formation of both superoxide and peroxide.[55] However due to the instability of lithium metal in contact with the solvent a platinum electrode was used as the counter electrode.

As an alternative to carbonate and ether solvents dimethyl sulfoxide (DMSO) has also been proposed for use in Li-O_2 cells. Similarly to MeCN, DMSO is also unstable when in direct contact with lithium metal but to a lesser extent. The use of DMSO was first investigated by Laoire *et al.* in 2010.[56] In their paper through the interpretation of cyclic voltammetry data they suggested that in DMSO the reduction of oxygen results in lithium peroxide and even lithium oxide (Figure 1.6), as indicated by different oxidation peaks.[56] However Gallant *et al.* suggest that rather than different oxidation peaks being associated with different lithium oxide discharge products they are infact due to the changing morphology of the lithium peroxide discharge product.[57] Similarly to the aforementioned report by Peng *et al.* in MeCN,[55] Laoire *et al.* required the use of platinum as a counter electrode rather than lithium.[56]

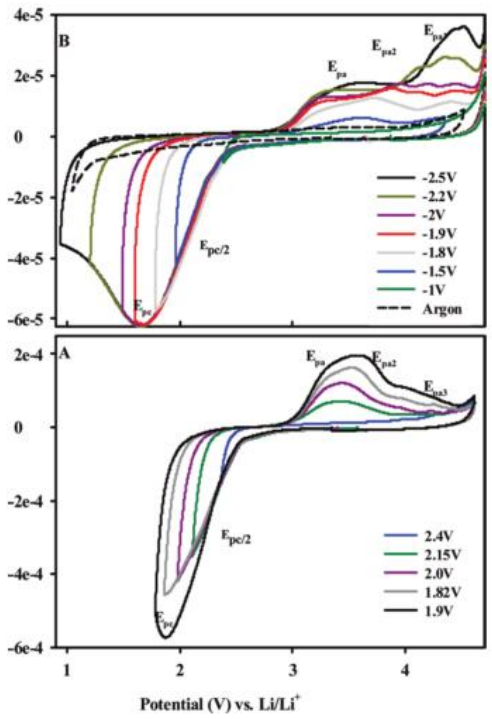

Figure 1.6. Cyclic voltammetry data collected in A) 0.1 M $LiPF_6$, DME and B)0.1 M $LiPF_6$, TEGDME at a glassy carbon working electrode and a scan rate of 100 mV s^{-1}. It was suggested that E_{pa} was due to lithium superoxide oxidation, E_{pa2} was due to lithium peroxide oxidation and E_{pa3} was the result of lithium oxide oxidation. **Reprinted with permission from "C. O. Laoire, S. Mukerjee, K. M. Abraham, E. J. Plichta, and M. A. Hendrickson, *J. Phys. Chem. C*, 114, 9178–9186, (2010)", Copyright 2010 American Chemical Society.**[56]

Following on from this in 2012 D. Xu *et al.* published a report in which it was demonstrated that by using DMSO as an electrolyte high capacities could be achieved.[58] The capacities achieved in DMSO were higher than the capacities that were obtained in TEGDME, this was true for all the current densities they investigated.[58] However, the difference in cell capacities is likely to be a result of the varying viscosities of the solvents.

Through the use of XRD it was also shown that on discharge Li_2O_2 was the primary product, with some LiOH found, presumably due to water incursion into the cell over the period of their experiments.[58] This water incursion may have been through the flexible rubber hosing used to introduce oxygen to the cells.

Crucially they did not identify any discharge products that could have resulted from parasitic reactions between superoxide and DMSO.[58]

Peng *et al.* went on to show that by exposing lithium metal to a solution of 0.1 M $LiClO_4$ in PC for several days an SEI formed on the lithium surface. This SEI allowed the stable cycling of lithium metal in DMSO.[59]

Through the use of FTIR and SERS spectroscopy it was again ascertained that Li_2O_2 was the primary discharge product, with the reversible formation of a small amount of Li_2CO_3.[58] This work represents the first true example of a Li-O_2 cell utilizing DMSO as an electrolyte. Several group have since continued to use DMSO in some of their publications.[60–64]

Sulfones have the same oxidation state as sulfoxides but exhibit lower volatility and better electrochemical stability.[65] It is undoubtedly these properties that have led to research into their use as solvents in Li-O_2 cells.

The electrochemical stability window of tetramethylene sulfoxide (TMS) was found to be greater than that of TEGDME, PC, DMSO and dimethylformamide (DMF).[65] In their report Xu *et al.* used XRD to show that Li_2O_2 was reversibly formed on the carbon cathode during cycling.[65]

Building on this initial investigation into the use of sulfones as electrolyte solvents Bardé *et al*. looked at the use of three different sulfones including TMS.[66] In contradiction to the result presented by Xu *et al.* by analysing charged and discharged electrodes using FTIR, PXRD (powder X-ray diffraction) and ^{1}H NMR they found that Li_2CO_3 was formed as a discharge product.[66] This resulted in capacity fading over several cycles.

It can therefore be concluded that sulfones are not suitable for use as electrolyte solvents in Li-O_2 cells.

DMF has also attracted a small amount of attention as a possible electrolyte solvent for use in Li-O_2 cells. DMF appears to be an attractive solvent due to its

known stability to attack by superoxide.[67] However this report along with others all used tetrabutyl ammonium cation (TBA^+) based salts which are known to stabilise the superoxide anion.[52]

When Chen *et al.* investigated the use of DMF with a Li^+ supporting electrolyte salt Li_2CO_3 was found to form during discharge and resulted in CO_2 being evolved during charge thus ruling out DMF as a possible electrolyte solvent for use in Li-O_2 cells.[68]

In summary it can be said that initial efforts into the realisation of a working Li-O_2 cell, utilising carbonates as the electrolyte solvent, were hampered by the discovery that carbonates are inherently unstable in the presence of superoxide anions that are generated during discharge. This has resulted in a large amount of research in to other non-aqueous solvents.

Out of this research ethers have emerged as being one of the more promising solvents, as long as they are sufficiently pure so as to avoid any degradation reactions. If the purification of solvents is a problem it appears that the use of shorter chain ethers such as DEGDME is preferable over longer chain ethers such as TEGDME.

DMSO also presents some hope if the problem of reactivity with lithium metal can be overcome. Indeed it has been shown that by using carbonate based electrolytes to first create an SEI on lithium metal the reactivity between lithium and DMSO can be eliminated. This method is suitable for CV experiments or galvanostatic experiments of one or two cycles, but during experiments over a greater timescale or with a large number of cycles the SEI would breakdown. Electrolyte additives such as vinylene carbonate (VC) would therefore be required to help replenish the SEI.

The use of ionic liquids has produced mixed results which appear to largely be down to the cation of the ionic liquid. The ionic liquid Pyr_{14}TFSI certainly appears

to show some promise. Due to the tuneable nature of ionic liquids and the sheer number of possible cation and anion combinations it's likely that ionic liquids will play a role in the future of Li-O_2 battery research. Their low vapour pressure is a highly desirable property for a battery that is going to be exposed to its surrounding environment. However as they can only support low current densities their use is likely to be limited.

Recently Xue *et al.* furthered the work of Johnson *et al.*, who looked into the role of electrolyte solvent in non-aqueous lithium-oxygen cells,[69] by developing a comprehensive model of the system to evaluate the role of the solvent.[70] Through the comparison of experimental and simulated results they were able to provide evidence of how changing the donor number of the solvent in a lithium-oxygen cell affects the capacity. Principally solvents with a higher donor number can partially solvate lithium superoxide to a greater extent than solvents with a low donor number.[70] When cycling at low current densities the greater solubility of lithium superoxide in high donor number solvents allows a greater proportion of lithium peroxide formed to escape pores, resulting in less pore blocking and in turn resulting in larger capacities.[70] However, at higher discharge rates the results are less noticeable.[70]

Carbonates			
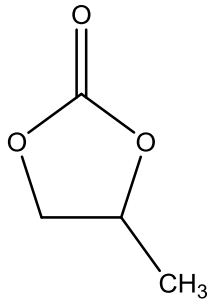		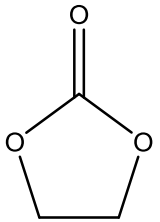	
Propylene Carbonate (PC)		Ethylene Carbonate (EC)	
Ethers			
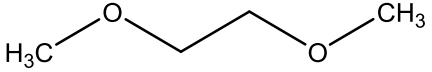	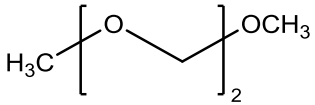	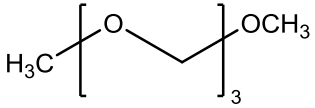	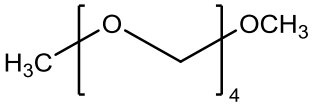
Monoglyme (DME)	Diglyme (DEGDME)	Triglyme	Tetraglyme (TEGDME)
Ionic liquid (Cations)			
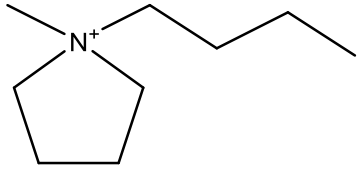	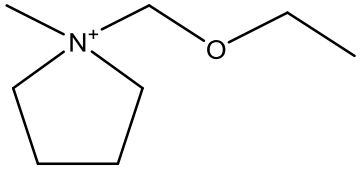	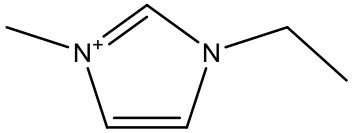	
1-Butly-1-methylpyrrolidinium (Pyr_{14}^{+})	1-methoxyethyl-1-methylpyrrolidinium ($Pyr_{1(2O1)}^{+}$)	1-Ethyl-3-methylimidiazolium (C_2mim^{+})	

Ionic liquid (anion)	
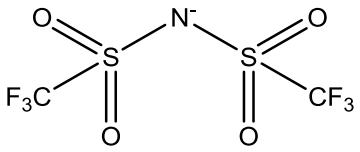	
bis(trifluoromethylsulfonyl)imide (TFSI-)	
Sulfoxides	
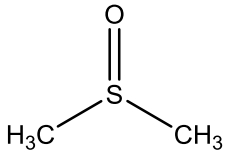	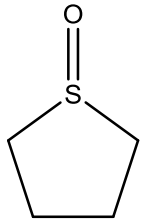
Dimethyl sulfoxide (DMSO)	Tetramethyl sulfoxide (TMS)
Formamide	**Nitrile**
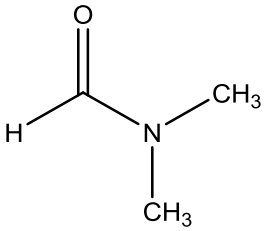	
Dimethyl formamide (DMF)	Acetonitrile (MeCN)

Table 1.2. Structures of solvent molecules commonly used in electrolytes in lithium-oxygen cells

1.6.2 Oxygen Reduction Reaction

Since the realisation that superoxide attacks carbonate based electrolytes in Li-O_2 cells, research into other areas was, to an extent, side lined.[32-35] With the identification of solvents that appear to be more stable to superoxide researchers were then able to focus on other problems that need to be addressed before Li-O_2 cells can be commercialized.

The oxygen reduction reaction (ORR) in a Li-O_2 cell is key to the cells performance. This is due to the fact that the primary discharge product that has been identified, in a cell with a suitable electrolyte, is lithium peroxide.[22] It is the insoluble and insulating nature of lithium peroxide that poses many problems.[71, 72] When first investigating the discharge products found in Li-O_2 cells using Raman spectroscopy Abraham and Jiang identified lithium peroxide as the principal discharge product.[22] Depending on the current density applied they found that the discharge voltage varied from $2.5\,V - 2.0\,V$ on a carbon acetylene black electrode. They calculated a standard potential of $3.10\,V$ for the formation of lithium peroxide, although it is now commonly accepted to be $2.96\,V$.[22, 73] Based on this it is clear that if it is possible to reduce the overpotential of the ORR it would provide greater efficiency within the cell.

To this end Abraham and Jiang investigated the use of an electrode bound, heterogeneous, cobalt catalyst.[22] The results obtained were promising as they showed a reduction in the overpotential of the cell during discharge. The capacity was however limited to $1/16^{th}$ that seen without a catalyst making a true comparison between the results with and without a catalyst difficult.

It is important to point out that it is now know that the primary reactions in cells containing carbonate based electrolytes are degradation reactions. Therefore, a large proportion of the capacity seen by Abraham and Jiang was likely to be due to the formation of lithium carbonate, lithium formate and lithium acetate.[33] The

subsequent determination of the primary discharge product being lithium peroxide may have resulted from the degradation products being removed from the electrode during treatment before *ex situ* Raman spectroscopy was carried out.

The use of heterogeneous catalysts in Li-O_2 research has since become a common occurrence. The use of transition metal oxides as heterogeneous catalysts in lithium-oxygen cells is somewhat unsurprising as they are widely used in Li-ion cells as insertion materials.[9] Their chemistry including redox potentials would have been well known to the battery researchers working on lithium-oxygen cells. Transition metal oxides were first investigated by Read, who incorporated λ-MnO_2 into the carbon electrode of a lithium-oxygen cell.[27] Although this wide ranging study was not focused on the effect of a catalyst it was noted that the plateaus resulting from the λ-MnO_2 disappeared after several cycles (Figure 1.7).[27] A possible explanation for this was that the sites were becoming blocked by discharge product. The product it was promoting was not investigated, and no significant effect on the overpotential on discharge was seen.

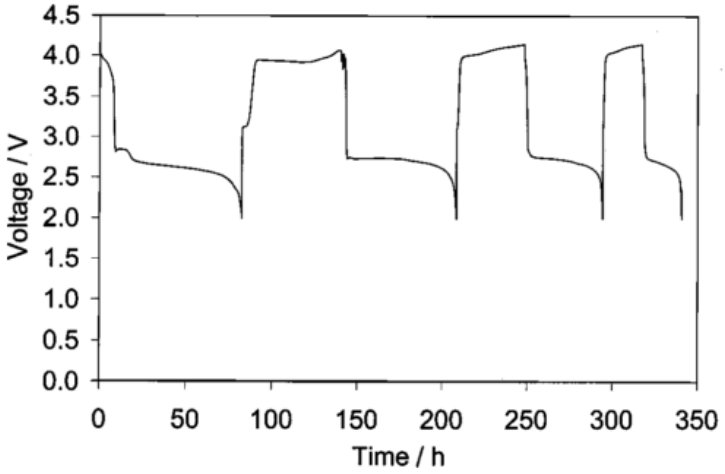

Figure 1.7. Galvanostatic cycling data of λ-MnO_2/carbon cycled in a 1 M $LiPF_6$ PC:DME electrolyte at 0.1 mA·cm^{-2}. The plateau due to λ-MnO_2 (seen between 3.0 – 2.75 V) disappears by the second cycle. **Reprinted with permission from "J. Read, *J. Electrochem. Soc.*, 149, A1190, (2002)". Copyright 2002, The Electrochemical Society.**[27]

The use of manganese dioxide as a catalyst for improving the capacity was then adopted by other researchers.[29, 74, 75] Debart *et al.* found that α-MnO_2 nanowires resulted in the largest capacities on discharge with better capacity retention over several cycles,[76] this is illustrated in Figure 1.8. This was supported by work that showed that MnO_2 of a certain structure could increase oxygen reduction activity, although in both cases these works studied the enhancement seen under aqueous conditions.[77, 78] The work carried out by Debart *et al*. was also carried out in carbonate based solvent,[76] so that although the trend seen undoubtedly holds true, the capacities seen cannot be relied upon. Following on from this work, manganese oxides were investigated primarily for their ability to reduce the overpotential required on charging (see section 1.6.3).

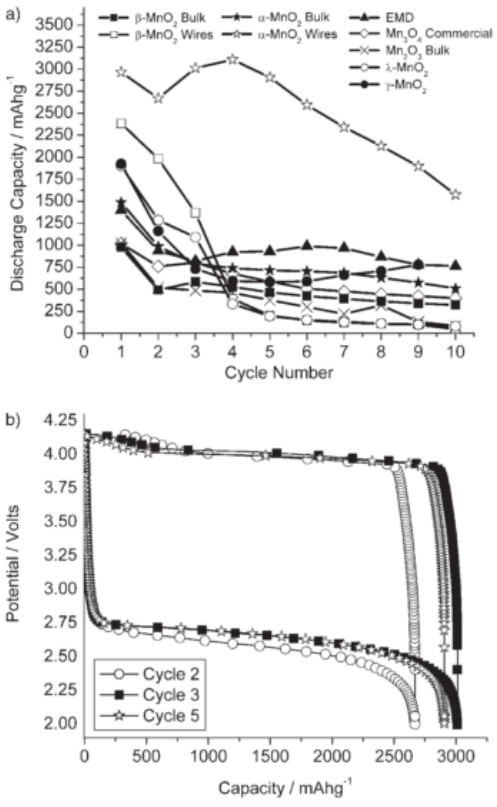

Figure 1.8. a) Discharge capacities with cycle number for various MnO_2 catalysts. **b)** Galvanostatic cycling data for α-MnO_2 cycled at a rate of 70 $mA \cdot g^{-1}$. **[α-MnO2 Nanowires: A Catalyst for the O2 Electrode in Rechargeable Lithium Batteries, Aurélie Débart, Allan J. Paterson, Jianli Bao, Peter G. Bruce, *Angew. Chem. Int. Edit.,* (27) 24. Copyright© 2008, John Wiley and Sons.**[76]

Cobalt oxide has also been the focus of some attention with Sun *et al.* showing better capacity retention over multiple cycles when CoO was incorporated into cathodes.[79] Kim *et al.* then went on to show that by dispersing polydopamine onto CoO particles prior to coating on to a carbon support, the resulting electrodes exhibited a more even distribution of CoO on the electrode surface and resulted in larger capacities.[80] The work of Kim *et al.* was also carried out in TEGDME adding credence to their results.[80]

Of particular interest for the oxygen reduction reaction are macrocyclic compounds containing transition metal ions. This no doubt stemmed from the use of phthalocyanine by Abraham and Jiang.[22] In a similar fashion to that of Abraham and Jiang, Zhang *et al.* investigated the use of electrode bound iron-copper phthalocycanine as a catalyst for the ORR.[81] The use of this catalyst resulted in a decrease in overpotential of the ORR.[81] Yoo *et al.* then furthered this research by developing an understanding of Fe phthalocyanine activity on different high surface area carbons. Their results showed that the activity of Fe phthalocyanine on oxygen reduction in aqueous media was better than that of platinum.[82] However Yoo *et al.* failed to provide evidence of Li_2O_2 production in non-aqeous media, while the work of Zhang *et al.* was carried out in an electrolyte containing carbonates making a true interpretation of their results difficult.[81, 82] Research into macrocyclic catalysts for lithium-oxygen batteries has not been limited to phthalocyanines.

The use of macrocyclic compounds without transition metals was investigated by Selvaraj *et al.*.[84] When investigating Di-lithium phthalocyanine they suggested that the phthalocyanine ring interacted with oxygen aiding the reduction process.[84] Although their work was carried out in carbonate based electrolytes their hypothesis may still hold true, and could be a useful insight for others investigating phthalocyanines.

The use of the metal complex Co phenanthroline was investigated by Wang *et al.*. They reported an increased capacity compared to carbon alone and a slight increase in the discharge potential.[83] However as with other works, the electrolyte used consisted of a mixture of two carbonate based electrolytes, leading to the possibility that the increased capacity was simply due to the catalysed breakdown of the electrolyte.

The inspiration for much of the oxygen reduction catalysts investigated for use in lithium-oxygen cells comes from other areas of energy storage research. In particular inspiration has been drawn from fuel cell work, where in hydrogen fuel cells the 4 e^- reduction of oxygen is desired. Unsurprisingly then a lot of research has focused on the use of noble metals such as gold, palladium, platinum and ruthenium.[85, 86] Lu *et al.* showed gold-platinum nanoparticles were effective catalysts, with gold working to reduce the overpotential of the ORR compared to carbon alone (Figure 1.9).[87]

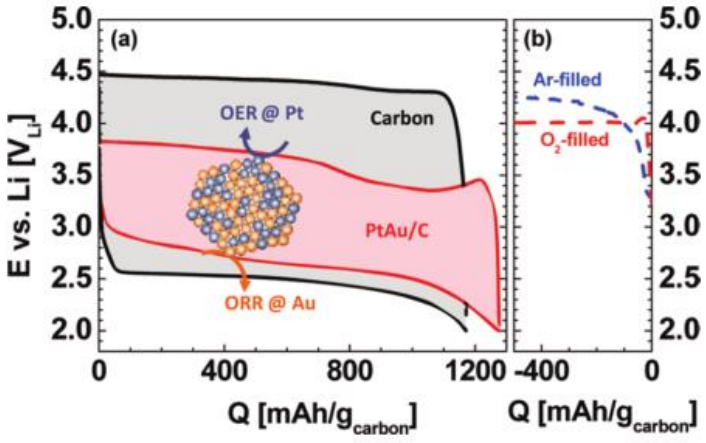

Figure 1.9. Galvanostatic discharge profiles of carbon (black, $85\,mA \cdot g_{carbon}^{-1}$) and PtAu catalysed carbon (red,$100\,mA \cdot g_{carbon}^{-1}$) in oxygen.The use of a catalyst shows a clear reduction of the overpotentials needed on discharge and charge. **Reprinted with permission from "Y.-C. Lu, Z. Xu, H. A. Gasteiger, S. Chen, K. Hamad-Schifferli, and Y. Shao-Horn, *J. Am. Chem. Soc.*, 132, 12170–12171, (2010)". Copyright 2010 American Chemical Society.**[87]

However, McCloskey *et al.* showed that, although platinum did reduce the overpotential on charging in a carbonate based electrolyte, it was catalysing the

oxidation of the degradation products rather than lithium peroxide.[88] In DME gold and manganese did not display any significant catalysis of oxygen reduction.[88] Rather than using expensive metal catalysts several groups have looked at how doping carbon can impact on oxygen reduction. Mi *et al.* doped carbon, in the form of CNTs, with nitrogen and showed an increase in the capacity compared to CNTs alone.[89] Although an ether based electrolyte was investigated stable cycling was not demonstrated.[89]

Yu *et al.* modified graphene with an iron-nitrogen-carbon catalyst. Their results showed an increase in the discharge capacity, but a lower average charging potential.[90] By limiting the capacity they were also able to show stable cycling over 50 cycles, in DMSO, however the cell had to be charged up to $> 4\,V$.[90]

Materials with perovskite structures, particularly but not exclusively those based on lanthanum, have also received attention as possible catalysts in Li-O_2 cells.[91] Meng *et al.* showed that the capacity of cells using $LaFe_{0.5}Mn_{0.5}O_3$ as a catalyst could be increased three fold by doping in a small amount of CeO_2.[92]

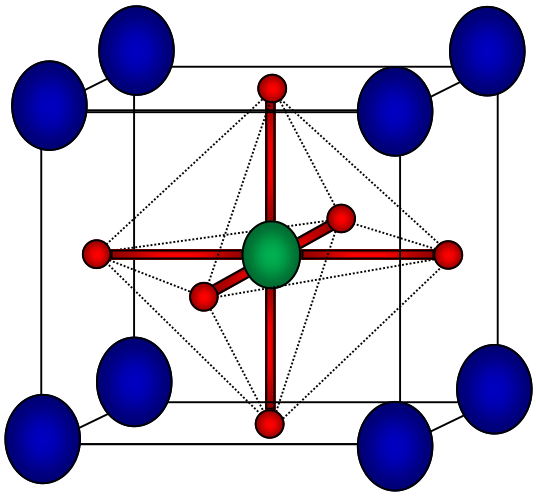

Figure 1.10. A perovskite unit cell where (●) is occupied by one transition metal ion, (●) is occupied by a different transition metal ion and (●) represent oxygen atoms.

Not only have perovskites been shown to be efficient at catalysing the ORR but some have been shown to be effective bifunctional catalysts.[93] In these cases the use of perovskite based materials has been shown to increase cycle life and enhance the round trip efficiency of cells.[94] Due to the wide variety of different compositions of material available some have been developed that appear to only be active during the OER.[95]

The catalysts that have been discussed so far have all been heterogeneous catalysts, that is catalysts that are in a different physical form to the reactants. In the case of the lithium-oxygen battery a heterogeneous catalyst will be solid while the reactant, oxygen, is in the solution phase (or gas phase).

As mentioned previously Read noted that when galvanostatically cycling a cell with manganese oxide in the cathode it was initially possible to discern regions of charge during discharge and charge that related to the oxidation and reduction of manganese oxide. However, after several cycles these regions of the charge and discharge profiles disappeared.[27] It was suggested that this maybe a result of the sites being blocked by lithium peroxide. Although the reason behind this disappearance is likely to be down to a multitude of factors it raises an important point. If the lithium peroxide formed around these electrode bound catalysts cannot be properly oxidised the catalyst site will soon become blocked rendering the catalyst ineffective. As a result of this the use of soluble, or homogeneous, catalysts is becoming an increasingly popular area of research.

As homogeneous catalysts are found in the solution they can move unhindered and therefore lithium peroxide formation can take place in solution rather than at the electrode surface.

The first paper exploring the use of a soluble catalyst for oxygen reduction was published in 2013. It explored the use of ethyl viologen to enhance oxygen reduction.[96] This has since been followed by work that has looked at various

alternative soluble catalysts. Sun *et al.* have explored the use of soluble iron phthalocyanine as a catalyst for both the ORR and the OER.[97] Through the use of this soluble catalyst they were able to show a significant increase in the discharge capacity particularly when in combination with a heterogeneous iron catalyst. Matsuda *et al*. showed similar improvements to the discharge capacity and discharge voltage by including Quinone derivatives in their work.[98]

In a similar vein to the use of soluble redox catalysts the use of electrolyte additives has been promoted as a possible solution to increase capacity. TPFPB has been shown to help solubilise Li_2O_2.[64, 99] This results in an increased capacity as the blocking effect of lithium peroxide on the electrode surface is reduced. However the solubility of peroxide increases as a function of TPFPB concentration, while the solubility of oxygen was found to decrease.[99] Pentafluorophenylboron oxalate (PFPBO) was also found to increase lithium peroxide solubility,[100] however more work needs to be carried out to establish how it affects oxygen concentrations. Perfluorotributyl-amine (FTBA) has also been shown to enhance the rate at which Li-O_2 cells can operate by increasing the oxygen solubility.[101]

Despite the discussion of the need for a catalyst a significant proportion of work has gone into researching catalyst free electrodes. This has obvious advantages with concern to cost and cell mass. The fewer additives required for a functioning cell reduces processing and materials cost. While the absence of heavy transition metal particle will significantly reduce the mass of a cell. This includes work by Meini *et al.* who examined high surface area carbons to determine their effect on cell capacity (Figure 1.11). Unsurprisingly they found that carbons with a larger surface area resulted in larger capacities.[102] However this did not address the problems associated with overpotential when using carbons.

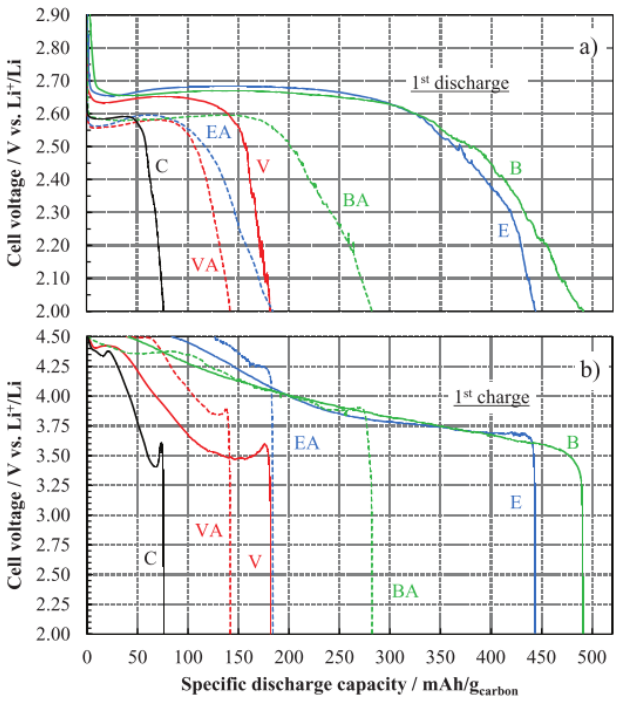

Figure 1.11. Galvanostatic discharge (a) and charge (b) data for various high surface area carbons. An electrolyte of 0.2 M LiTFSI DEGDME was used. The carbon surface area increases in the order C < VA < EA < V < BA < E < B. **Reprinted with permission from "S. Meini, M. Piana, H. Beyer, J. Schwammlein, and H. A. Gasteiger, *J. Electrochem. Soc.*, 159, A2135-A2142, (2012)". Copyright 2012, The Electrochemical Society.**[102]

Zhai *et al.* went further by suggesting that the type of activated carbon used plays an important role in determining the morphology of the discharge product and therefore the overpotential required during charging.[57, 103] While Yoo and Zhou suggest that the large proportion of SP^3 bonding in graphene plays a catalytic role during oxygen reduction, resulting in smaller overpotentials during discharge compared to platinum on carbon.[104]

Whether or not carbon is truly a catalyst of either the ORR or OER the variation in the discharge and charge potential seen on different carbons certainly suggest that if the right carbon can be identified there may not be such a need for expensive catalysts.

It is also worth noting that of the differing approaches discussed here many of them have only been tested in electrolytes that have since been found to be

unstable to oxygen reduction products. There is therefore a wide scope to retest some of these catalysts in more stable electrolyte systems.

1.6.3 Oxygen Evolution Reaction

When considering the charge reaction in a Li-O_2 cell there are two areas that require improvement; complete oxidisation of lithium peroxide and a reduction in the overpotential required on charging. If complete oxidation of the discharge product can be achieved the cycle life of the cell can be vastly improved as well as the capacity retention. While if the overpotential can be reduced this will lead to better round trip efficiencies and help to avoid problems associated with charging to high potentials (*e.g.* electrolyte degradation).

To be able to develop systems that can operate at low overpotentials it is important to first understand what it is that influences the oxidation potentials seen in Li-O_2 cells. The literature on this rather fundamental area was until recently rather sparse. However several recent high profile publications have helped to shed some light on lithium peroxide oxidation.

In 2013 Gallant *et al.* showed that the discharge profiles seen in Li-O_2 cells without a catalyst influence the charge profiles seen during galvanostatic charging.[57] They identified lithium peroxide deposits with a toroidal morphology as being the primary morphology of deposits formed on CNTs (Figure 1.12).[57] This resulted in charge plateaus above $3.4\,V\ vs\ Li^+/Li$. They also demonstrated that small lithium peroxide particles resulted in sloping charge profiles, but with lower average charging potentials than what was seen for toroidal deposits.[57]

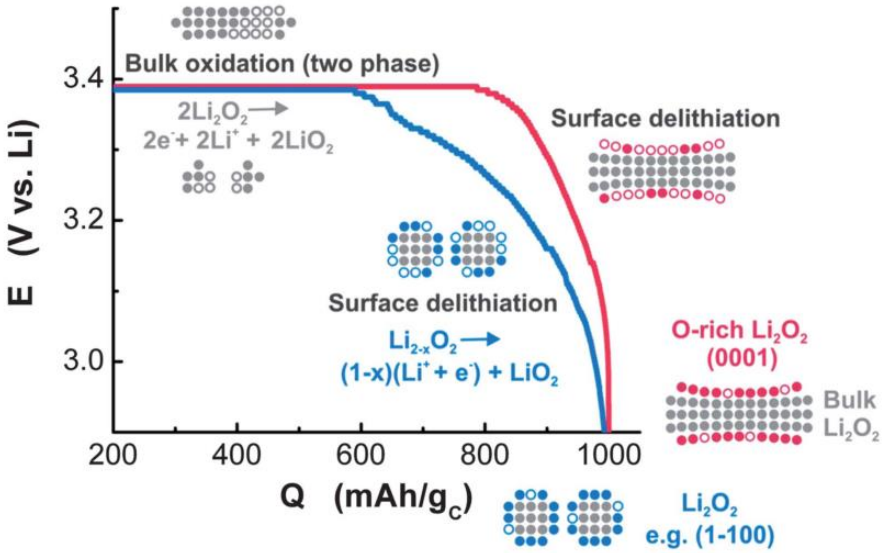

Figure 1.12. Proposed charging process of lithium peroxide in a Li-O_2 cell. **Reproduced from Ref [57] with permission of The Royal Society of Chemistry.**

Schwenke *et al.* then went on to suggest that the shape of the deposit formed is the result of the proton/water concentration in the electrolyte.[105] With the toroidal morphology reported by Gallant *et al.* found to be the result of protons present in the solution. These protons, formed during the oxidation of water at high potentials, were found to be able to solubilise small amounts of lithium peroxide through the formation of hydrogen peroxide according to:[105]

$$2H^+ + Li_2O_2 \rightarrow H_2O_2 + 2Li^+$$

While water present in cells created an equilibrium between lithium peroxide, hydrogen peroxide and lithium hydroxide:[105]

$$2H_2O + Li_2O_2 \rightleftharpoons 2LiOH + H_2O_2$$

Equation 1.8

These reactions therefore enable lithium peroxide deposits to form in areas that are not in direct electrical contact with the electrode surface, when water is present in the cell.

In the absence of protons a uniform layer of lithium peroxide was found on the electrode surface.[105] The charge profile of this uniform layer was found to be similar to the small particles reported by Gallant *et al.*.[57, 105] However the formation of toroids in the absence of proton molecules should not be ruled out if the right hydrodynamic conditions are employed.

Xia *et al.* also furthered the work of Gallant *et al.* by investigating the conductivity of toroid deposits. They found that the outer shell of the toroid structures were lithium deficient affording them a high degree of conductivity and allowing them to be charged at lower overpotentials.[106] The core of the toroid's were found to be formed of insulating bulk lithium peroxide that required higher charging potentials.[106]

This series of work is in contrast to the earlier work of Allen *et al.* in which it had been suggested that the different oxidation processes seen were the result of lithium superoxide oxidation at lower potentials, followed by lithium peroxide oxidation at higher potentials and lithium oxide at potentials above that.[48]

Although it had also been suggested by Gallant *et al.* that the oxidation reaction did proceed *via* lithium superoxide, it is not crystalline lithium superoxide but lithium deficient lithium peroxide.[58]

Around the same time that it was established that the discharge reaction in the presence of carbonate based electrolytes proceeded *via* a series of degradation reactions,[32–35] work by several groups led to the realisation that degradation reactions also occurred during charging.[41, 107]

McCloskey *et al.* and Xu *et al.* published research into the source of CO_2 seen during charging of Li-O_2 cells within quick succession of each other.[41, 107]

McCloskey *et al.* found that lithium carbonates were formed as a result of the reaction between lithium peroxide and the electrolyte (DME in their case) as well as the reaction between lithium peroxide and the carbon electrode.[107] This was in

contrast to what was reported by Xu *et al.* who claimed that the lithium carbonate seen was a direct result of the reaction between lithium peroxide and the electrolyte with very little contribution from reactions with the electrode.[41] In both cases they reported that large overpotentials were required during charging if lithium carbonates were to be removed from the electrode surface.[41, 107]

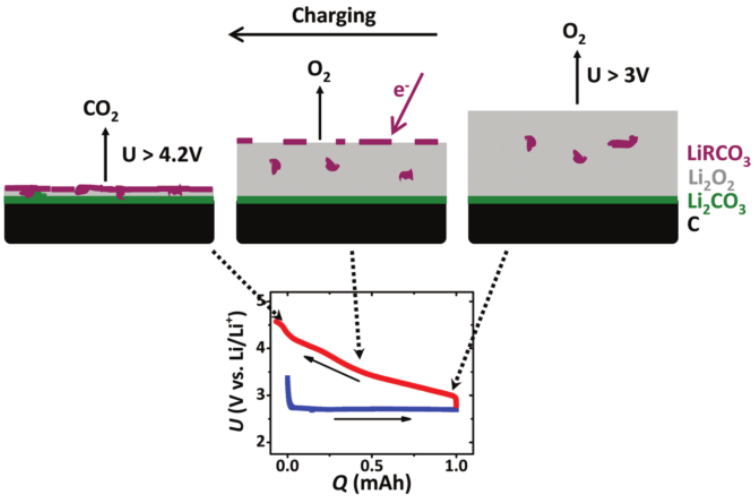

Figure 1.13. Schematic representation of the oxidation of discharge deposits on the positive electrode in a Li-O_2 cell. In this scheme it is suggested that the lithium carbonates present are the result of a reaction with the electrolyte. **Reprinted with permission from "B. D. McCloskey, A. Speidel, R. Scheffler, D. C. Miller, V. Viswanathan, J. S. Hummelshøj, J. K. Nørskov, and A. C. Luntz, *J. Phys. Chem. Lett.*, 3, 997–1001, (2012)". Copyright 2012 American Chemical Society.**[107]

Ottakam Thotiyl *et al.* showed that the decomposition of the electrode was not related to a direct reaction between lithium peroxide and the carbon, i.e. in the absence of a potential biased, as claimed by McCloskey *et al.* but a result of the high potentials used during charging.[108] They reported that carbon decomposition occurred, in the presence of lithium peroxide, above $3.5\,V$.[108]

In agreement with what had already been published, Ottakam Thotiyl *et al.* also found that the biggest contributing factor to lithium carbonate formation was degradation of the electrolyte.[108] It was also found that carbons with a hydrophilic

surface promoted electrolyte breakdown, during charging, to a greater extent than carbons with a hydrophobic surface.[108]

To avoid problems associated with oxidation of the carbon electrode work has gone into developing electrodes based on more stable materials. To this end tin carbide and nanoporous gold electrodes have been proposed as possible alternatives.[62, 109]

Knowledge of the charge process is valuable, particularly when developing catalyst free cells, as control of the discharge product can result in cells with lower over charge potentials. However control of the discharge product may not always be simple, particularly when developing commercially viable batteries. As a result the use of catalysts to assist lithium peroxide oxidation by both reducing overpotentials and promoting complete oxidation of the discharge product is essential.

Abraham and jiang used phthalocyanine molecules as the first heterogeneous catalyst in Li-O_2 cells.[22] They found that the inclusion of a catalyst reduced the overpotential on charging and that when charging a cell at half the current density used during discharge the performance of the cell was improved.[22] Since this initial work on phthalocyanines by Abraham and Jiang they have primarily been investigated for use as catalysts for the ORR.[82, 110]

As mentioned in section 1.6.2 manganese oxides were initially hailed as promising catalyst for Li-O_2 cells. They appeared to increase the capacity during discharge.[76] During the charge reaction manganese oxide was also shown to decrease the overpotential required while at the same time increasing the charge efficiency.[111-113] The promise of manganese oxides was soon put in to question by uncertainties in the reaction pathways followed during discharge.

Ling and Mizuno proposed that when using a MnO_2 catalyst when charging a lithium-oxygen cell the low overpotential seen was due to lithium, from lithium

peroxide, inserting into the MnO_2 matrix reducing the energy required to oxidise the deposit.[114] However, lithium was then not released from the matrix resulting in a change in the shape of the lattice and eventually to a decrease in activity of the material.[114] This suggests that MnO_2 was therefore not actually acting as a catalyst. As a result of this work there are now far fewer studies into the use of MnO_2 as a catalysts in Li-O_2 cells.

Black *et al.* showed that through the use of Co_3O_4 the overpotential on charging could be reduced by approximately $400\,mV$ bringing the average charging potential to below $4.0\,V$.[115] They suggest that this was the result of metal oxides being 'less sticky' than carbon and thus promoting the transport of lithium-oxygen species.[115] However the effectiveness of the catalyst was shown to decrease significantly after several cycles. This result was echoed in the work of Kim *et al.*.[80]

The use of ruthenium oxide as a catalyst for the OER was examined by Jian *et al.* who reported a decrease in the average charging potential of $\sim 900\,mV$.[116] The potential during charging was also seen to not exceed $4.0\,V$ over 20 cycles when limiting the discharge capacity.[116]

As mentioned in section 1.6.2 perovskites have received attention as bifunctional catalysts in Li-O_2 cells. Yang *et al.* first reported their use and showed that they were effective at reducing the overpotential seen on discharge.[93] Similar results were also seen by Jin *et al.*.[94] In both cases the potential was seen to rise above $4.0\,V$ in order for complete oxidation of the discharge product, this suggests that they may not be practical for use in commercial Li-O_2 cells.[93, 94]

Precious metals have received a considerable amount of attention as possible candidates for both the ORR (section 1.6.2) and for the OER. Platinum was first proposed for use as a catalyst for the OER by Yi-Chun Lu *et al*. who found that it considerably reduced the overpotential on charging from above $4.0\,V$ to $\sim 3.6\,V$ on

average.[87] Similar results were seen by McCloskey *et al*. when they looked into the use of platinum.[88] However McCloskey *et al*. showed that this reduction in the overpotential was linked to an increase in the amount of CO_2 given off, suggesting that platinum was in fact catalysing electrolyte breakdown.[88] CO_2 evolution was seen in both carbonate based electrolytes and ether based electrolytes.[88]

Palladium has also been investigated as a possible catalyst for the OER with Thapa *et al.* reporting a decrease in the overpotential of $\sim 200\, mV$ when it was employed within a cell.[111, 117] Reasonable cycling was also reported when limiting the discharge capacity. However as carbonate electrolytes were used during these investigations it is likely that it is the breakdown of the electrolyte that is being catalysed rather than lithium peroxide oxidation.

Although some of the catalysts mentioned so far have shown promise with regards to the oxygen evolution reaction of Li-O_2 cells they have also been shown to have limitations. In particular the insoluble nature of lithium peroxide deposits means that a high coverage of catalyst is required to completely oxidise all deposits. To try and counter this a new trend is emerging with regards to catalysis of lithium peroxide oxidation in Li-O_2 cells, this is the move away from heterogeneous catalysts to homogeneous catalysts. These homogeneous catalysts are catalyst molecules that are dissolved in the electrolyte. The motives behind their use are similar to that of their use in catalysing the ORR. That is that they are able to move in solution and therefore, they can travel to the location of lithium peroxide deposits and oxidise them back to oxygen.

Chen *et al.* first proposed the use of the soluble redox molecule tetrathiafulevene (TTF), as a catalyst for the OER, in 2013.[60] Through the use of this soluble molecule they reported charging potentials of $< 3.6\, V$ at high current densities.[60] They also demonstrated reproducible cycling over 100 cycles, albeit with a limited

discharge capacity. Through the use of DEMS it was shown that the capacity seen on charge (and discharge) related to almost exactly two electrons per di-oxygen molecule over 100 cycles.[60] Combined with the absence of any CO_2 this confirms the successful reduction to and oxidation of lithium peroxide. This represented one of the first instances of a truly reversible Li-O_2 cell.

Since this paper a slew of other soluble catalysts have been proposed. Bergner *et al.* proposed the use of TEMPO (2,2,6,6- tetramethylpiperidinyloxyl).[118] Although their work produced some promising results complete oxidation required charging to $4.0\,V$ and therefore does not represent an improvement on the results reported by Chen *et al.*.[60, 118]

Matsuda *et al.* more recently reported the use of cobalt phthalocyanine complexes as mobile catalysts.[119] A reduction of the charge potential similar to that reported by Chen *et al.* was seen.[60] However they did not demonstrate how this catalyst system fared over multiple cycles.

The use of iodide as a soluble catalyst has also been reported several times.[120–122] Lim *et al.* reported particularly good results where the cell was reported to operate at current of $6000\,mA \cdot g^{-1}$ with an average charge potential $< 3.5\,V$.[121] On top of this the cell was reported to operate for 900 cycles.[121]

Iron Phthalocyanine has also been reported to be an effective bifunctional soluble catalyst.[123] The authors demonstrated a reduction in the discharge potential of the charge process and reasonable cycling behaviour.[123]

As mentioned in section 1.6.1 it was recently suggested by Johnson *et al.* and Xue *et al.* that the nature of the solvent affects the solubility of the lithium superoxide intermediate product.[69, 70] Solvents with high donor numbers were identified as being able to increase the solubility of superoxide, similarly the use of soft acid cations can also increase the solubility of superoxide.[56] This results in systems where the solution phase formation of lithium peroxide is promoted. In systems

such as this and systems that have utilised soluble catalysts of the ORR, soluble catalysts of the OER will be essential as they will be able to reach lithium peroxide deposits that may not have electrical contact with the electrode.

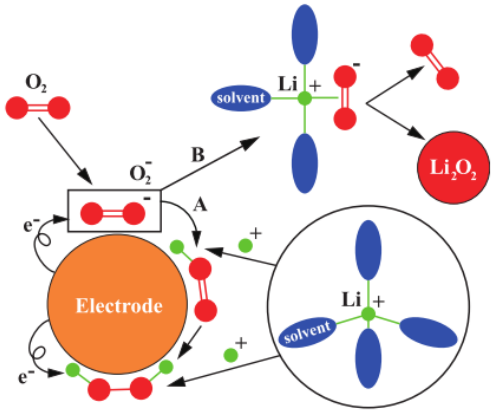

Diagram 1.4. Illustration of the two mechanisms for oxygen reduction in aprotic solvents. In route A, the second reduction occurs at the electrode surface, while in route B, O_2^- is slightly bonded to the lithium ion, which may wander to an existing solid Li_2O_2 core which promotes a disproportionation reaction. **Reprinted with permission from "K. Xue, E. Mcturk, L. Johnson, P. G. Bruce, and A. A. Franco, *J. Electrochem. Soc.*, 162, 614–621, (2015)". Copyright 2015, The Electrochemical Society.**[70]

1.6.4 Oxygen Selective Membranes

The Li-O_2 battery system is often referred to as the Li-Air battery. This implies that the oxygen required for the discharge process is accessed from the air. If Li-O_2 cells are to become commercially viable it would be desirable for this to be the case. If it cannot be achieved the cell would require oxygen from another source such as an oxygen storage tank. This has many drawbacks as it would increase the weight of the system, reducing its specific energy, as well as presenting a potential safety risk.

In an effort to avoid the need for an oxygen storage tank several groups have looked into the use of oxygen selective membranes. An effective membrane must be oxygen permeable while preventing the diffusion of other gasses, particularly

nitrogen and carbon dioxide. They must also prevent the ingression of water and water vapour.

Various approaches have been suggested, Zhang *et al.* proposed the use of silicon oils immobilised in a PTFE membrane.[124, 125] Cells were discharged in air at 20 % relative humidity. Operational discharge times of 16 days and 21 days were achieved however in both cases the cells were not charged and the discharge products were not probed.[124, 125] Further to this the electrolyte solvent used in both cases was EC:PC and as a result it is possible that the capacities seen simply relate to electrolyte breakdown.

J. Zhang *et al.* investigated the use of high density polyethylene (HDPE) and a heat sealable polymer (Melinex®) as separate oxygen selective membranes.[126] It was shown that the cell utilising the Melinex® membrane could operate under ambient conditions for 33 days. However the discharge products were again not investigated, the cell was not recharged and the electrolyte was composed of EC and PC.

The work of D. Zhang *et al.* looked into the use of complex membranes consisting of hydrophobic ionic liquids-silica-PVdF-HFP (polyvinylidene fluoride and hexafluoropropylene respecitvely).[127] Cells using these membranes were shown to work for >10 days and were able to perform three galvanostatic discharge-charge cycles with reasonable capacity retention.[127] Again the electrolyte used was composed of PC and EC and the discharge product was not analysed. However the lithium electrode showed clear signs of water ingression.

Crowther *et al.* developed a membrane from PTFE coated onto a fibreglass cloth.[128] Cells using this membrane operated for 40 days with minimal electrolyte loss. Further to this the lithium metal anode appeared to be less affected by moisture than a control sample without the membrane.[128] This membrane was developed around the idea of a primary cell so the cycle life was not investigated.

These works represent the key experimental efforts to date in the development of suitable membranes for Li-O_2 cells. Although they show some promise a great deal more work is required. In particular the testing of these membranes with stable electrolytes is required. More recent work has looked to model the effect of membranes for Li-O_2 cells,[129] it is hoped that this type of modelling will eventually lead to better membranes for Li-O_2 cells. As it currently stands it appears that there will be a need for oxygen tanks on any Li-O_2 cell that reaches commercial production in the close future.

1.7 Aims

The overall aim of this work is to investigate the lithium-oxygen battery system and identify techniques and methods that can be used to further develop our understanding of the system and improve it. The use of *in situ* Raman spectroscopy will be demonstrated as an efficient method for identifying stable ionic liquids. The electrochemical reduction reactions in two ionic liquids, one of which is known to be unsuitable for use in lithium-oxygen cells and one of which is thought to be stable to the reduction products of oxygen, will be investigated using *in situ* Raman spectroscopy.

The identification of molecules that may act as soluble redox catalysts and the methods for assessing their activity on the ORR and OER will then be explored. The use of soluble redox molecules for catalysing the ORR in lithium oxygen cells promises to increase cell capacity while also helping to specify a specific reaction pathway. The use of soluble redox molecules for catalysing the OER can help to avoid degradation reactions associated with charging to high potentials while also increasing the round trip efficiency of cells.

1.8 References

[1] G. C. Hegerl, F. W. Zwiers, P. Braconnot, N. P. Gillett, Y. Luo, J. A M. Orsini, N. Nicholls, J. E. Penner, and P. A. Stott, *Climate Change: The Physical Science Basis*, IPCC, (2007).

[2] A. J. Appleby, *J. Power Sources*, **53**, 187–197, (1995).

[3] E. Peled, D. Golodnitsky, H. Mazor, M. Goor, and S. Avshalomov, *J. Power Sources*, **196**, 6835–6840, (2011).

[4] D. Linden and T. B. Reddy, *Handbook of Batteries*, 3rd ed. McGraw-Hill, 2002.

[5] C. A. Vincent and B. Scrocati, *Modern Batteries* 2nd ed. J.W.Arrowsmith, 1997.

[6] D. Pletcher, *A First Course in Electrode Processes*, 2nd ed. RSC Publishing, 2009.

[7] M. Wakihara, *Mat. Sci. Eng. R*, **33**. 109–134, (2001).

[8] J. B. Goodenough and K. S. Park, *J. Am. Chem. Soc.*, **135**, 1167–1176, (2013).

[9] J. M. Tarascon and M. Armand, *Nature*, **414**, 359–367, (2001).

[10] A. S. Aricò, P. Bruce, B. Scrosati, J.-M. Tarascon, and W. Van Schalkwijk, *Nat. Mater.*, **4**, 366–377, (2005).

[11] V. Etacheri, R. Marom, R. Elazari, G. Salitra, and D. Aurbach, *Energ. Environ. Sci.*, **4**, 3243–3262, (2011).

[12] B. J. Landi, M. J. Ganter, C. D. Cress, R. A. DiLeo, and R. P. Raffaelle, *Energ. Environ. Sci.*, **2**, 638–654, (2009).

[13] M. Park, X. Zhang, M. Chung, G. B. Less, and A. M. Sastry, *J. Power Sources*, **195**, 7904–7929, (2010).

[14] O. Crowther and A. C. West, *J. Electrochem. Soc.*, **155**, A806, (2008).

[15] D. Aurbach, Y. Talyosef, B. Markovsky, E. Markevich, E. Zinigrad, L. Asraf, J. S. Gnanaraj, and H. J. Kim, *Electrochim. Acta*, **50**, 247–254, (2004).

[16] E. Peled, D. Bar Tow, A. Merson, A. Gladkich, L. Burstein, and D. Golodnitsky, *J. Power Sources*, **97–98**, 52–57, (2001).

[17] B. G. Dixon, R. S. Morris, and S. Dallek, *J. Power Sources*, **138**, 274–276, (2004).

[18] S. S. Zhang, *J. Power Sources*, **162**, 1379–1394, (2006).

[19] P. G. Bruce, S. A. Freunberger, L. J. Hardwick, and J.-M. Tarascon, *Nat. Mater.*, **11**, 19–29, (2011).

[20] E. L. Littauer and K. Tsai, *J. Electrochem. Soc.*, **123**, 771–776, (1976).

[21] E. L. Littauer and K. Tsai, *J. Electrochem. Soc.*, **125**, 521–524, (1980).

[22] K. M. Abraham and Z. Jiang, *J. Electrochem. Soc.*, **143**, 1–5, (1996).

[23] J. Herranz, A. Garsuch, and H. A. Gasteiger, *J. Phys. Chem. C*, **116**, 19084–19094, (2012).

[24] Y. Xu and W. Shelton, *J. Chem. Phys.*, **133**, 024703, (2010).

[25] K. M. Abraham, Z. Jiang, and B. Carroll, *Chem. Mater.*, **9**, 1978–1988, (1997).

[26] J.-M. Tarascon, E. Wang, and F. K. Shokoohi, *J. Electrochem. Soc.*, **138**, 2859–2864, (1991).

[27] J. Read, *J. Electrochem. Soc.*, **149**, A1190–A1195, (2002).

[28] J. Read, K. Mutolo, M. Ervin, W. Behl, J. Wolfenstine, A. Driedger, and D. Foster, *J. Electrochem. Soc.*, **150**, A1351–A1356, (2003).

[29] T. Ogasawara, A. Débart, M. Holzapfel, P. Novák, and P. G. Bruce, *J. Am. Chem. Soc.*, **128**, 1390–1393, (2006).

[30] S. Mohamed, N. Johari, A. Ali, M. Harun, and M. Yahya, *J. Power Sources*, **183**, 351–354, (2008).

[31] B. Kumar, J. Kumar, R. Leese, J. P. Fellner, S. J. Rodrigues, and K. M. Abraham, *J. Electrochem. Soc.*, **157**, A50, (2010).

[32] F. Mizuno, S. Nakanishi, Y. Kotani, S. Yokoishi, and H. Iba, *Electrochemistry*, **78**, 403–405, (2010).

[33] S. A. Freunberger, Y. Chen, Z. Peng, J. M. Griffin, L. J. Hardwick, F. Bardé, P. Novák, and P. G. Bruce, *J. Am. Chem. Soc.*, **133**, 8040–8047, (2011).

[34] B. D. McCloskey, D. S. Bethune, R. M. Shelby, G. Girishkumar, and A. C. Luntz, *J. Phys. Chem. Lett.*, **2**, 1161–1166, (2011).

[35] G. M. Veith, N. J. Dudney, J. Howe, and J. Nanda, *J. Phys. Chem. C*, **115**, 14325–14333, (2011).

[36] J. Lee and M. H. Litt, *Macromolecules*, **33**, 1618–1627, (2000).

[37] J. Read, *J. Electrochem. Soc.*, **153**, A96–A100, (2006).

[38] W. Xu, J. Xiao, J. Zhang, D. Wang, and J.-G. Zhang, *J. Electrochem. Soc.*, **156**, A773–A779, (2009).

[39] W. Xu, J. Xiao, D. Wang, J. Zhang, and J.-G. Zhang, *J. Electrochem. Soc.*, **157**, A219–A224, (2010).

[40] C. O. Laoire, S. Mukerjee, E. J. Plichta, M. A. Hendrickson, and K. M. Abraham, *J. Electrochem. Soc.*, **158**, A302–A308, (2011).

[41] W. Xu, J. Hu, M. H. Engelhard, S. A. Towne, J. S. Hardy, J. Xiao, J. Feng, M. Y. Hu, J. Zhang, F. Ding, M. E. Gross, and J.-G. Zhang, *J. Power Sources*, **215**, 240–247, (2012).

[42] H. Wang and K. Xie, *Electrochim. Acta*, **64**, 29–34, (2012).

[43] R. Black, S. H. Oh, J. Lee, T. Yim, B. Adams, and L. F. Nazar, *J. Am. Chem. Soc.*, **134**, 2902–5, (2012).

[44] K. U. Schwenke, S. Meini, X. Wu, H. A. Gasteiger, and M. Piana, *Phys. Chem. Chem. Phys*, **15**, 11830–11839, (2013).

[45] T. Kuboki, T. Okuyama, T. Ohsaki, and N. Takami, *J. Power Sources*, **146**, 766–769, (2005).

[46] A. W. Lodge, M. J. Lacey, M. Fitt, N. Garcia-Araez, and J. R. Owen, *Electrochim. Acta*, **140**, 168–173, (2014).

[47] Y. Katayama, H. Onodera, M. Yamagata, and T. Miura, *J. Electrochem. Soc.*, **151**, A59–A63, (2004).

[48] C. J. Allen, S. Mukerjee, E. J. Plichta, M. A. Hendrickson, and K. M. Abraham, *J. Phys. Chem. Lett.*, **2**, 2420–2424, (2011).

[49] F. De Giorgio, F. Soavi, and M. Mastragostino, *Electrochem. Commun.*, **13**, 1090–1093, (2011).

[50] S. Monaco, A. M. Arangio, F. Soavi, M. Mastragostino, E. Paillard, and S. Passerini, *Electrochim. Acta*, **83**, 94–104, (2012).

[51] C. J. Allen, J. Hwang, R. Kautz, S. Mukerjee, E. J. Plichta, M. A. Hendrickson, and K. M. Abraham, *J. Phys. Chem. C*, **116**, 20755–20764, (2012).

[52] C. O. Laoire, S. Mukerjee, K. M. Abraham, E. J. Plichta, and M. A. Hendrickson, *J. Phys. Chem. C*, **113**, 20127–20134, (2009).

[53] M. C. Buzzeo, O. V Klymenko, J. D. Wadhawan, C. Hardacre, K. R. Seddon, and R. G. Compton, *J. Phys. Chem. A*, **107**, 8872–8878, (2003).

[54] V. S. Bryantsev, J. Uddin, V. Giordani, W. Walker, D. Addison, and G. V Chase, *J. Electrochem. Soc.*, **160**, A160–A171, (2012).

[55] Z. Peng, S. A. Freunberger, L. J. Hardwick, Y. Chen, V. Giordani, F. Bardé, P. Novák, D. Graham, J. Tarascon, and P. G. Bruce, *Angew. Chem. Int. Ed.*, **50**, 6351–6355 (2011).

[56] C. O. Laoire, S. Mukerjee, K. M. Abraham, E. J. Plichta, and M. A. Hendrickson, *J. Phys. Chem. C*, **114**, 9178–9186, (2010).

[57] B. M. Gallant, D. G. Kwabi, R. R. Mitchell, J. Zhou, C. V. Thompson, and Y. Shao-Horn, *Energ. Environ. Sci.*, **6**, 2518–2528, (2013).

[58] D. Xu, Z. Wang, J. Xu, L. Zhang, and X. Zhang, *Chem. Commun.*, **48**, 6948–50, (2012).

[59] Z. Peng, S. A. Freunberger, Y. Chen, and P. G. Bruce, *Science*, **337**, 563–566, (2012).

[60] Y. Chen, S. A. Freunberger, Z. Peng, O. Fontaine, and P. G. Bruce, *Nat. Chem.*, **5**, 489–494, (2013).

[61] C. Li, O. Fontaine, S. A. Freunberger, L. Johnson, S. Grugeon, S. Laruelle, P. G. Bruce, and M. Armand, *J. Phys. Chem. C*, **118**, 3393–3401, (2014).

[62] M. M. Ottakam Thotiyl, S. A. Freunberger, Z. Peng, Y. Chen, Z. Liu, and P. G. Bruce, *Nat. Mater.*, **12**, 1050–6, (2013).

[63] Y. Shao, S. Park, J. Xiao, J. Zhang, Y. Wang, and J. Liu, *ACS Catal.*, **2**, 844–857, (2012).

[64] D. Zheng, Q. Wang, H.-S. Lee, X.-Q. Yang, and D. Qu, *Chemistry*, **19**, 8679–8683, (2013).

[65] D. Xu, Z. Wang, J. Xu, L. Zhang, L. Wang, and X. Zhang, *Chem. Commun. (Camb).*, **48**, 11674–6, (2012).

[66] F. Bardé, Y. Chen, L. Johnson, S. Schaltin, J. Fransaer, and P. G. Bruce, *J. Phys. Chem. C*, **118**, 18892–18898, (2014).

[67] D. Vasudevan and H. Wendt, *J. Electroanal. Chem.*, **192**, 69–74, (1995).

[68] Y. Chen, S. A. Freunberger, Z. Peng, F. Bardé, and P. G. Bruce, *J. Am. Chem. Soc.*, **134**, 7952–7, (2012).

[69] L. Johnson, C. Li, Z. Liu, Y. Chen, S. A. Freunberger, P. C. Ashok, B. B. Praveen, K. Dholakia, J.-M. Tarascon, and P. G. Bruce, *Nat. Chem.*, **6**, 1091–1099, (2014).

[70] K. Xue, E. Mcturk, L. Johnson, P. G. Bruce, and A. A. Franco, *J. Electrochem. Soc.*, **162**, 614–621, (2015).

[71] M. D. Radin, J. F. Rodriguez, F. Tian, and D. J. Siegel, *J. Am. Chem. Soc.*, **134**, 1093–103, (2012).

[72] V. Viswanathan, K. S. Thygesen, J. S. Hummelshøj, J. K. Nørskov, G. Girishkumar, B. D. McCloskey, A. C. Luntz, J. S. Hummelshøj, and J. K. Nørskov, *J. Chem. Phys.*, **135**, 214704 1–10, (2011).

[73] B. M. Gallant, D. G. Kwabi, R. R. Mitchell, J. Zhou, C. V Thompson, and Y. Shao-Horn, *Energ. Environ. Sci.*, **6**, 2518–2528, (2013).

[74] J. Luo, J. Zhang, and Y. Xia, *Chem. Mater.*, **18**, 5618–5623, (2006).

[75] A. Débart, J. Bao, G. Armstrong, and P. G. Bruce, *J. Power Sources*, **174**, 1177–1182, (2007).

[76] A. Débart, A. J. Paterson, J. Bao, and P. G. Bruce, *Angew. Chemie - Int. Ed.*, **47**, 4521–4524, (2008).

[77] W. Xiao, D. Wang, and X. W. Lou, *J. Phys. Chem. C*, **114**, 1694–1700, (2010).

[78] R. S. Kalubarme, M.-S. Cho, K.-S. Yun, T.-S. Kim, and C.-J. Park, *Nanotechnology*, **22**, 395402, (2011).

[79] B. Sun, H. Liu, P. Munroe, H. Ahn, and G. Wang, *Nano Res.*, **5**, 460–469, (2012).

[80] D. S. Kim and Y. J. Park, *J. Alloys Compd.*, **575**, 319–325, (2013).

[81] S. S. Zhang, X. Ren, and J. Read, *Electrochim. Acta*, **56**, 4544–4548, (2011).

[82] E. Yoo and H. Zhou, *J. Power Sources*, **244**, 429–434, (2013).

[83] H. Wang, X. Liao, Q. Jiang, X. Yang, Y. He, and Z. Ma, *Chinese Sci. Bull.*, **57**, 1959–1963, (2012).

[84] C. Selvaraj, N. Munichandraiah, and L. G. Scanlon, *J. Porphyr. Phthalocya.*, **16**, 255–259, (2012).

[85] H. Cheng and K. Scott, *Appl. catal. B-Environ.*, **108–109**, 140–151, (2011).

[86] J. Chen, J. S. Hummelshøj, K. S. Thygesen, J. S. G. Myrdal, J. K. Nørskov, and T. Vegge, *Catal. Today*, **165**, 2–9, (2011).

[87] Y.-C. Lu, Z. Xu, H. A. Gasteiger, S. Chen, K. Hamad-Schifferli, and Y. Shao-Horn, *J. Am. Chem. Soc.*, **132**, 12170–12171, (2010).

[88] B. D. McCloskey, R. Scheffler, A. Speidel, D. S. Bethune, R. M. Shelby, and A. C. Luntz, *J. Am. Chem. Soc.*, **133**, 18038–41, (2011).

[89] R. Mi, H. Liu, H. Wang, K. Wong, J. Mei, and Y. Chen, *Carbon N. Y.*, **67**, 744–752, (2013).

[90] L. Yu, Y. Shen, and Y. Huang, *J. Alloys Compd.*, **595**, 185–191, (2014).

[91] C. Jin, X. Cao, L. Zhang, C. Zhang, and R. Yang, *J. Power Sources*, **241**, 225–230, (2013).

[92] T. Meng, M. Ara, L. Wang, R. Naik, and K. Y. S. Ng, *J. Mater. Sci.*, **49**, 4058–4066, (2014).

[93] W. Yang, J. Salim, S. Li, C. Sun, L. Chen, J. B. Goodenough, and Y. Kim, *J. Mater. Chem.*, **22**, 18902–18907, (2012).

[94] J. J. Xu, D. Xu, Z. L. Wang, H. G. Wang, L. L. Zhang, and X. B. Zhang, *Angew. Chemie - Int. Ed.*, **52**, 3887–3890, (2013).

[95] K.-N. Jung, J.-I. Lee, W. Bin Im, S. Yoon, K.-H. Shin, and J.-W. Lee, *Chem. Commun.*, **48**, 9406–9408, (2012).

[96] M. J. Lacey, J. T. Frith, and J. R. Owen, *Electrochem. Commun.*, **26**, 74–76, (2013).

[97] D. Sun, Y. Shen, W. Zhang, L. Yu, Z. Yi, W. Yin, D. Wang, Y. Huang, J. Wang, D. Wang, and J. B. Goodenough, *J. Am. Chem. Soc.*, **136**, 8941–6 (2014).

[98] S. Matsuda, K. Hashimoto, and S. Nakanishi, *J. Phys. Chem. C*, **118**, 18397–18400, (2014).

[99] J. Xiao, W. Xu, D. Wang, and J. J.-G. Zhang, *J. Electrochem. Soc.*, **157**, A219–A224, (2010).

[100] L. F. Li, H. S. Lee, H. Li, X. Q. Yang, and X. J. Huang, *Electrochem. Commun.*, **11**, 2296–2299, (2009).

[101] Y. Wang, D. Zheng, X.-Q. Yang, and D. Qu, *Energ. Environ. Sci.*, **4**, 3697–3702, (2011).

[102] S. Meini, M. Piana, H. Beyer, J. Schwammlein, and H. A. Gasteiger, *J. Electrochem. Soc.*, **159**, A2135–A2142, (2012).

[103] D. Zhai, H.-H. Wang, J. Yang, K. C. Lau, K. Li, K. Amine, and L. A. Curtiss, *J. Am. Chem. Soc.*, **135**, 15364–72, (2013).

[104] E. Yoo and H. Zhou, *ACS Nano*, **5**, 3020–3026, (2011).

[105] K. U. Schwenke, M. Metzger, T. Restle, M. Piana, and H. A. Gasteiger, *J. Electrochem. Soc.*, **162**, A573–A584 (2015).

[106] C. Xia, M. Waletzko, L. Chen, K. Peppler, P. J. Klar, and J. Janek, *ACS Appl. Mater. Interfaces*, **6**, 12083–12092 (2014).

[107] B. D. McCloskey, A. Speidel, R. Scheffler, D. C. Miller, V. Viswanathan, J. S. Hummelshøj, J. K. Nørskov, and A. C. Luntz, *J. Phys. Chem. Lett.*, **3**, 997–1001, (2012).

[108] M. M. Ottakam Thotiyl, S. A. Freunberger, Z. Peng, and P. G. Bruce, *J. Am. Chem. Soc.*, **135**, 494–500 (2013).

[109] Z. Peng, S. A. Freunberger, Y. Chen, and P. G. Bruce, *Science*, **337**, 563–6, (2012).

[110] S. S. Zhang, X. Ren, and J. Read, *Electrochim. Acta*, **56**, 4544–4548, (2011).

[111] A. K. Thapa and T. Ishihara, *J. Power Sources*, **196**, 7016–7020, (2011).

[112] G. Q. Zhang, J. P. Zheng, R. Liang, C. Zhang, B. Wang, M. Au, M. Hendrickson, and E. J. Plichta, *J. Electrochem. Soc.*, **158**, A822–A827, (2011).

[113] J. Li, N. Wang, Y. Zhao, Y. Ding, and L. Guan, *Electrochem. Commun.*, **13**, 698–700, (2011).

[114] C. Ling and F. Mizuno, *Chem. Mater.*, **24**, 3943–3951, (2012).

[115] R. Black, J.-H. Lee, B. Adams, C. A. Mims, and L. F. Nazar, *Angew. Chem. Int. Ed. Engl.*, **52**, 392–6, (2013).

[116] Z. Jian, P. Liu, F. Li, P. He, X. Guo, M. Chen, and H. Zhou, *Angew. Chem. Int. Ed.*, **53**, 442–446, (2014).

[117] A. K. Thapa, T. H. Shin, S. Ida, G. U. Sumanasekera, M. K. Sunkara, and T. Ishihara, *J. Power Sources*, **220**, 211–216, (2012).

[118] B. J. Bergner, A. Schürmann, K. Peppler, A. Garsuch, and J. Janek, *J. Am. Chem. Soc.*, **136**, 15054–15064, (2014).

[119] S. Matsuda, S. Mori, K. Hashimoto, and S. Nakanishi, *J. Phys. Chem. C*, **118**, 28435–28439, (2014).

[120] D. S. Kim and Y. J. Park, *J. Alloys Compd.*, **591**, 164–169, (2014).

[121] H. Lim, H. Song, J. Kim, H. Gwon, Y. Bae, K. Park, J. Hong, H. Kim, T. Kim, Y. H. Kim, X. Lepró, R. Ovalle-Robles, R. H. Baughman, and K. Kang, *Angew. Chem. Int. Ed. Engl.*, **53**, 3926–31, (2014).

[122] T. H. Yoon and Y. J. Park, *RSC Adv.*, **4**, 17434–17442, (2014).

[123] D. Sun, Y. Shen, W. Zhang, L. Yu, Z. Yi, W. Yin, D. Wang, Y. Huang, J. Wang, D. Wang, and J. B. Goodenough, *J. Am. Chem. Soc.*, **136**, 8941–6, (2014).

[124] J. Zhang, W. Xu, and W. Liu, *J. Power Sources*, **195**, 7438–7444, (2010).

[125] J. Zhang, W. Xu, X. Li, and W. Liu, *J. Electrochem. Soc.*, **157**, A940–A946, (2010).

[126] J.-G. Zhang, D. Wang, W. Xu, J. Xiao, and R. E. Williford, *J. Power Sources*, **195**, 4332–4337, (2010).

[127] D. Zhang, R. Li, T. Huang, and A. Yu, *J. Power Sources*, **195**, 1202–1206, (2010).

[128] O. Crowther, D. Keeny, D. M. Moureau, B. Meyer, M. Salomon, and M. Hendrickson, *J. Power Sources*, **202**, 347–351, (2012).

[129] U. Sahapatsombut, H. Cheng, and K. Scott, *J. Power Sources*, **249**, 418–430, (2014).

Chapter 2 : Experimental Procedures & Techniques

This chapter discusses the methods and techniques, which have been used across several chapters, for the preparation of materials and cells and their analysis. Preparation of materials and techniques that are specific to a particular chapter are discussed in the experimental section of those chapters.

2.1 Solvent and Electrolyte Preparation

The ionic liquids 1-ethyl-3-methylimidazolium bis(trifluoromethylsulfonyl)imide (C_2mimTFSI, IoLiTec, $99\ \%$) and 1-butly-1-methylpyrrolidinium bis(trifluoromethylsulfonyl)imide (Pyr_{14}TFSI, IoLiTec, $99.5\ \%$) were dried under vacuum at $120\ ^{\circ}C$ for a minimum of $24\ h$, with longer times used when drying quantities greater than 100 *ml*. After drying the water content of the electrolyte was found to be $< 10\ ppm$.

Diglyme (anhydrous, $99.5\ \%$, Sigma-Aldrich) was dried further using dry $3\ Å$ molecular sieves (beads, $4-8$ mesh, Sigma-Aldrich) the water content of the dried solvent was found to be between $10-15\ ppm$. As received molecular sieves were dried by heating at $120\ ^{\circ}C$ under vacuum for $48\ h$.

The lithium salt lithium bis(trifluoromethylsulfonyl)imide (LiTFSI, Sigma-Aldrich, $99.95\ \%$) was dried under vacuum at $120\ ^{\circ}C$ for $48\ h$. Following on from drying the reagents were stored in a dry argon filled glovebox ($<\ 10$ *ppm* O_2, $<\ 10$ *ppm* H_2O, mBraun).

Electrolyte solutions were prepared in a dry argon filled glovebox ($<\ 10$ *ppm* O_2, $<\ 10$ *ppm* H_2O, mBraun) by dissolving an appropriate mass of lithium salt into the desired solvent. Electrolytes were prepared when needed to avoid any contamination that could occur from storage over a long period of time.

The water content of solvents was investigated *via* Karl-Fischer (KF) titrations using a Metrohm 831 KF coulometer. Karl-Fischer titrations determine the quantity of water in a solvent by electrochemically generating iodine from iodide.

The iodine then goes on to react with water (Scheme 2.1). When all the water present in the sample has been consumed the concentration of iodine in the electrolyte increases, this is monitored by an indicator electrode and represents the end point of the titration. The charge passed to convert iodide to iodine, up until the end point, can then be directly correlated to the quantity of water present in the sample.

$$I_2 + SO_2 + H_2O + CH_3OH \rightarrow 2HI + HSO_4CH_3$$

Scheme 2.1

2.2 Cell Construction

2.2.1 Two Compartment Glass 'U' Cells

In general cyclic voltammetry experiments were carried out in a two compartment glass 'U' cell. This allowed separation of the working electrode and electrolyte from the counter/reference electrode and electrolyte. The working electrode consisted of a 3 *mm* diameter glassy carbon rod (Alfa-Aesar) encased in glass resulting in a 3 *mm* diameter glassy carbon disk electrode. The counter/reference electrode was lithium metal (Lithium foil battery grade, Rockwood lithium) mechanically stamped onto a stainless steel mesh. When placed in the cell only lithium extending below the stainless steel mesh was immersed in the electrolyte. Cells were built under an argon atmosphere allowing measurements to be recorded in argon without purging the cell. To carry out measurements under an oxygen atmosphere the cell was bubbled with oxygen (BOC) for 40 *mins* at a flow rate of 50 $ml \cdot min^{-1}$ and a pressure of 1.5 atmospheres. In an effort to ensure the gas was dry before entering cells it was first flown over 3 *Å* molecular sieves

(beads, $4-8$ mesh, Sigma-Aldrich) and silica gel indicating beads (Fisher scientific).

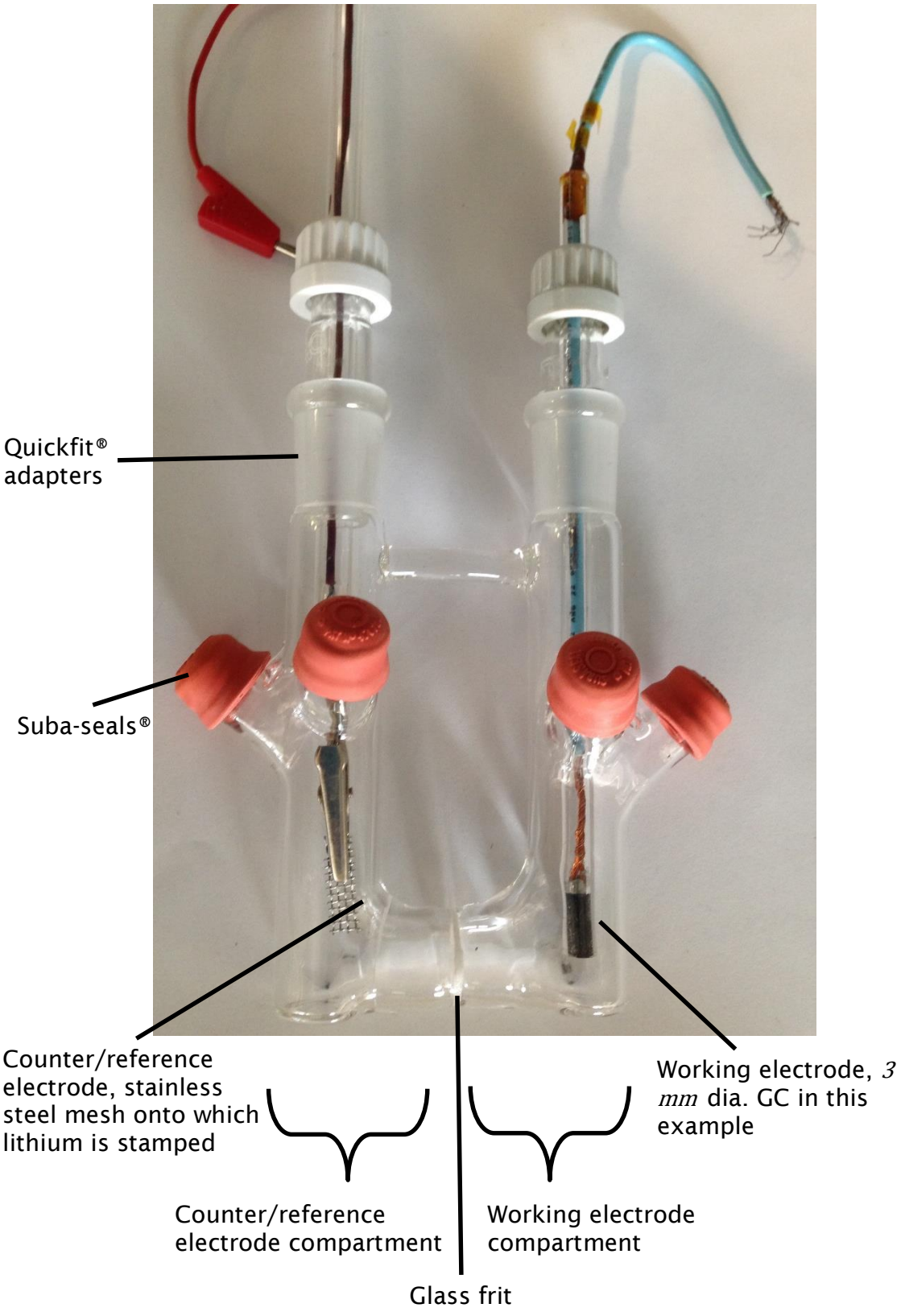

Diagram 2.1. Two compartment glass 'U' cell

2.2.2 Swagelok Cells utilising a Stacked Cell Geometry

To carry out galvanostatic cycling in cells with a stacked geometry Swagelok style cells were designed that allowed cells to be purged with oxygen (Diagram 2.2). The cell design consisted of a lithium metal anode separated from a CNT working electrode by an Ohara glass separator (Ohara inc, $1''$ Ø). The lithium electrode was a $24\ mm$ Ø lithium disk (Lithium foil battery grade, Rockwood lithium), this was separated from the Ohara glass by a $1''$ Ø Celguard separator (Celgard M824) that was wetted with $17\ \mu L$ of a specified electrolyte. The electrolyte on the lithium anode side of the cell only ever consisted of a lithium salt and solvent *i.e.* no soluble redox molecule was added. The inside of the stainless steel Swagelok® cell was kept electronically isolated from the cell stack by an insulating sheet of FEP (fluorinated ethylene propylene, $0.127\ mm$ thick, RS components).

The working electrode consisted of a CNT ink applied to Celgard M824 *via* Mayer-rod coating. The ink was prepared by mixing acid treated CNTs (Fullerene CNTs, multi-walled $95\ \%$, Alfa-Aesar) with PVdF (Solvay Solexis LTD) in the ratio $0.66/0.33$. NMP (1-methyl-2-pyrrolidone, anhydrous, $99.5\ \%$, Sigma-Aldrich) was then added and the solution homogenised, using an IKA digital ultra TURRAX, at $20{,}000$ rpm for 15 minutes. $13\ mm$ Ø disks were cut and dried under vacuum at room temperature for $48\ hr$ prior to cell assembly. The carbon loading of the electrodes was $0.20\ mg \cdot cm^2\ \pm 0.05\ mg \cdot cm^2$ The CNT working electrode was separated from the Ohara glass by two Celgard separators. $17\ \mu L$ of electrolyte was then added on top of the two Celgard seperators and a further $17\ \mu L$ of electrolyte was added on top of the CNT working electrode. The electrolyte on the working electrode side of the Ohara glass consisted of lithium salt a solvent and a soluble redox molecule when appropriate.

Cells were constructed under an argon atmosphere allowing measurements in argon to be carried out without gas purging. To oxygenate cells, cells were first

attached to a gas line *via* Swagelok connections. While the valves connected to the cell remained closed the gas line was put under vacuum for 10 minutes to remove any residual water vapour. Oxygen (BOC), at $1.1\ atm$, was then allowed into the system and the cell. Oxygen was flown through the cell for $30\ s$, the cell was then left to rest for $30\ minutes$ before cycling.

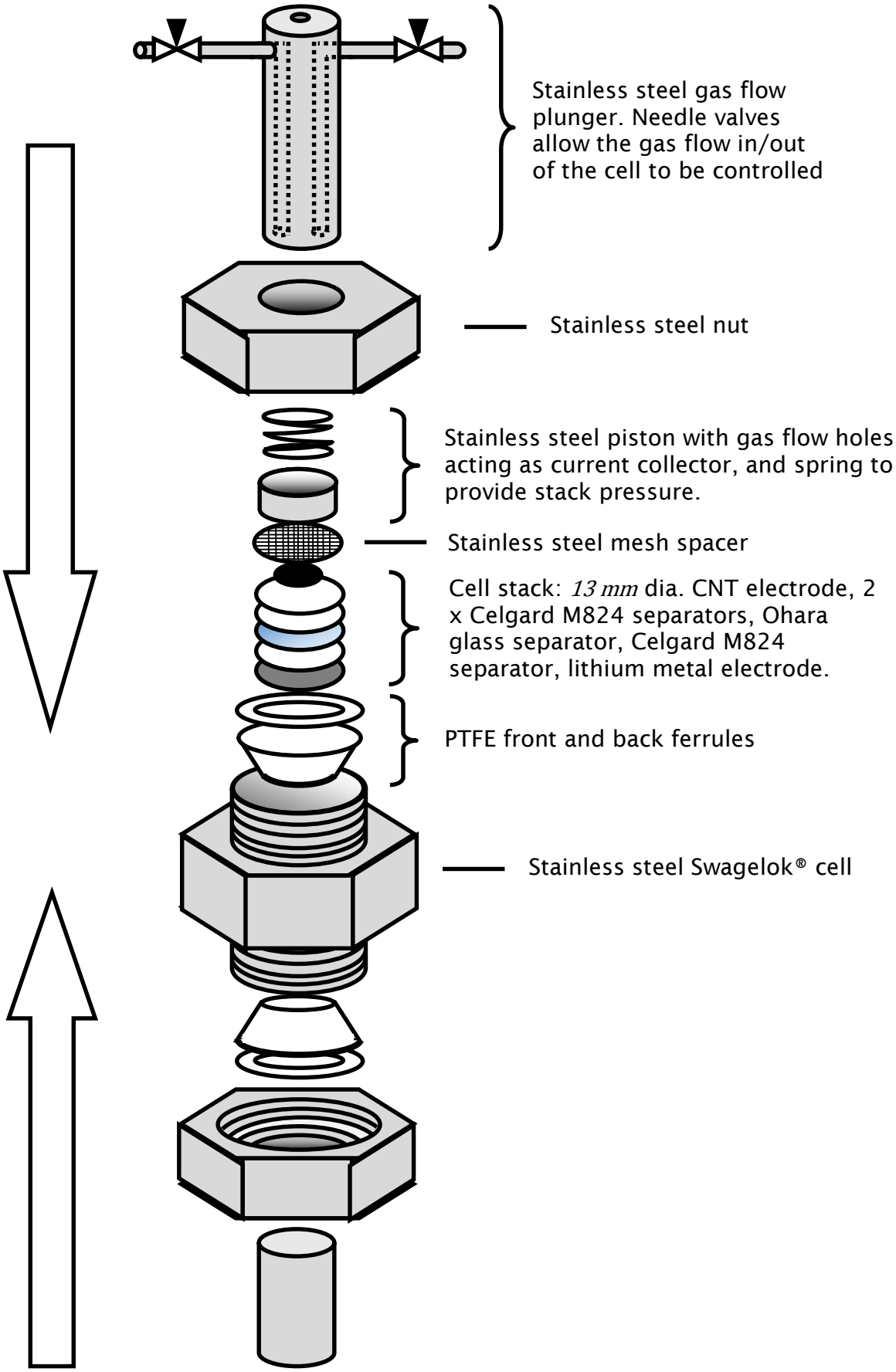

Diagram 2.2. Stainless steel Swagelok® cell for Li-O_2 cell testing. The design allows the cell to be oxygenated.

2.3 Electrochemical Techniques

Unless otherwise specified electrochemical techniques were carried out using a Bio-Logic variable multichannel potentiostat (VMP2). Potentiostats commonly operate using a three electrode connection setup; a working electrode, a counter electrode and a reference electrode.

The working electrode is the electrode under investigation in the system, changes to the potential are applied and recorded at this electrode. While the counter electrode is there to complete the circuit undergoing electrochemical reactions as required to balance the flow of charge at the working electrode. The current flow between the working and counter electrodes can be controlled or monitored depending on the process under investigation. The reference electrode, in an ideal system, does not undergo an electrochemical reaction. Instead it should be poised at the equilibrium potential of a redox couple to provide a stable reference. The potential that is applied or measured at the working electrode is done so with regards to the reference electrode.

2.3.1 Cyclic Voltammetry

Cyclic voltammetry is a commonly used and versatile electrochemical technique that allows the investigation of many electrochemical systems, and in particular irreversible and reversible (Nernstian) redox reactions. During cyclic voltammetry experiments the potential of the working electrode is changed linearly with time (Figure 2.1) between two potential limits. The current flowing through the system is measured and is then plotted *vs* the potential. The rate at which the potential is changed is known as the scan rate and has units of $mV \cdot s^{-1}$. There are several factors which can affect the flow of current through the system; the thermodynamic conditions, the kinetics of the system, and the mass transport properties of the species under investigation and its reaction products.

The potential of a system with equal concentrations of the oxidised form and reduced form of a species would therefore sit at the standard potential. If the potential at the electrode surface is changed, for an electrochemically reversible reaction, the concentration of each species should change according to the Nernst equation:

$$E = E^o + \frac{2.3RT}{nF} log \frac{c_o}{c_r}$$

Equation 2.1. Nernst equation

Where:

E = Potential (V)

E^o = Standard reaction potential ($V\ vs\ Ref$)

R = Gas constant ($8.314\ J \cdot K^{-1} mol^{-1}$)

T = Temperature (K)

n = number of electrons involved in the reaction

F = Faradays constant ($96485\ C \cdot mol^{-1}$)

c = concentration of oxidised or reduced species ($mol \cdot l^{-1}$)

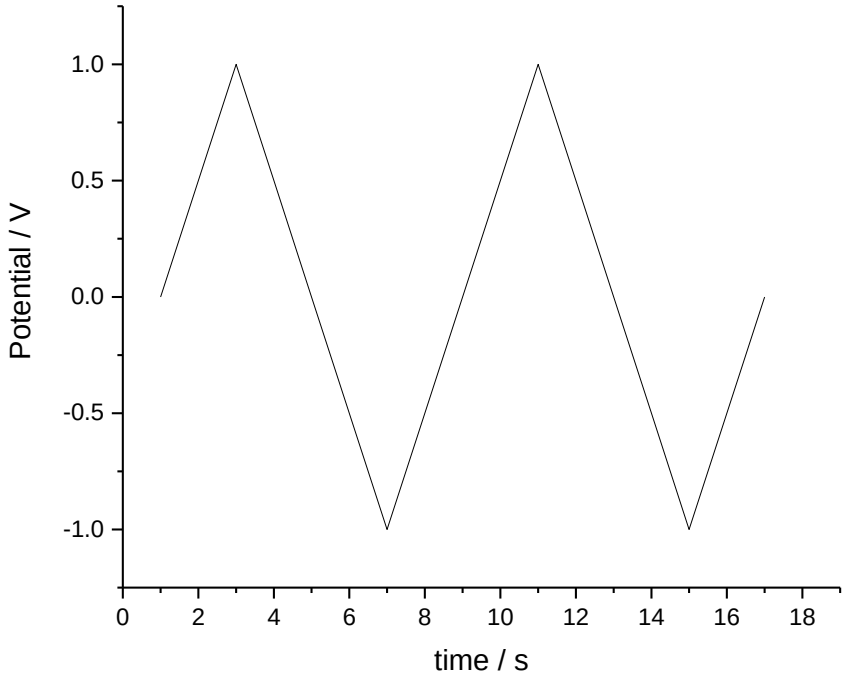

Figure 2.1. Voltage-time profile of a cyclic voltammogram, in this example voltage limits of +/- 1 V are used with a scan rate of 500 $mV \cdot s^{-1}$.

An electrochemically reversible reaction can be identified from the first cycle of a cyclic voltammogram. If a system is electrochemically reversible the peak current, i_p, for the oxidation or reduction process will change proportionally with the square root of the scan rate, $v^{1/2}$, as the scan rate is changed. The peak-to-peak separation, that is the potential difference between the oxidation peak potential and the reduction peak potential, for a reversible system should be $\frac{59\,mV}{n}$. If a system does not satisfy these conditions completely it is not necessarily an indicator that the system is not electrochemically reversible. It may be that experimental conditions are affecting the observed results. An example of something that may skew the results is the iR drop across the cell.

Cyclic voltammetry is useful for gaining an insight into the electrochemical processes occurring at the working electrode in a system. As the potential can be

scanned both positive and negative it is possible to investigate both oxidation reactions and reduction reactions. It is possible to scan the potential anywhere from extremely slow scan rates ($mV \cdot s^{-1}$) to extremely fast scan rates ($kV \cdot s^{-1}$).

The data collected during cyclic voltammetry experiments is generally plotted as a current *vs* voltage plot. Figure 2.2 illustrates the CV of a one electron oxidation of a species in solution to give an oxidised species in solution:

$$R_{Bulk} \rightarrow R_{Surface}$$

$$R_{Surface} \rightarrow O_{Surface} + e^-$$

$$O_{Surface} \rightarrow O_{Bulk}$$

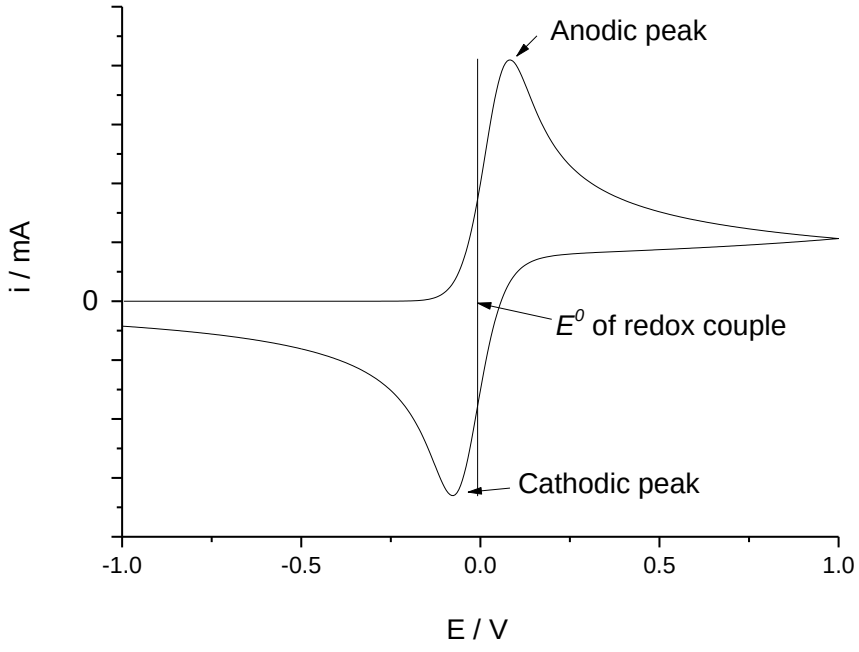

Figure 2.2. Theoretical current *vs* potential plot for data obtained during a cyclic voltammetry experiment. Simulated using DigiElch: $\mathbf{20\ mV \cdot s^{-1}}$, $\boldsymbol{k^s} = \mathbf{1} \times \mathbf{10^{-3}\ cm \cdot s^{-1}}$, semi-infinite 2D diffusion.

The shape of a cyclic voltammogram, such as that shown in Figure 2.2, with a low k^s, is determined by the both the kinetics and the mass transport of the system.

The initial increase in the current seen follows the Butler-Volmer equation which models the kinetics for simple electron transfer reactions.[1]

$$j = j_0(exp\frac{\alpha nF\eta}{RT} - exp - \frac{(1-\alpha)nF\eta}{RT})$$

Equation 2.2. Butler-Volmer equation

Where:

j = Current density ($A \cdot cm^{-2}$)

j_0 = exchange current density ($A \cdot cm^{-2}$)

α = charge transfer coefficient

n = number of moles of electrons

F = Faradays constant ($96485\ C \cdot mol^{-1}$)

η = overpotential (V)

R = Gas constant ($8.314\ J \cdot K^{-1}mol^{-1}$)

T = Temperature (K)

In Figure 2.2 the peak and corresponding decline in the current is a result of the mass transport limitations of the system, which in general is a diffusion limitation. In a reversible system the peak current can be used to determine the diffusion coefficient of a species in a certain electrolyte according to the Randles-Sevcik equation:[1]

$$i_p = 0.4463nFAc(\frac{nFvD}{RT})^{1/2}$$

Equation 2.3. Randles-Sevcik equation

Where:

$i_p =$ Peak current (A)

$n =$ number of moles of electrons

$F =$ Faradays constant $(96485\ C \cdot mol^{-1})$

$A =$ geometric surface area of electrode (cm^2)

$c =$ concentration of species $(mol \cdot L^{-1})$

$v =$ scan rate $(V \cdot s^{-1})$

$D =$ diffusion coefficient $(cm^2 \cdot s^{-1})$

$R =$ Gas constant $(8.314\ J \cdot K^{-1}mol^{-1})$

$T =$ Temperature (K)

From a plot of current *vs* voltage it is possible to calculate the charge, q, for the oxidation and reduction processes by integrating the area under the curve according to:

$$q = \frac{idE}{v}$$

Equation 2.4

Where:

$q =$ charge (As)

$i =$ current (A)

$dE =$ voltage change (V)

$v =$ scan rate $(V \cdot s^{-1})$

The charge can then be related to the number of moles of a species being oxidised or reduced according to:

$$q = nFm$$

Equation 2.5

Where:

$q =$ charge (As)

$n =$ number of moles of electrons

$F =$ Faradays constant $(96485\ C \cdot mol^{-1})$

$m =$ number of moles (mol)

2.3.2 Galvanostatic Cycling

Conditions under which a commercial battery would operate are more easily simulated through the use of galvanostatic cycling. This technique involves a constant current being applied to the cell while the voltage response is recorded. The current is normally switched between positive and negative values, Figure 2.3, to allow the investigation of discharge and charge processes. Potential limits are often applied when performing galvanostatic cycling, however it is also possible to limit the time for which each current is applied. This allows the total charge passed to be controlled.

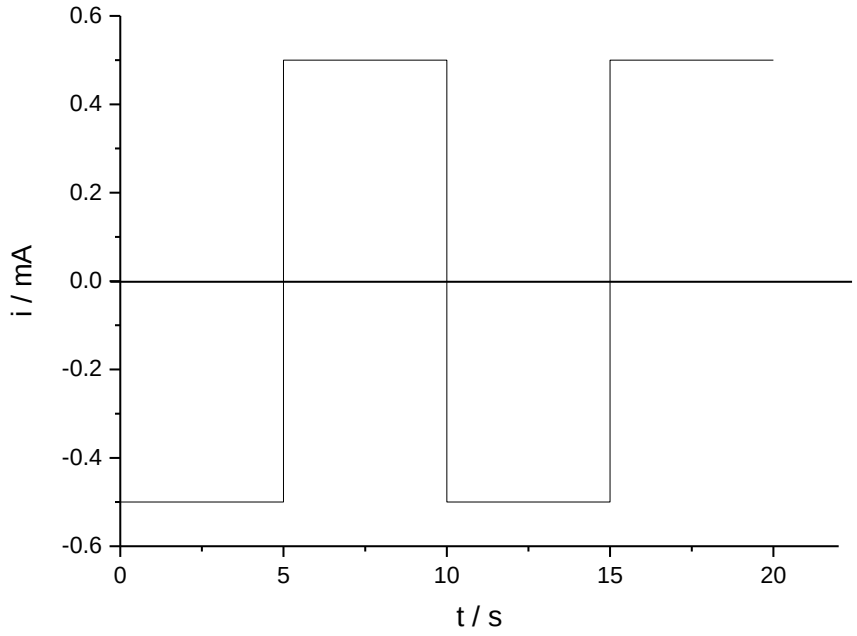

Figure 2.3. Representation of how the current changes with time during a galvanostatic experiment.

The data collected during galvanostatic cycling is often plotted as a voltage *vs* charge, q, graph, however when discussing the electrochemistry of batteries it is more common to plot the data in the form of a voltage *vs* capacity graph as shown in Figure 2.3.

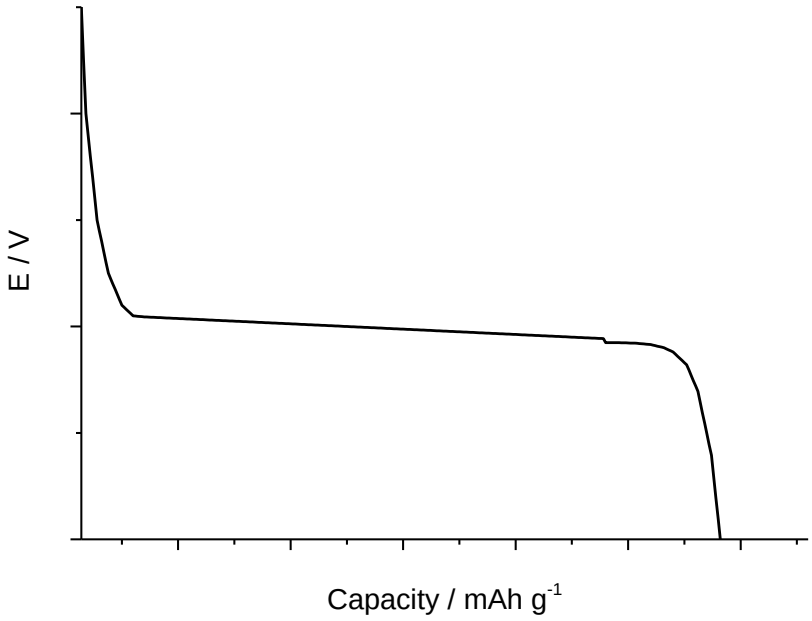

Figure 2.4. Theoretical potential *vs* capacity graph for the galvanostatic discharge of a battery cell.

When investigating the cycling behaviour of a reversible redox couple it is possible to estimate the expected capacity based on the transition time calculated form the Sand equation:[1]

$$\frac{i\tau^{1/2}}{c} = \frac{nFAD^{1/2}\pi^{1/2}}{2}$$

Equation 2.6

Where:

i = applied current (A)

τ = transition time (s)

c = concentration of species ($mol \cdot L^{-1}$)

n = number of electrons involved in reaction

F = Faradays constant ($96485\ C \cdot mol^{-1}$)

A = geometric surface area of electrode (cm^2)

D = diffusion coefficient ($cm^2 \cdot s^{-1}$)

To determine the transition time the diffusion coefficient of the species and the bulk concentration of the species must both be known. The transition time can then be converted to a charge which in turn can be converted to a capacity.

The sand equation can be used to model both reversible processes (Nernstian) and irreversible processes. It is possible to derive Nernstian style equations to describe the potential change seen during a constant current experiment for both the reversible and irreversible case. A reversible process can be described as:[1]

$$E = E_{\tau/4} + \frac{RT}{nF} ln \frac{\tau^{1/2} - t^{1/2}}{t^{1/2}}$$

Where:

$E_{\tau/4}$= The quarter wave potential (V)
R = Gas constant ($8.314\ J \cdot K^{-1} mol^{-1}$)
T = Temperature (K)
n = number of electrons involved in the reaction
F = Faradays constant ($96485\ C \cdot mol^{-1}$)
τ =transition time (s)
t = time (s)

While the potential change of an irreversible process can be described as:[1]

$$E = E^0 + \frac{RT}{\alpha F} ln \left[\frac{2k^0 \tau^{1/2}}{(\pi D)^{1/2}}\right] + \frac{RT}{\alpha F} \ln \left[1 - \left(\frac{t}{\tau}\right)^{1/2}\right]$$

Where:

k^0= standard heterogeneous rate constant ($cm \cdot s^{-1}$)
α =activity of the species under investigation
D = diffusion coefficient of the species under investigation ($cm^2 \cdot s^{-1}$)
R = Gas constant ($8.314\ J \cdot K^{-1} mol^{-1}$)
T = Temperature (K)
n = number of electrons involved in the reaction
F = Faradays constant ($96485\ C \cdot mol^{-1}$)
τ =transition time (s)
t = time (s)

When carrying out galvanostatic cycling, when the time of the experiment surpasses the transition time, τ, the flux of the reacting species to the electrode surface will not be sufficient to support the applied current. This then results in a change in the potential of the electrode to potentials where other electrode processes may occur.

It should be considered that during experiments other processes may also occur and contribute to the observed transition time. For example during an experiment as well as a faradaic process double layer charging may also be observed. Therefore of the total applied current only a certain proportion contributes to the faradaic reaction, this is expressed as:

$$\frac{i\tau^{1/2}}{c} = \frac{i_f\tau^{1/2}}{c} + \frac{i_c\tau}{c\tau^{1/2}}$$

Where:

i = Currrent (A)
τ =transition time (s)
i_f = Faradaic current (A)
i_c = current corresponding to double layer charging (A)
c = concentration of species reacting ($mol \cdot l^{-1}$)
t = time (s)

When the applied current is reversed, *i.e.* when changing from a reduction process to an oxidation process, the transition time for the new process, τ_2, is approximately $1/3$ of the time of initial process:

$$\tau_2 = t_1/3$$

Where:

τ_2 = Transition time of the reverse process (s)

t_1 = time of initial process (s)

2.4 References

[1] A. J. Bard and L. R. Faulkner, *Electrochemical Methods: Fundamentals and Applications,* 2nd ed. New York, NY: John Wiley & Sons, 2001.

Chapter 3: An Investigation of Electrolyte Stability through the use of *In Situ* Raman Spectroscopy

3.1 Introduction

As discussed in the introduction the role of the electrolyte in the Li-O_2 cell is vital for the correct operation of the cell. This oversight marred Li-O_2 research for many years. Since the realisation that the highly reactive nature of the superoxide anion intermediate makes many solvents,[1] particularly traditional carbonate based solvents, unsuitable for use in Li-O_2 cells there has been a push to find suitable alternatives.[2–5] Although there are many other solvents to choose from some present problems other than instability to superoxide; acetonitrile and DMSO for example are known to react with lithium metal.[6] This can be overcome by using something other than lithium metal as an anode or by pre-treatment of the lithium metal anode to form a protective coating.[7, 8]

When investigating the discharge products in different solvents great care must be taken to maintain the electrode in an air tight environment due to the instability of Li_2O_2 when exposed to moisture. This means that *in situ* or *in operando* identification is preferable. To date the majority of the techniques used for identifying Li_2O_2 have involved *ex situ* XRD,[2, 9–14] Fourier Transition-Infrared (FTIR) spectroscopy and Raman spectroscopy.[9, 12, 13, 15–20] Other techniques used include Electron Energy Loss Spectroscopy (EELS) and various forms of NMR spectroscopy.[11, 15, 21–23]

Recently *in situ* DEMS has been used to differentiate between reactive and unreactive solvents used in Li-O_2 cells.[23–26] *In situ* Surface Enhanced Raman Scattering (SERS) spectroscopy has also recently been adopted for the identification of oxygen reduction products.[15, 23, 25, 27–29]

The use of ionic liquids as electrolytes in Li-O_2 cells was investigated by Kuboki *et al*. before the realisation that the superoxide anion reacts with a large number of solvents.[30] This was driven by the highly desirable properties ionic liquids possess; hydrophobic nature, low volatility and low flammability. In

electrochemical cells that are highly sensitive to moisture, potentially open to the atmosphere and related to a family of batteries (Li-ion cells) that have recently been under intense scrutiny due to their safety, the appeal of ionic liquids is obvious. Unfortunately there are also undesirable properties associated with ionic liquids in particular their high viscosity, which can result in slow diffusion of ions through the solution. It is the benefits offered by ionic liquids (ILs) that led to their proposed use in the EU funded 'LABOHR' project. The work presented here was carried out as part of this project.

It is important to point out that the term ionic liquids covers a broad range of liquids consisting purely of ions, and that by this definition any salt that is heated to a temperature high enough to break the ionic interactions between molecules and form a liquid is classed as an ionic liquid. Therefore the type of ILs we are interested in are those that become liquid at low temperatures, below $298\ K$, hence the term room temperature ionic liquid (RTIL) can be used. These RTILs have been studied for use as electrolyte solvents in electrochemical cells since the 1970s.[31]

As mentioned Raman spectroscopy is a key technique used for the identification of Li_2O_2 in Li-O_2 cells and was used in Abraham and Jiang's first paper on lithium-air cells to identify the discharge product.[4, 8, 19, 32-36] They observed a strong peak after discharge at *ca.* $795\ cm^{-1}$, this was assigned to lithium peroxide.

Raman spectroscopy works by analysing the light inelastically scattered from a sample that has been excited by a laser beam. Upon interacting with a material the laser photons lose part of their energy (Stokes, see Diagram 3.1), which is transferred to the material causing the atoms to vibrate. The Raman effect is based on the change in the electric field of the molecule, and the induced dipole moment caused by the incident beam. Raman spectroscopy often gives relatively weak results as most light that is scattered back is done so elastically, this is

known as Rayleigh scattering (see Diagram 3.1) and does not result in a Raman shift. Studying the vibrations of atoms provides valuable information about the chemical composition of different materials and their chemical make-up.

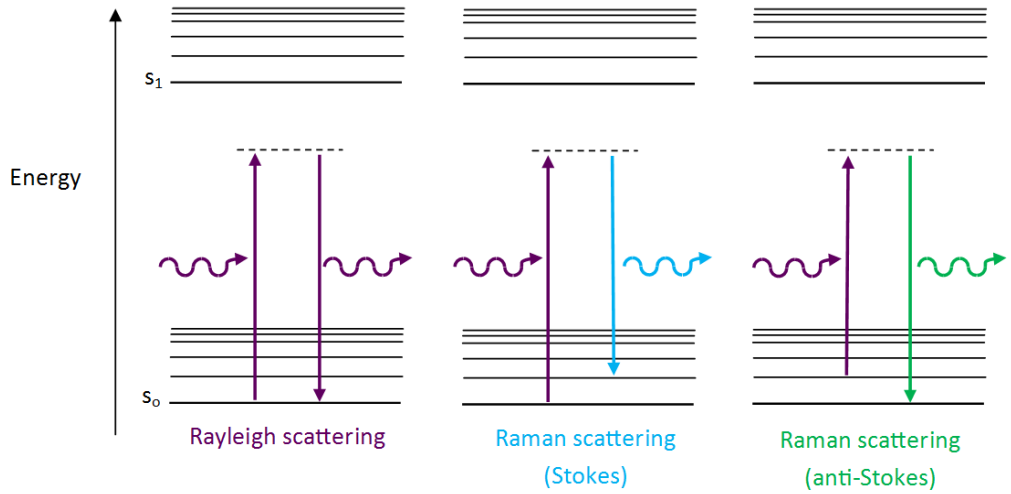

Diagram 3.1. Visual representation of the energy changes related to Raman effect

In 1973 a strange effect was noted by a University of Southampton research team led by Martin Fleischmann whereby the Raman signal of a pyridine molecule was unusually intense when measured on the surface of a roughened silver electrode.[37] This enhancement was later determined to be due to the rough surface of the silver electrode and was described as Surface Enhanced Raman Scattering and is known to enhance a Raman signal by as much as 10^6.[38]

The signal enhancement that results from SERS is now a widely used technique and is an extremely useful analytical tool as it allows the investigation of molecules that would otherwise give a very low Raman signal. The cause of SERS enhancement is a harmonic interaction between a surface Plasmon and a molecule on the surface of the substrate. A Plasmon with the correct wavelength

helps to couple the laser excitation into and out of the molecular bonds (Diagram 3.2).

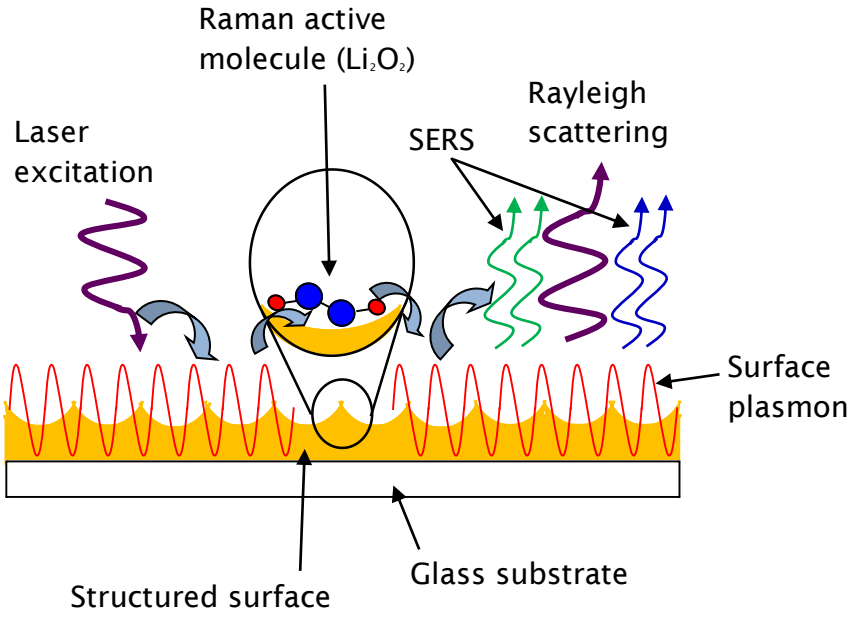

Diagram 3.2. Mechanism of SERS enhancement on a plasmonic substrate.

In this chapter the use of SERS spectroscopy as a powerful tool for the identification of stable electrolytes in Li-O_2 cells is investigated. The results presented here show the first instance of *in situ* SERS spectroscopy to monitor the oxygen reduction reaction in ionic liquid electrolytes in Li-O_2 cells.

3.2 Experimental

3.2.1 Chemical Reagents

Electrolytes were prepared as described in chapter 2, section 2.1.

$Li_2Mn_2O_4$ was prepared in house by combining $Li_1Mn_2O_4$ (Sigma-Aldrich, spinel, powder, $< 99\ \%$) with LiI (Sigma-Aldrich, beads, $99\ \%$) in a 1:1 ratio and heating at $200\ ^\circ C$ under vacuum overnight. $Li_{1.5}Mn_2O_4$ was prepared by mixing Li_1MnO_2 with $Li_2Mn_2O_4$ in a 1:1 ratio. $Li_{1.5}MnO_2$ was then prepared as an ink by mixing $Li_{1.5}Mn_2O_4$ with acetylene carbon black (Shewenigan) and the binder polyvinylidene fluoride (PVDF, DuPont) in ratio of 20:70:10 by weight percent.

3.2.2 Instrumentation

Raman spectra were acquired using a 50X objective in combination with a Renishaw 2000 microscope equipped with a $632.8\ nm$ He-Ne laser. The diameter of the laser spot on the electrode surface was approximately $1\ \mu m$.

Raman spectra presented were baseline corrected using a linear multipoint fitting function. The Raman intensities of the peaks were taken as the height above the baseline. Spectra were plotted using Origin 8.5.1.

Electrochemical measurements were carried out at room temperature on an EcoChemie μAutolabIII potentiostat/galvanostat.

Prior to any electrochemical experiments being carried out the Raman cell was dried at $80\ ^\circ C$ in an oven overnight and the SERS substrate was dried under vacuum at $100\ ^\circ C$ before being transferred to a dry glovebox. The cell was assembled under an argon atmosphere and then saturated with oxygen (BOC) outside of the glovebox by flowing oxygen saturated electrolyte through the cell.

3.2.3 Cell Design

A spectro-electrochemical Raman cell was designed and built in consultation with Ventacon Ltd. (Diagram 3.3). The design of the cell allows for viewing under the microscope, while maintaining a thin electrolyte film on the substrate of $150\ \mu L$. Electrochemistry was carried out in the cell using a three electrode setup, where a SERS substrate was used as the working electrode, a platinum wire counter electrode and a platinum wire coated in $Li_{1.5}Mn_2O_4$ was used as the reference electrode. Structured sphere segment void (Diagram 3.4) SERS substrates were prepared in-house, as described by Johnson *et al.*,[39] using $600\ nm$ polystyrene spheres as a template.

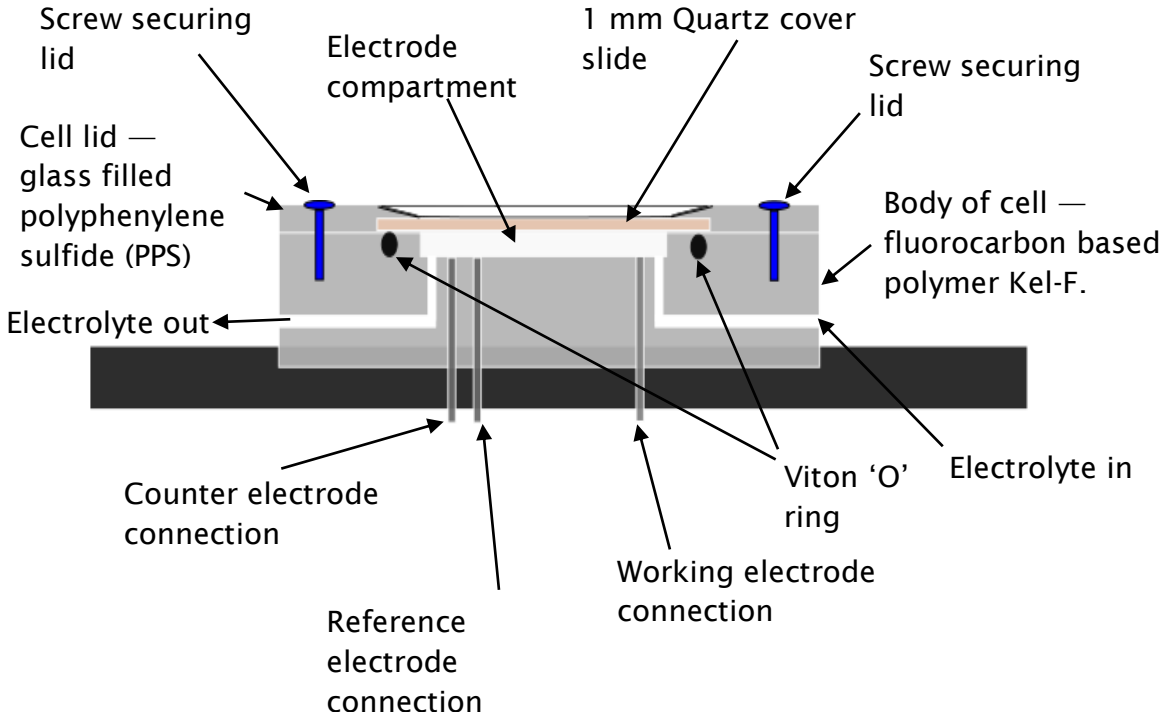

Diagram 3.3. Side-on view of *in situ* Raman spectroscopy cell constructed in consultation with Ventacon Ltd.

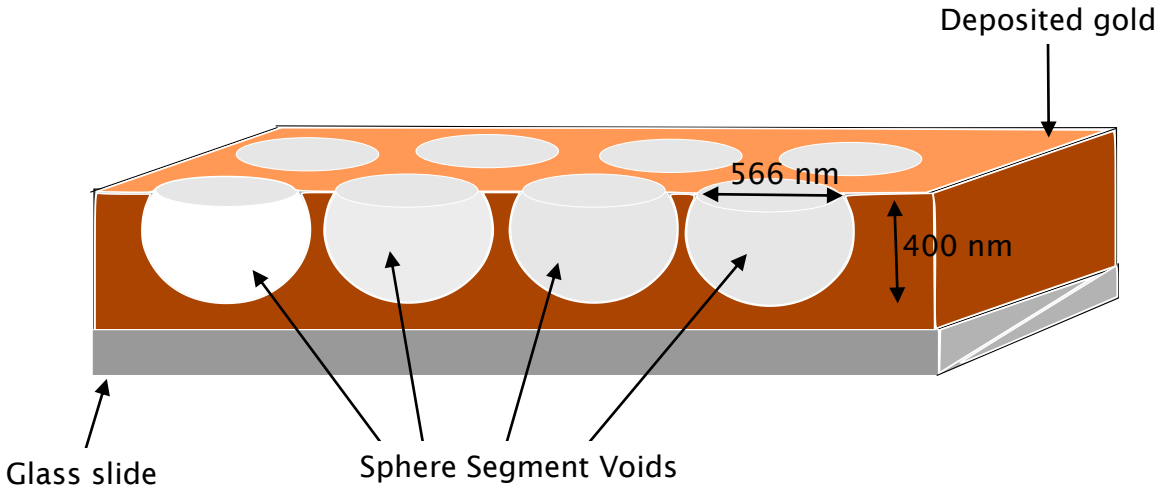

Diagram 3.4. Sphere Segment Void (SSV) electrode surface offering plasmonic enhancement.

3.3 Results and Discussion

3.3.1 SERS Investigation of Oxygen Reduction in 1-Ethyl-3-Methylimidazolium Bis(trifluoromethanylsulfonyl)imide

One of the first ILs investigated for use in a Li-O_2 cell was the ionic liquid C_2mimTFSI (EMIMTFSI),[30] the chemical structure of the C_2mim cation and TFSI anion are shown in Figure 3.1. Kuboki *et al*. reported extremely high capacities when using this solvent. Later reports suggested that the capacities seen did not relate to the formation of lithium peroxide but breakdown products,[40] GC-MS and FTIR were used to identify the breakdown products. In this work the electrochemical reduction of oxygen at a structured gold electrode was probed *in situ* using Raman spectroscopy.

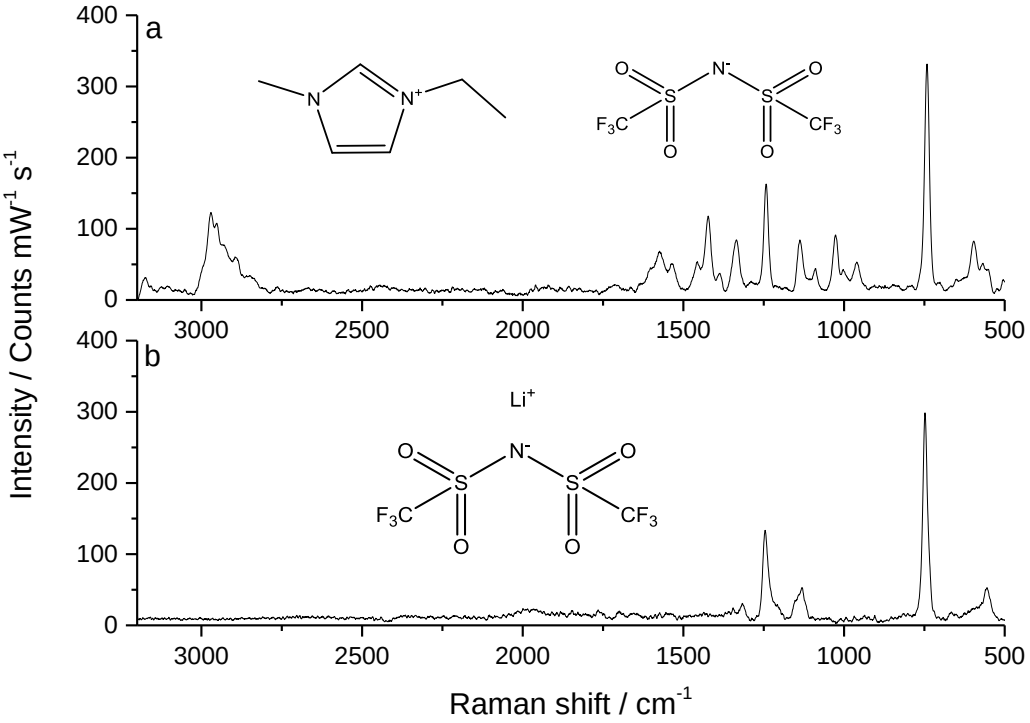

Figure 3.1. a) Raman spectrum of the ionic liquid C_2mimTFSI. **b)** Raman spectrum of the lithium salt LiTFSI.

Figure 3.1 shows the Raman spectra of both the ionic liquid C_2mimTFSI (top spectrum) and LiTFSI powder (bottom spectrum). Through the comparison of the two spectra it is possible to determine the peak contributions from both the C_2mim cation and the TFSI anion. It is apparent that the most intense band, at $742\ cm^{-1}$, is due to the TFSI anion.

The spectrum collected for both C_2mimTFSI and the LiTFSI are in good agreement with the literature.[41, 42] Through the comparison of these reference spectra with the spectra recorded during *in situ* experiments it is hoped that it will be possible to identify any new bands that arise as a result of oxygen reduction. This in turn will allow the determination of the stability of this electrolyte to the superoxide anion.

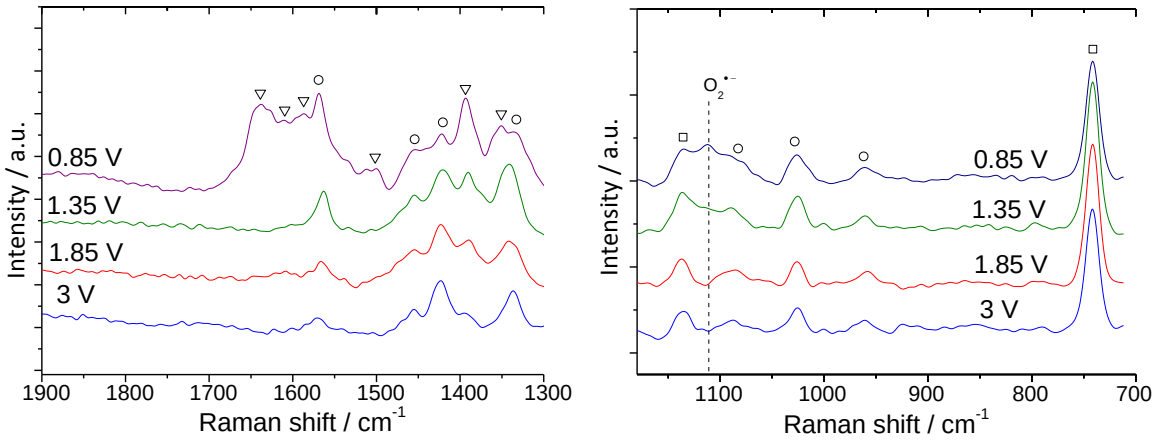

Figure 3.2. Raman Spectra recorded during a stepped chronoamperometry experiment at different potentials as indicated in the figure. The electrochemical cell comprised a Au SSV W_e, $Li_{1.5}Mn_2O_4$ R_e and Pt C_e in O_2 saturated $\mathbf{10}\ \boldsymbol{mM}$ LiTFSI C_2mimTFSI. The potentials shown are relative to the Li^+/Li couple.

Figure 3.2 shows *in-situ* Raman spectra that were collected on a gold SSV SERS electrode in O_2 saturated C_2mimTFSI $10\ mmol \cdot L^{-1}$ LiTFSI. The spectrum collected at OCV, $3\ V\ vs\ Li^+/Li$, is in close agreement with that seen in Figure 3.1 of the pure C_2mimTFSI IL (a comparison is shown in Figure **3.3**). This is as would be expected as no electrochemical reactions have yet been carried out. As a reductive overpotential was applied it can be seen that a new band emerges at

$1110\ cm^{-1}$, through comparison with the literature it can be concluded that this new band is due to the formation of the superoxide anion, $O_2^{\bullet-}$,[43] *via* the electrochemical reduction of oxygen (Scheme 3.1).

$$O_2 + e^- \rightarrow O_2^{\bullet-}$$

Scheme 3.1

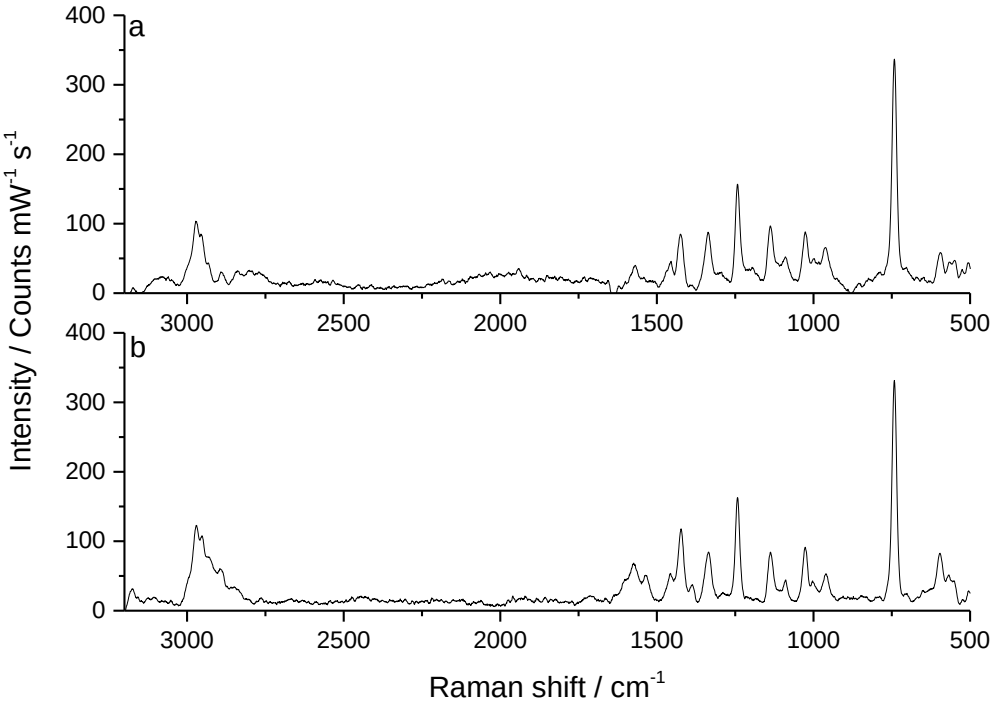

Figure 3.3. a) Raman spectrum of the ionic liquid C_2mimTFSI at OCV, 3 $\boldsymbol{V\ vs\ Li^+/Li}$, taken in-situ. **b)** Background Raman spectrum of the ionic liquid C_2mimTFSI taken ex-situ.

The formation of a new band at $1110\ cm^{-1}$ represents the only emergence of a new band at low wavenumbers, $700 - 1175\ cm^{-1}$. In the higher wavenumber region, $1300 - 1900\ cm^{-1}$, new bands emerge around $1600\ cm^{-1}$ after the appearance of the band at $1110\ cm^{-1}$. Bands in this region are often ascribed to C=O stretches of amides.[44] This formation of amides results from the nucleophilic attack of the superoxide anion on the C_2mim^+ cation. The findings shown here are in agreement with the literature where 1-ehtyl-3-methylimidazolone has

previously been identified as the main product of the reaction between superoxide and C_2mim^+ (Scheme 3.2).[40] The imidazolone product reportedly accounts for 98 % of the breakdown product. The remaining 2 % can be accounted for by "ring-opening" products.[45] The absence of a lithium peroxide peak supports the assumption in the literature that the superoxide anion and the imidazolium react in a 1:1 ratio.

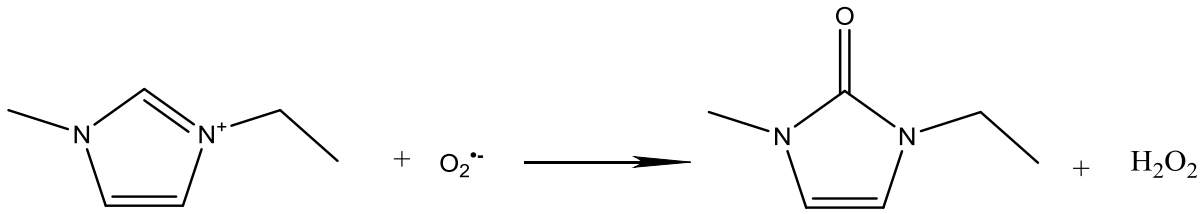

Scheme 3.2. 2-imidazolone formation *via* the reaction between superoxide and C_2mim^+.[40]

Based on these finding it appears that although we do see the generation of the superoxide anion, which is a precursor to peroxide formation. The formation of lithium peroxide its self is hampered by side reactions between the superoxide anion and the C_2mim^+ cation. This confirms that the capacities seen by Kuboki *et al.* were not the result of lithium peroxide formation,[30] but were due to the generation of superoxide that then went on to react with the electrolyte.

3.3.2 SERS Investigation of Oxygen Reduction in 1-Butyl-1-Methylpyrrolidinium Bis(trifluoromethylsulfonyl)imide

Having successfully employed the use of *in situ* SERS spectroscopy to monitor the reduction of oxygen on a structured gold electrode in the ionic liquid C_2mimTFSI the same technique was then employed to investigate the reaction pathway of oxygen reduction in the ionic liquid Pyr_{14}TFSI. According to the literature the Pyr_{14}^+ cation is more stable to nucleophilic attack than the C_2mim^+ cation, with lithium peroxide having previously been identified, *via ex situ* measurements, as a discharge product.[12] The work detailed below represents the first *in situ* measurements of oxygen reduction in this solvent.

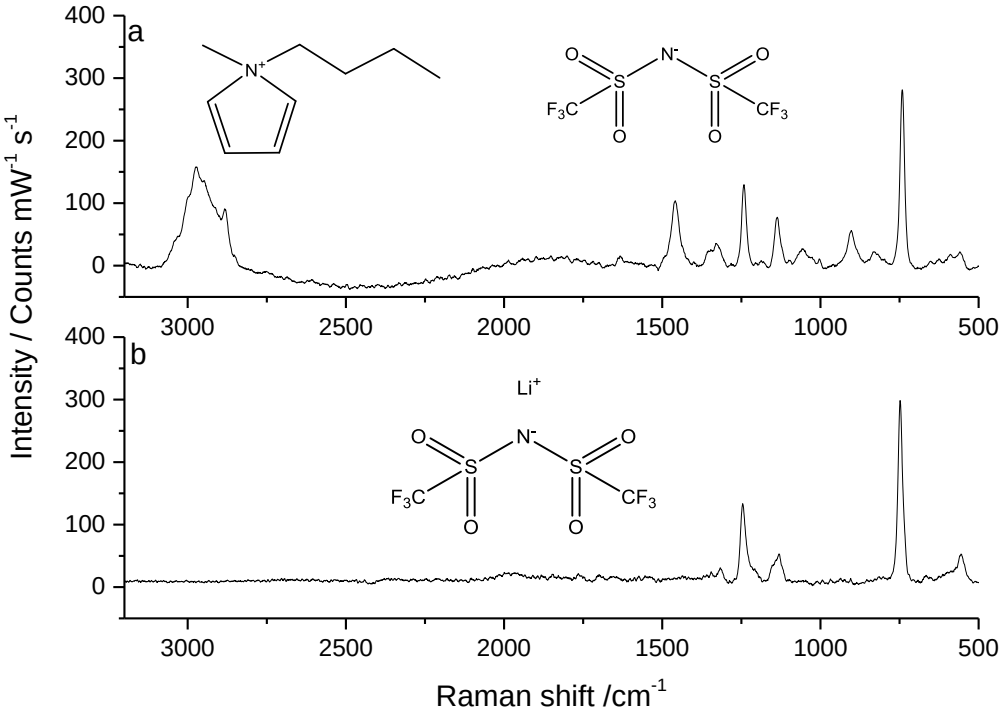

Figure 3.4. a) Raman spectrum of the ionic liquid Pyr_{14}TFSI. **b)** Raman spectrum of the lithium salt LiTFSI.

Figure 3.4 compares the Raman spectra of the ionic liquid Pyr_{14}TFSI with a powder sample of LiTFSI. This again allows us to identify the peaks that are present due

to the Pyr_{14}^{+} cation and $TFSI^{-}$ anion. It can again be seen that the most intense band present is that at $742\ cm^{-1}$, this is assigned to a complex molecular vibration that involves both the bending of the $-CF_3$ group and the stretching of the S-N bond.[46]

The spectra collected are in good agreement with those reported in the literature.[41, 42, 46] Through comparison of these reference spectra with those recorded during *in situ* experiments it will again be possible to follow the reduction of oxygen in this electrolyte.

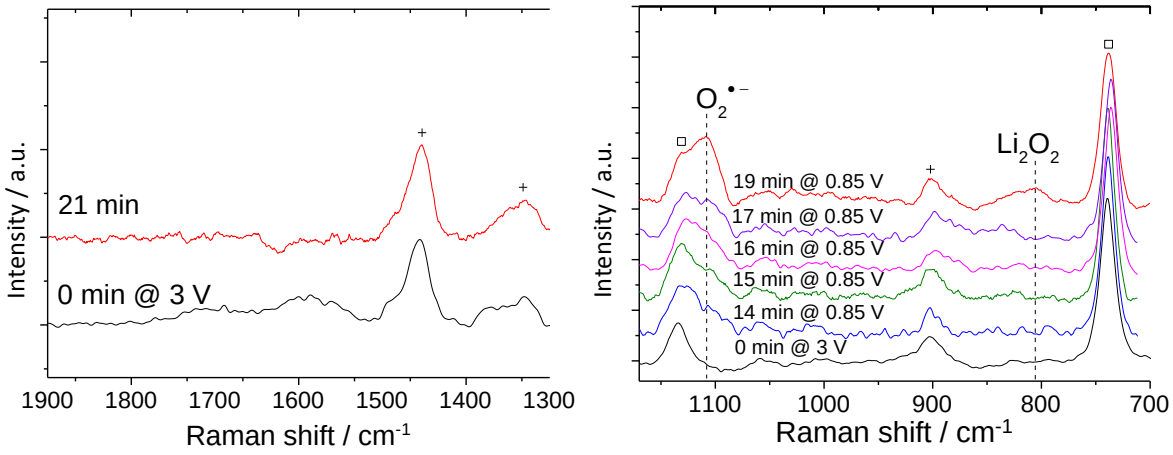

Figure 3.5. Raman spectra recorded during a stepped chronoamperometry experiment. The cell was comprised of a Au SSV W_e, $Li_{1.5}Mn_2O_4$ R_e and Pt C_e in O_2 saturated $\mathbf{10\ mM}$ LiTFSI $Pyr_{14}TFSI$.

Figure 3.5 shows *in situ* SERS spectra recorded in O_2 saturated $10\ mM$ LiTFSI, $Pyr_{14}TFSI$. During the experiment the potential of the cell was stepped from the OCV to $0.85\ V\ vs\ Li^{+}/Li$. The spectra presented in Figure 3.5, other than the spectrum collected at the OCV, were collected while the potential of the working electrode was held at $0.85\ V\ vs\ Li^{+}/Li$.

The spectrum at $3\ V\ vs\ Li^{+}/Li$, OCV, agrees with both the reference spectrum of $Pyr_{14}TFSI$ that is shown in Figure 3.4 and with previously reported spectra from the literature.[41, 42, 46] In a similar fashion to that which was seen when examining oxygen reduction in C_2mimTFSI a new band appears first at $1107\ cm^{-1}$, this was

again ascribed to the superoxide anion and was in good agreement with the frequency of the superoxide band at $1109\ cm^{-1}$ measured in tetraalkylammonium solutions of acetonitrile.[29, 33, 43]

Furthermore the formation of superoxide by the 1 e^- reduction of oxygen, as indicated by the new band at $1107\ cm^{-1}$, is followed by the emergence of a second band at $805\ cm^{-1}$. Through comparison with the literature this second band is ascribed to the formation of peroxide, and more specifically lithium peroxide.[12, 27, 33, 36] The pathway taken to form lithium peroxide is not clear, with the possibility of the reaction following an electrochemical pathway, Scheme 3.3, a chemical pathway, Scheme 3.4, or a mixture of the two.

$$O_2^{\bullet -} + Li^+ \rightarrow LiO_2$$

$$LiO_2 + Li^+ + e^- \rightarrow Li_2O_2$$

Scheme 3.3

$$O_2^{\bullet -} + Li^+ \rightarrow LiO_2$$

$$2LiO_2 \rightarrow Li_2O_2$$

Scheme 3.4

In contrast to what was seen in C_2mimTFSI no new bands emerge at higher wavenumbers in the spectrum of Pyr_{14}TFSI. This demonstrates the chemical stability of Pyr_{14}^+ based ionic liquid to nucleophilic attack by the superoxide anion and is in agreement with previous *ex situ* studies.[12]

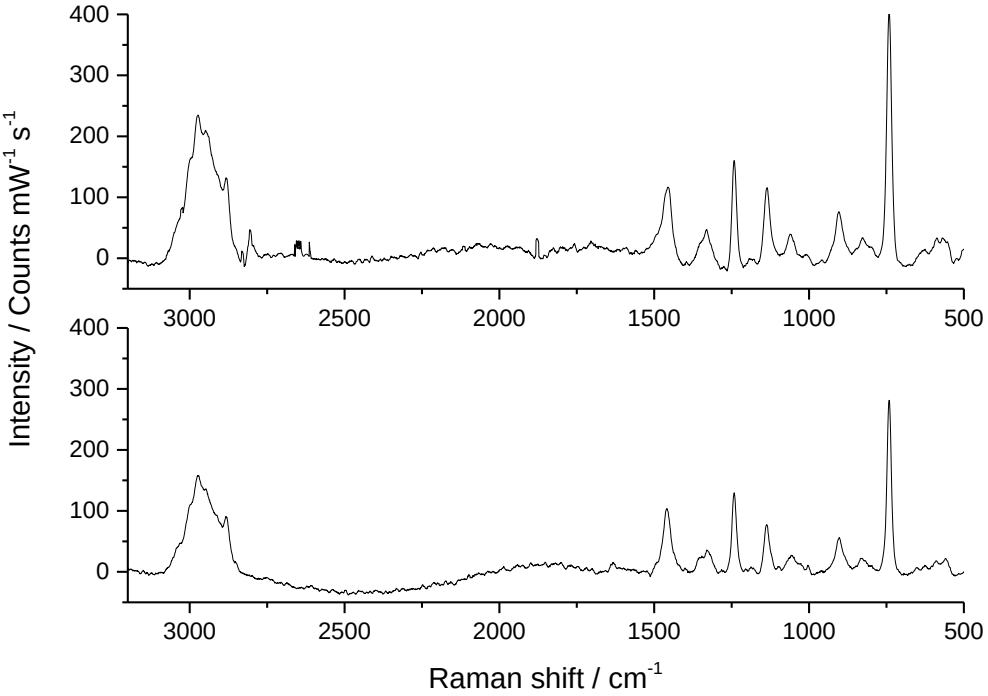

Figure 3.6. a) Raman spectrum of the ionic liquid $Pyr_{14}TFSI$ at OCV, $\boldsymbol{3\ V\ vs\ Li^{+}/Li}$, recorded in-situ. **b)** Background Raman spectrum of the ionic liquid $Pyr_{14}TFSI$ recorded *ex situ*.

In this experiment the main reaction product of oxygen reduction found in $Pyr_{14}TFSI$ was superoxide, at least near the electrode surface. This suggests that, under these experimental conditions where a relatively low lithium salt concentration was used, the superoxide anion may be stabilised to some extent by the large number of soft cations present from the ionic liquid. This effect, in relation to the Li-O_2 cell, was first reported by Laoire *et al.*.[47] This may pose an added advantage when using this solvent as the inhibition of the disproportionation reaction will allow added time for the superoxide anions to diffuse away from the electrode surface. As the disproportionation reaction would then occur away from the electrode surface the electrode would not become passivated by the lithium peroxide as quickly. As the passivation of the electrode surface by the deposition of lithium peroxide is widely viewed as the biggest

limitation to the practical capacities of Li-O_2 cells,[48] this could be hugely beneficial.

This finding could present an alternative explanation to previously reported results in this solvent by Monaco *et al.* who found that when using a rotating disk electrode (RDE) the biggest limiting factor to cell capacity was oxygen mass transport at high current densities.[49] This was demonstrated through the attainment of higher capacities at higher rotation rates. It was suggested that the observed endpoint of their galvanostatic discharges, where there was a sharp drop in voltage, was due to oxygen starvation. This only considers the possibility that the current used was higher than the oxygen diffusion limiting current for all rotation rates meaning that no steady state was achieved. By rearranging the Sand equation to give Equation 3.1 it is possible to estimate the expected capacity under the conditions used by Monaco *et al.* if oxygen diffusion was the limiting factor.

$$q = \frac{n^2 F^2 D \pi C^2}{4j}$$

Equation 3.1

Where:

q = charge ($mC \cdot cm^{-2}$)

n = the number of electrons

F = Faradays constant ($96485\ C \cdot mol^{-1}$)

D = the diffusion coefficient ($cm^2 \cdot s^{-1}$)

C = the concentration ($mol \cdot cm^{-3}$)

j = the current density ($mA \cdot cm^{-2}$)

Based on Equation 3.1 using $n = 2$, $D_{O_2} = 12 \times 10^{-6}\ cm^2 \cdot s^{-1}$ [50], $C_{O_2} = 2.9 \times 10^{-6}\ mol \cdot cm^{-3}$ [50] and $j = 0.5\ mA \cdot cm^{-2}$ for temperatures of $30\ °C$ we calculated $q = 5.9\ mC \cdot cm^{-2}$. If you then consider that the value of the diffusion coefficient

doesn't take into account the addition of $100\ mM$ LiTFSI which changes the viscosity of the electrolyte and therefore the diffusion coefficient of the oxygen. Through the use of the Stokes-Einstein relationship Equation 3.2 we can estimate a new value for the diffusion coefficient.

$$D = \frac{k_B T}{6\pi\eta r}$$

Equation 3.2

Where:

D = Diffusion coefficient ($m^2 \cdot s^{-1}$)

k_B = Boltzmann constant ($1.38 \times 10^{-23} m^2 kg \cdot s^{-2} K^{-1}$)

T = the temperature (K)

r = the radius (m)

η = the kinematic viscocity ($kg \cdot s^{-1} m^{-1}$)

Using $r = 3 \times 10^{-10}\ m$ and $\eta = 0.085\ kg \cdot s^{-1} m^{-1}$ in 100 mM LiTFSI, $Pyr_{14}TFSI$ a new value is estimated, $D = 8.6 \times 10^{-12}\ m^2 \cdot s^{-1}$. Using this new value of D we can calculate $q = 4.2\ mC \cdot cm^{-2}$. If we then consider that the carbon loading used in Monaco's work was $1\ mg \cdot cm^{-2}$, we can calculate values of the specific capacity of $1.64\ mAh \cdot g^{-1}$ and $1.17\ mAh \cdot g^{-1}$ respectively. The specific capacities obtained in their work was in fact in great excess, $> 300\ mAh \cdot g^{-1}$, of the values calculated here. This suggest that in fact oxygen mass transport was not the limiting factor affecting the obtainable capacities. Based on our findings that lithium peroxide is not detected on the surface of the electrode for some time after the formation of superoxide, we believe that the increase in capacity seen by Monaco *et al.* at higher rotation rates is due to the removal of some superoxide from the electrode surface. This would then result in the formation of some lithium peroxide away

from the electrode surface allowing the continued reduction of oxygen at the electrode surface.

3.4 Conclusions and Further Work

Through the use of *in situ* SERS spectroscopy we have provided the first *in situ* spectroscopic evidence of the instability of the C_2mimTFSI ionic liquid in the presence of superoxide, and more specifically the instability of the C_2mim^+ cation. Further to this we have shown that the Pyr_{14}^+ cation found in the ionic liquid Pyr_{14}TFSI was stable to superoxide over the timescale of this experiment. We have also shown that lithium peroxide, the desired product of the discharge reaction in Li-O_2 cells, is formed on discharge in this electrolyte. This is in agreement with previous *ex situ* results in this electrolyte.[51] It should be taken into consideration that although we have shown that the Pyr_{14}^+ cation is stable to the superoxide radical, a recent article by Piana *et al*. detected breakdown products *via* ^{1}H NMR and OEMS.[52] They suggest that this is the result of charging the cell above $4.0\,V$ and the reaction of the Pyr_{14}^+ cation with the lithium metal anode. The eventual use of Pyr_{14}TFSI as an electrolyte in a Li-O_2 cell may not be practical, unless the charging potential can be kept below $4\,V$ and suitable electrolyte additives can be utilized to help form an SEI on the lithium and prevent the reaction between the cation and the lithium metal.

From the data we obtained and analysis of results from other work it appears that the large cations present in the Pyr_{14}TFSI electrolyte help to stabilize the superoxide anion radical.[49, 50, 53] This results in a slow conversion to lithium peroxide, in cells with controlled hydrodynamic conditions this can lead to increased capacities. However this is not necessarily practical for most Li-O_2 cells. The possibility of moving the site of lithium peroxide formation away from the electrode surface offers the possibility of Li-O_2 cells with extremely large capacities, where the specific capacity would no longer be dependent on the surface area of the carbon but the volume of the electrolyte compartment.

To further investigate the longevity of the superoxide cation in the ionic liquid $Pyr_{14}TFSI$ it is suggested that a series of UV-Vis experiments could be carried out. Through the use of readily available reagents, such as potassium superoxide, valuable kinetic information could be gained. By then combining this with Raman or SERS spectroscopy the stability of the ionic liquid over long time scales, not looked at in our work, could be investigated.

Capitalization of the displacement of lithium peroxide so as to increase the capacity of cells was seen as a key focus. To do this we suggest the use of soluble redox catalysts that can be reduced at the electrode surface and then diffuse into solution where it can reduce oxygen. This idea is explored further in Chapter 4.

3.5 References

[1] F. Mizuno, S. Nakanishi, Y. Kotani, S. Yokoishi, and H. Iba, *Electrochemistry*, **78**, 403–405, (2010).

[2] W. Xu, J. Hu, M. H. Engelhard, S. A. Towne, J. S. Hardy, J. Xiao, J. Feng, M. Y. Hu, J. Zhang, F. Ding, M. E. Gross, and J.-G. Zhang, *J. Power Sources*, **215**, 240–247, (2012).

[3] K. U. Schwenke, S. Meini, X. Wu, H. A. Gasteiger, and M. Piana, *Phys. Chem. Chem. Phys*, **15**, 11830–11839, (2013).

[4] B. D. McCloskey, D. S. Bethune, R. M. Shelby, G. Girishkumar, and A. C. Luntz, *J. Phys. Chem. Lett.*, **2**, 1161–1166, (2011).

[5] V. S. Bryantsev, J. Uddin, V. Giordani, W. Walker, D. Addison, and G. V. Chase, *J. Electrochem. Soc.*, **160**, A160–A171, (2012).

[6] D. Xu, Z. Wang, J. Xu, L. Zhang, and X. Zhang, *Chem. Commun.*, **48**, 6948–50, (2012).

[7] Y. Chen, S. A. Freunberger, Z. Peng, O. Fontaine, and P. G. Bruce, *Nat. Chem.*, **5**, 489–94, (2013).

[8] Z. Peng, S. A. Freunberger, Y. Chen, and P. G. Bruce, *Science.*, **337**, 563–566, (2012).

[9] P. Du, J. Lu, K. C. Lau, X. Luo, J. Bareño, X. Zhang, Y. Ren, Z. Zhang, L. A. Curtiss, Y.-K. Sun, and K. Amine, *Phys Chem Chem Phys*, **15**, 5572–81, (2013).

[10] A. K. Thapa and T. Ishihara, *J. Power Sources*, **196**, 7016–7020, (2011).

[11] J. Xiao, J. Hu, D. Wang, D. Hu, W. Xu, G. L. Graff, Z. Nie, J. Liu, and J.-G. Zhang, *J. Power Sources*, **196**, 5674–5678, (2011).

[12] F. Soavi and M. Mastragostino, *J. Power Sources*, **224**, 115–119, (2013).

[13] C. Xia, M. Waletzko, L. Chen, K. Peppler, P. J. Klar, and J. Janek, *ACS Appl. Mater. Interfaces*, **6**, 12083–12092 (2014).

[14] I. Landa-Medrano, I. Ruiz de Larramendi, N. Ortiz-Vitoriano, R. Pinedo, J. Ignacio Ruiz de Larramendi, and T. Rojo, *J. Power Sources*, **249**, 110–117, (2014).

[15] F. Mizuno, K. Takechi, S. Higashi, T. Shiga, T. Shiotsuki, N. Takazawa, Y. Sakurabayashi, S. Okazaki, I. Nitta, T. Kodama, H. Nakamoto, H. Nishikoori, S. Nakanishi, Y. Kotani, and H. Iba, *J. Power Sources*, **228**, 47–56, (2013).

[16] R. Black, S. H. Oh, J. Lee, T. Yim, B. Adams, and L. F. Nazar, *J. Am. Chem. Soc.*, **134**, 2902–5, (2012).

[17] M. Yu, X. Ren, L. Ma, and Y. Wu, *Nat. Commun.*, **5**, 5111, (2014).

[18] K. M. Abraham and Z. Jiang, *J. Electrochem. Soc.*, **143**, 1–5, (1996).

[19] H. Wang and K. Xie, *Electrochim. Acta*, **64**, 29–34, (2012).

[20] G. M. Veith, N. J. Dudney, J. Howe, and J. Nanda, *J. Phys. Chem. C*, **115**, 14325–14333, (2011).

[21] B. D. Adams, C. Radtke, R. Black, M. L. Trudeau, K. Zaghib, and L. F. Nazar, *Energy Environ. Sci.*, **6**, 1772, (2013).

[22] L. A. Huff, J. L. Rapp, L. Zhu, and A. A. Gewirth, *J. Power Sources*, **235**, 87–94, (2013).

[23] S. A. Freunberger, Y. Chen, Z. Peng, J. M. Griffin, L. J. Hardwick, F. Bardé, P. Novák, and P. G. Bruce, *J. Am. Chem. Soc.*, **133**, 8040–8047, (2011).

[24] Y. Chen, S. A. Freunberger, Z. Peng, F. Bardé, and P. G. Bruce, *J. Am. Chem. Soc.*, **134**, 7952–7, (2012).

[25] Z. Peng, S. A. Freunberger, L. J. Hardwick, Y. Chen, V. Giordani, F. Bardé, P. Novák, D. Graham, J.-M. Tarascon, and P. G. Bruce, *Angew. Chem. Int. Ed.*, **50**, 6351–5, (2011).

[26] F. Bardé, Y. Chen, L. Johnson, S. Schaltin, J. Fransaer, and P. G. Bruce, *J. Phys. Chem. C*, **118**, 18892–18898, (2014).

[27] F. S. Gittleson, W. Ryu, and A. D. Taylor, *ACS Appl. Mater. Interfaces*, **6**, 19017–25, (2014).

[28] D. Zhai, H.-H. Wang, J. Yang, K. C. Lau, K. Li, K. Amine, and L. a Curtiss, *J. Am. Chem. Soc.*, **135**, 15364–72, (2013).

[29] C. Li, O. Fontaine, S. A. Freunberger, L. Johnson, S. Grugeon, S. Laruelle, P. G. Bruce, and M. Armand, *J. Phys. Chem. C*, **118**, 3393–3401, (2014).

[30] T. Kuboki, T. Okuyama, T. Ohsaki, and N. Takami, *J. Power Sources*, **146**, 766–769, (2005).

[31] M. C. Buzzeo, R. G. Evans, and R. G. Compton, *ChemPhysChem*, **5**, 1106–1120, (2004).

[32] T. Ogasawara, A. Débart, M. Holzapfel, P. Novák, and P. G. Bruce, *J. Am. Chem. Soc.*, **128**, 1390–1393, (2006).

[33] Z. Peng, S. A. Freunberger, L. J. Hardwick, Y. Chen, V. Giordani, F. Bardé, P. Novák, D. Graham, J.-M. Tarascon, and P. G. Bruce, *Angew. Chem. Int. Ed.*, **50**, 6351–5, (2011).

[34] A. K. Thapa, T. H. Shin, S. Ida, G. U. Sumanasekera, M. K. Sunkara, and T. Ishihara, *J. Power Sources*, **220**, 211–216, (2012).

[35] V. S. Bryantsev, V. Giordani, W. Walker, M. Blanco, S. Zecevic, K. Sasaki, J. Uddin, D. Addison, and G. V Chase, *J. Phys. Chem. A*, **115**, 12399–409, (2011).

[36] K. M. Abraham and Z. Jiang, *J. Electrochem. Soc.*, **143**, 1–5, (1996).

[37] M. Fleischmann, P. J. Hendra, and A. J. McQuillan, *Chem. Phys. Lett.*, **26**, 163–166, (1974).

[38] G. Albrecht and A. Creighton, *J. Am. Chem. Soc.*, **99**, 5215–5217, (1976).

[39] R. P. Johnson, S. Mahajan, M. E. Abdelsalam, R. M. Cole, J. J. Baumberg, A. E. Russell, and P. N. Bartlett, *Phys. Chem. Chem. Phys.*, **13**, 16661–5, (2011).

[40] I. M. AlNashef, M. A. Hashim, F. S. Mjalli, M. Q. A. Ali, and M. Hayyan, *Tetrahedron Lett.*, **51**, 1976–1978, (2010).

[41] K. Matsumoto and R. Hagiwara, *Inorg. chem.*, **48**, 7350–8, (2009).

[42] M. Herstedt, M. Smirnov, P. Johansson, M. Chami, J. Grondin, L. Servant, and J. C. Lassègues, *J. Raman Spectrosc.*, **36**, 762–770, (2005).

[43] Z. Peng, S. A. Freunberger, L. J. Hardwick, Y. Chen, V. Giordani, F. Bardé, P. Novák, D. Graham, J. Tarascon, and P. G. Bruce, *Angew. Chem. Int. Ed.*, (2011).

[44] J. Mink, L. Hajba, I. Pápai, J. Mihály, C. Neméth, M. Y. Skripkin, and M. Sandström, *Appl. Spectrosc. Rev.*, **45**, 274–326, (2010).

[45] M. M. Islam, T. Imase, T. Okajima, M. Takahashi, Y. Niikura, N. Kawashima, Y. Nakamura, and T. Ohsaka, *J. Phys. Chem. A*, **113**, 912–6, (2009).

[46] M. Castriota, T. Caruso, R. G. Agostino, E. Cazzanelli, W. a Henderson, and S. Passerini, *J. Phys. Chem. A*, **109**, 92–6, (2005).

[47] C. O. Laoire, S. Mukerjee, K. M. Abraham, E. J. Plichta, and M. A. Hendrickson, *J. Phys. Chem. C*, **114**, 9178–9186, (2010).

[48] V. Viswanathan, K. S. Thygesen, J. S. Hummelshøj, J. K. Nørskov, G. Girishkumar, B. D. McCloskey, A. C. Luntz, J. S. Hummelshoj, and J. K. Nørskov, *J. Chem. Phys.*, **135**, 214704 1–10, (2011).

[49] S. Monaco, F. Soavi, and M. Mastragostino, *J. Phys. Chem. Lett.*, **4**, 1379–1382, (2013).

[50] S. Monaco, A. M. Arangio, F. Soavi, M. Mastragostino, E. Paillard, and S. Passerini, *Electrochim. Acta*, **83**, 94–104, (2012).

[51] F. Soavi, S. Monaco, and M. Mastragostino, *J. Power Sources*, **224**, 115–119, (2013).

[52] M. Piana, J. Wandt, S. Meini, I. Buchberger, N. Tsiouvaras, and H. A. Gasteiger, *J. Electrochem. Soc.*, **161**, A1992–A2001, (2014).

[53] C. O. Laoire, S. Mukerjee, K. M. Abraham, E. J. Plichta, and M. A. Hendrickson, *J. Phys. Chem. C*, **113**, 20127–20134, (2009).

3.6 Related Publications

J. T. Frith, A. E. Russell, N. Garcia-Araez, and J. R. Owen, *Electrochem. Commun.*, **46**, 33–35, (2014).

Chapter 4 : Ethyl Viologen as a Homogeneous Catalyst for the Oxygen Reduction Reaction

4.1 Introduction

When considering catalysis in Li-O_2 cells it is important to note that this is an area where the Li-O_2 cell behaves in a way that is similar to a fuel cell, rather than a Li-ion cell.

Li-ion cells operate by changing the redox state of transition metal ions in a lattice. Lithium ions are then inserted into or removed from the matrix so as to balance the change in the oxidation state of the material. There is therefore no chemical reaction to catalyse as no bonds are broken or formed. An example of this is shown in Diagram 4.1 using the Li-ion cathode material lithium cobalt oxide ($LiCoO_2$).

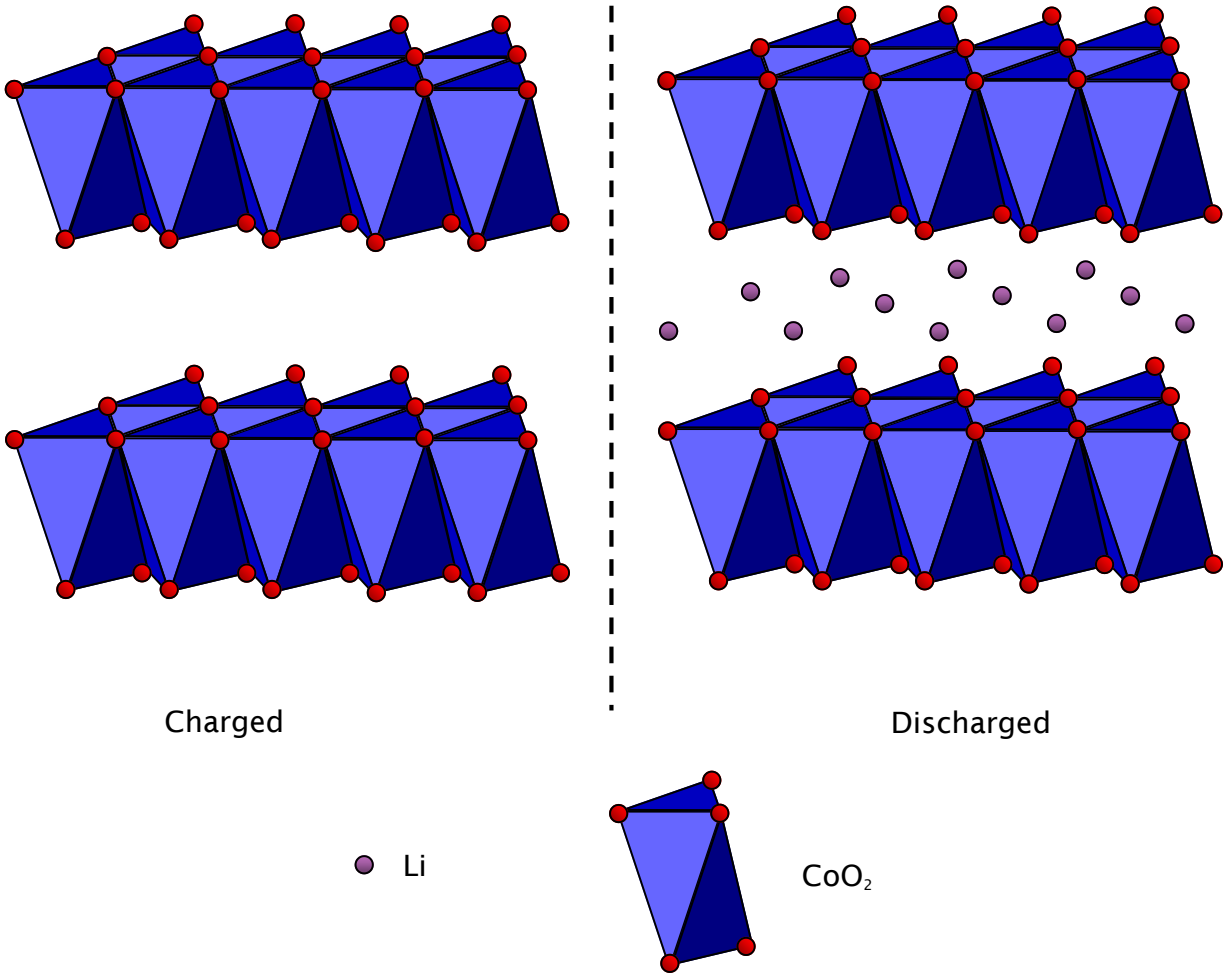

Diagram 4.1. Lithium cobalt oxide positive electrode in the charged and discharged state.

This is in contrast to fuel cells where, in a hydrogen fuel cell, a catalyst can be used to both lower the overpotential required for a particular reaction and at the same time promote a specific reaction pathway; in most cases the 4 e^- reduction of O_2 to H_2O in the cathode and the oxidation of H_2 in the anode (Diagram 4.2). In the case of fuel cells, where the product is soluble, the catalyst tends to be evenly dispersed particles on a support material (often high surface carbons). As the products are soluble these catalyst reaction sites can be accessed multiple times during discharge.

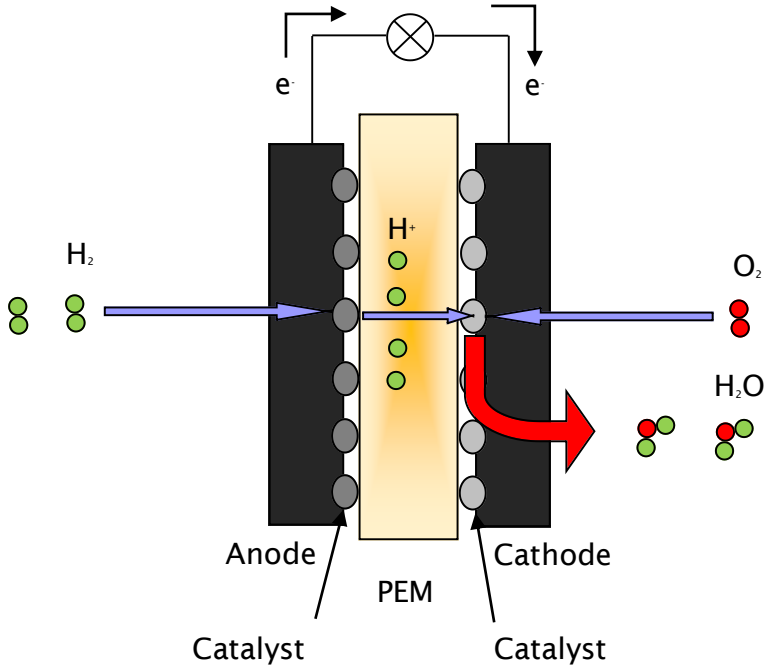

Diagram 4.2. Diagram of a hydrogen fuel cell utilizing a polymer electrolyte membrane (PEM).

Li-O_2 cells are similar to fuel cells. However the nature of the primary discharge product, Li_2O_2, in a Li-O_2 cell creates problems not seen in fuel cells. This is due to the insolubility and insulating properties of lithium peroxide.

When utilizing heterogeneous catalysts to promote the reduction of oxygen to Li_2O_2 in Li-O_2 cells, using a dry solvent with a low donor number, the discharge product will deposit close to the catalyst (Diagram 4.3).[1,2] The use of a catalyst

will therefore increase the rate at which the catalyst sites are covered in an insoluble and insulating layer. The effect of this will be seen as an increase in the rate at which the electrode is passivated, resulting in a decreased capacity.

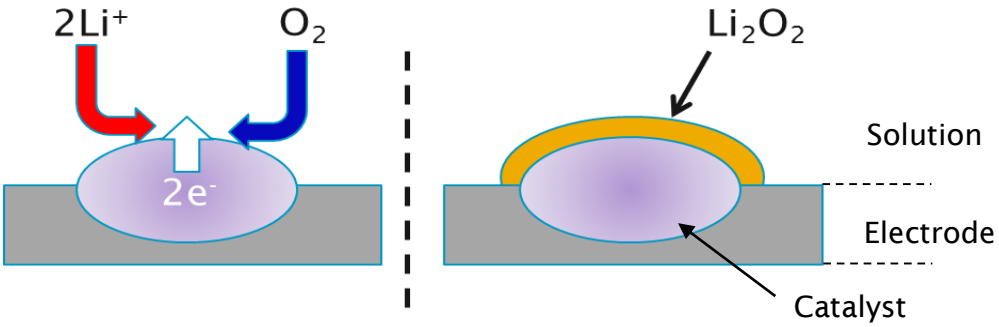

Diagram 4.3. Heterogeneous catalysis of the oxygen reduction reaction in lithium oxygen cells.

A majority of the work carried out to date on catalysts for the oxygen reduction reaction in Li-O_2 cells has focused on the use of heterogeneous catalysts.[3-10] While these works tend to focus on the use of catalysts to reduce the overpotential during discharge the catalyst does not specify the route the reaction takes i.e. the 1 e^- or 2 e^- reduction of oxygen.

The use of the term catalyst in these incidences therefore refers to the very basic definition of a catalyst being a species that aids a reaction without undergoing any permanent changes itself. A more complex definition of a catalyst is a species that is not only unchanged by a reaction but also helps in the selection of a specific product.

The next step in the development of catalysts for Li-O_2 cells should therefore focus on the identification of species that can direct the reduction of oxygen *via* the 2 e^- reaction pathway while at the same time reduce the overpotential and negate the effects of electrode passivation resulting from lithium peroxide formation.

The use of soluble redox molecules as catalysts (homogeneous catalysis) that can move the site of oxygen reduction away from the electrode surface may provide the answer.

A soluble redox catalyst moves the site of lithium peroxide formation away from the electrode surface by transferring electrons to oxygen in solution *via* a redox reaction (Diagram 4.4). This would keep the electrode free of any insoluble and insulating deposits as the lithium peroxide would not form directly on the electrode surface. This in turn would result in an increase in the discharge capacity of the cell.

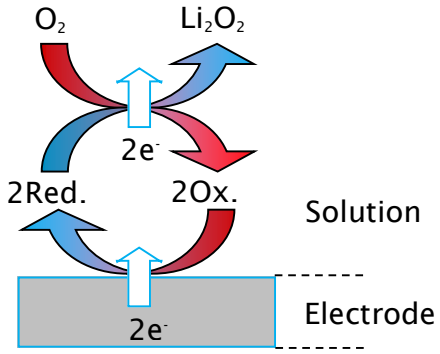

Diagram 4.4. Mode of action a soluble redox catalyst (homogeneous catalyst) when catalysing the oxygen reduction reaction of a Li-O_2 cell. Red./Ox. represents the redox molecule in its reduced and oxidised form respectively.

The distance from the electrode surface at which the redox molecule transfers an electron to oxygen may depend on the experimental conditions. Here we refer to a redox mediator as a molecule that is catalysing oxygen reduction close to the electrode surface, from electron tunnelling distance to several hundred nanometres distance. While a redox shuttle refers to a molecule that is catalysing oxygen reduction at a distance greater than several hundred nanometres from the electrode surface. It is important to note that a molecule that is acting as a redox mediator may be able to act as a redox shuttle under different conditions and

vice versa. They may also be acting as both a redox mediator and a redox shuttle simultaneously under certain conditions.

The work shown here presents a summary of investigations into the use of ethyl viologen as a homogeneous catalyst in Li-O_2 cells. Ethyl viologen was chosen as it is analogous to methyl viologen but exhibits slightly higher redox potentials.[11] Methyl viologen is well known for mediating the reduction of oxygen to superoxide in biological reactions.[12] This production of superoxide has previously been cited as the primary route of toxicity for the herbicide paraquat (methyl viologen).[13, 14] However in both aqueous and aprotic media viologen has been shown to ultimately promote peroxide formation.[12, 15]

This investigation focuses on the use of electrochemical techniques to probe the enhancement of the oxygen reduction reaction resulting from the use of a solution phase redox molecule with a potential that allows the reduced form of the redox molecule to reduce oxygen, in turn regenerating the oxidised form of the redox molecule (Diagram 4.4).

The reaction route that is promoted through the use of ethyl viologen as a homogeneous catalyst was also investigated, using UV-Vis spectroscopy, although this is not shown here (a summary is shown in Figure1, Appendix A). The results of this study provided evidence of the first catalyst to be used in a Li-O_2 cell that promotes the two electron reduction of oxygen *via* superoxide to form Li_2O_2.[16]

4.2 Experimental

4.2.1 Electrochemical Techniques

Cyclic voltammetry, galvanostatic cycling and potential step measurements have been used in this chapter. These techniques are explained in detail in Chapter 2, section 2.3.

4.2.2 Chemical Reagents

Electrolytes were prepared as detailed in Chapter 2, section 2.1.

4.2.3 Synthesis of Chemical Reagents

Ethyl viologen triflate was prepared *via* an ion exchange reaction. Ethyl viologen diiodide ($EtVI_2$, 99 %, Sigma-Aldrich) was dissolved in distilled water. To this solution an aqueous solution of silver triflate (Ag(OTf), $\geq$ 99.9 %, Sigma-Aldrich) was added in the molar ratio of 1:2. This caused silver iodide to crash out of solution, this was then filtered off and the remaining solution was allowed to evaporate. The resulting solid was collected and dried under vacuum at $120\,^{\circ}C$ overnight before being transferred to a dry argon filled glovebox ($< 1\,ppm$ H_2O, $< 10\,ppm$ O_2).

4.2.4 Instrumentation

Electrochemical experiments were carried out on a Bio-Logic VMP2 (Variable Multi-channel Potentiostat).

4.2.5 Cell Design

The cyclic voltammetry shown in this chapter was carried out in two compartment glass cells as described in Chapter 2, section 2.2. This allowed a certain amount of separation of ethyl viologen in the working electrode compartment from the lithium metal anode in the counter/reference electrode compartment. The

electrolyte used in these cells consisted of $100\ mM$ LiTFSI, $Pyr_{14}TFSI$. In the working electrode compartment ethyl viologen was added as specified.

The potential step experiments shown in this chapter warranted the design of new cells. To accommodate the high surface area working electrode a one compartment cell was used with a porous separator as shown in Diagram 4.5. The design of the cell allowed for the electrolyte to be agitated during electrochemical reduction thus increasing the rate at which the ethyl viologen was reduced, rather than relying on diffusion alone. The electrolyte in these cells consisted of $100\ mM$ LiTFSI, $Pyr_{14}TFSI$. $5\ mM$ $EtV(OTf)_2$ was added as specified.

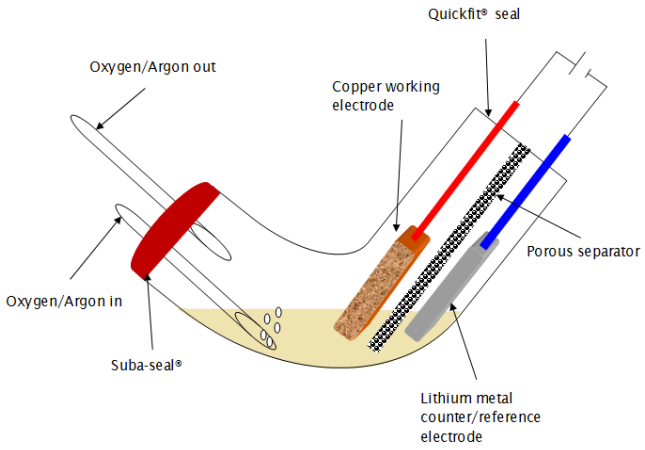

Diagram 4.5. Ethyl viologen electrolysis cell.

A second ethyl viologen reduction cell was then designed to try and overcome some of the limitations associated with the initial cell shown in Diagram 4.5. In this cell rather than using lithium metal as a counter/reference electrode, Li_1FePO_4 was used as the counter electrode and $Li_{0.5}FePO_4$ was used as the reference electrode. Copper foam was again used as the working electrode. The electrolyte used in these cells was $100\ mM$ LiTFSI, acetonitrile with $2\ mM$ $EtV(OTf)_2$. A diagram showing the cell geometry of this redesigned cell is shown in Diagram 4.6.

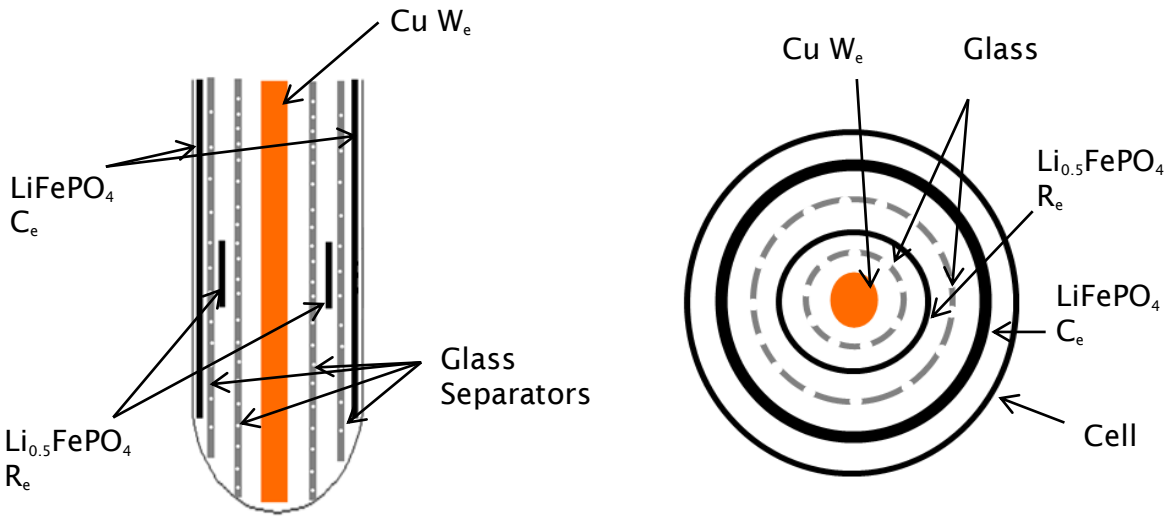

Diagram 4.6. Redesigned ethyl viologen electrolysis cell.

The galvanostatic work shown in this chapter was carried out in a mixture of two compartment glass cells and Swagelok cells as described in Chapter 2, section 2.2.

4.3 Results and Discussion

4.3.1 Electrochemical Investigation of Ethyl Viologen Ditriflate

To understand how a catalyst might affect the discharge reaction of a Li-O_2 cell it is important to first understand the oxygen reduction reaction in an uncatalysed system. To this end the voltammetry of oxygen reduction in $100\,mM$ LiTFSI, $Pyr_{14}TFSI$ at a scan rate of $20\,mV\,s^{-1}$ is shown in Figure 4.1 (red trace). The voltammetry under an argon atmosphere is also shown (black trace). It is clear from the CV carried out in argon that in the absence of oxygen only double layer charging was seen.

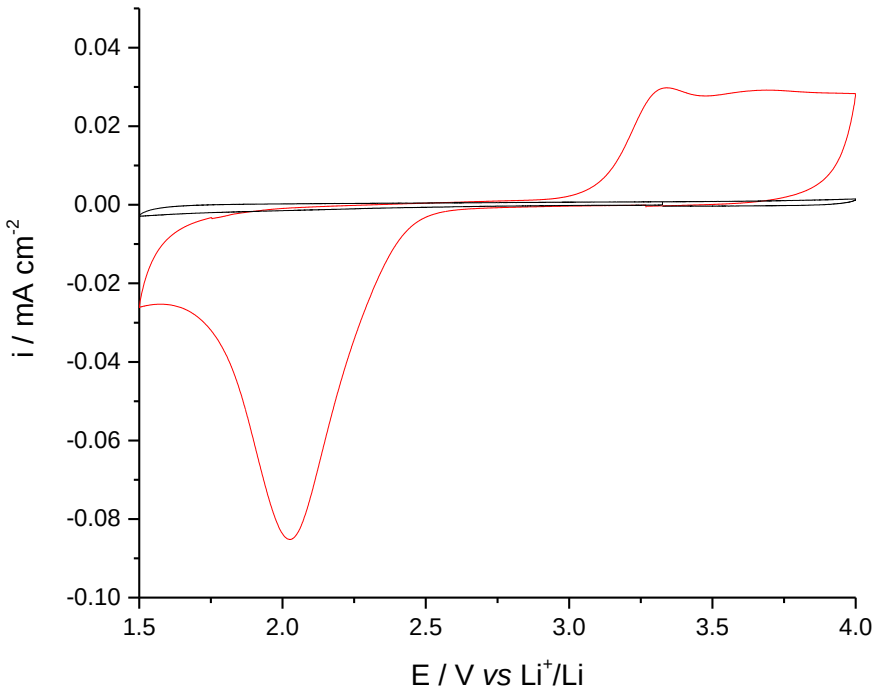

Figure 4.1. Cyclic voltammetry data recorded in $\mathbf{100\,mM}$ LiTFSI, $Pyr_{14}TFSI$ on a $\mathbf{3\,mm}$ Ø glassy carbon (GC) electrode. The scans were recorded at a scan rate of $\mathbf{20\,mV\,s^{-1}}$. (—) Recorded under an argon atmosphere. (—) Recorded in an oxygen saturated electrolyte.

When cycling in oxygen, as the potential of the working electrode was scanned below $2.5\ V\ vs\ Li^+/Li$ a large reductive current was observed with a peak at ~$2.0\ V\ vs\ Li^+/Li$. This is ascribed to the reduction of oxygen on the electrode surface that results in the formation of lithium peroxide as the final product. This is in accordance with the data reported in the literature for the $Pyr_{14}TFSI$ electrolyte.[17-19] This reaction proceeds *via* one or both of the reaction pathways shown in Scheme 4.1 and Scheme 4.2.

$$O_2 + e^- + Li^+ \rightarrow LiO_2 \qquad step\ 1$$

$$2LiO_2 \rightarrow Li_2O_2 + O_2 \qquad step\ 2$$

Scheme 4.1

$$O_2 + e^- + Li^+ \rightarrow LiO_2 \qquad step\ 1$$

$$LiO_2 + e^- + Li^+ \rightarrow Li_2O_2 \qquad step\ 2$$

Scheme 4.2

The reaction path that is followed is likely to be dependent on the conditions present in the cell. Xue *et al.* have recently highlighted the importance of the donor number of a solvent on the solubility of lithium superoxide.[2] In a solvent with a greater lithium superoxide solubility the lithium superoxide is liable to diffuse away from the electrode surface, therefore the formation of lithium peroxide is likely to follow the disproportionation route shown in Scheme 4.1. Yang *et al.* recently demonstrated conditions under which lithium superoxide was shown to be stable in solution over a number of hours.[16] In a cell operating under these conditions it would be expected that the formation of lithium peroxide over short time periods would proceed *via* Scheme 4.2. However, Scheme 4.1 could be

favoured by the presence of an electrode surface (*via* the heterogeneous catalysis of the disproportionation reaction).

As the potential of the working electrode was scanned positive from $1.5\ V\ vs\ Li^+/Li$ only a small amount of current was seen between $1.5 - 3.0\ V\ vs\ Li^+/Li$. This is indicative of electrode passivation, a process which is not seen in electrolytes that do not contain lithium salt.[17, 20]

Above $3.0\ V\ vs\ Li^+/Li$ current responses due to oxidation were seen. These oxidation processes are associated with the oxidation of lithium peroxide back to lithium and oxygen (Scheme 4.3). The exact reaction pathway still remains unclear however Peng *et al.* have provided spectroscopic evidence that suggests the reaction pathway during oxidation does not proceed *via* lithium superoxide.[21]

$$Li_2O_2 \rightarrow 2Li^+ + O_2 + 2e^-$$

Scheme 4.3

The cause of the multiple oxidation processes seen in Li-O_2 cells has previously been ascribed to the oxidation of lithium superoxide followed by the oxidation of lithium peroxide.[22] In theory this could be seen in cells using electrolytes that prolong the lifetime of lithium superoxide. However it is now more commonly accepted that the multiple oxidation processes seen are a result of the oxidation of lithium peroxide that has been deposited in differing morphologies.[23, 24]

By integrating between $2.0 - 1.5\ V\ vs\ Li^+/Li$ and $3.0 - 4.0\ V\ vs\ Li^+/Li$ respectively the reductive and oxidative charge was found to be $0.153\ mC$ and $0.092\ mC$ respectively. This shows an imbalance between the number of moles of Li_2O_2 formed on reduction ($7.9 \times 10^{-10}\ moles$) and the number of moles that are oxidised ($4.7 \times 10^{-10}\ moles$). To increase the number of moles of Li_2O_2 that are

oxidised the potential limits the cell was cycled between could be extended above $4.0\ V\ vs\ Li^+/Li$. However it has been shown that when using carbon positive electrodes, including glassy carbon electrodes, when the potential was increased above $4.0\ V\ vs\ Li^+/Li$ the electrode began to degrade.[25] Therefore to quantify the increase in the amount of Li_2O_2 oxidised when charging above $4.0\ V\ vs\ Li^+/Li$, cyclic voltammetry would have to be linked with a quantative method of analysis such as differential electrochemical mass spectroscopy (DEMS). It is also recommended that DEMS be used even when cycling below $4.0\ V\ vs\ Li^+/Li$, to confirm that only lithium peroxide is being oxidised.

The effect of the incomplete oxidation of Li_2O_2 is evident during subsequent cycles where the current passed, and therefore the capacity, on both reduction and oxidation is seen to decrease (Figure 2, Appendix A). This passivation is caused by the build-up of lithium peroxide on the electrode surface and is one of the major limitations of the Li-O_2 cell.

Having investigated the behaviour of oxygen reduction and evolution in $100\ mM$ LiTFSI, $Pyr_{14}TFSI$ the electrochemical behaviour of ethyl viologen ditriflate ($EtV(OTf)_2$) in this electrolyte was investigated.

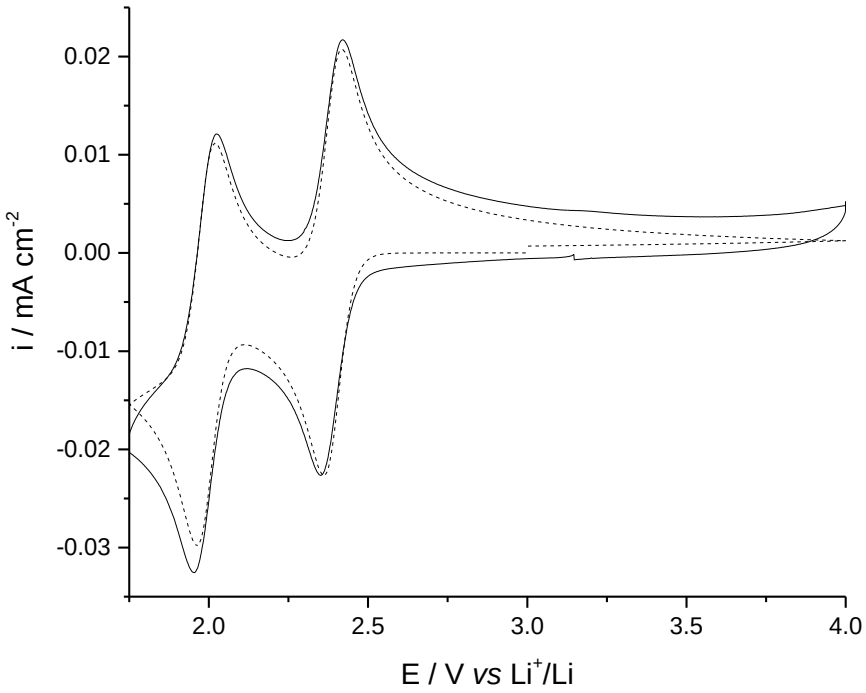

Figure 4.2. Cyclic voltammetry of $\mathbf{2}\,\boldsymbol{mM}$ EtV(OTf)$_2$ in $\mathbf{100}\,\boldsymbol{mM}$ LiTFSI, Pyr$_{14}$TFSI under an argon atmosphere. A GC electrode was used as the working electrode with a lithium counter/reference electrode. A scan rate of $\mathbf{20}\,\boldsymbol{mV\,s^{-1}}$ was used. A fit of the experimental data is also shown and is indicated by the dotted line; $\boldsymbol{D = 8.87 \times 10^{-8}\,cm^2 \cdot s^{-1}}$, $\boldsymbol{k_s > 0.1\,cm \cdot s^{-1}}$, $\boldsymbol{v = 20\,mV \cdot s^{-1}}$.

The electrochemical behaviour of $2\ mM$ ethyl viologen ditriflate was investigated in an electrolyte of $100\ mM$ LiTFSI, Pyr$_{14}$TFSI using cyclic voltammetry at a scan rate of $20\ mV\ s^{-1}$ the results of which are shown in Figure 4.2.

The viologen dication undergoes two electrochemically reversible redox processes according to Scheme 4.4. The first redox process seen when scanning negative is associated with step 1, this is in accordance with the literature.[26] The second redox process is therefore associated with the process shown in step 2.

$$EtV^{2+} + e^- \rightleftharpoons EtV^+ \qquad E^0 = 2.39\ V\ vs\ Li^+/Li \qquad step\ 1$$

$$EtV^+ + e^- \rightleftharpoons EtV^0 \qquad E^0 = 1.99\ V\ vs\ Li^+/Li \qquad step\ 2$$

Scheme 4.4

Through the application of the Randles-Sevcik equation (Equation 4.1) it is possible to estimate a diffusion coefficient, $8.87 \times 10^{-8}\ cm^2 \cdot s^{-1}$, for the EtV^{2+} cation in $100\ mM$ LiTFSI, $Pyr_{14}TFSI$.

$$i_p = 0.4463nFAC(\frac{nF\nu D}{RT})^{1/2}$$

Equation 4.1. Randles-Sevcik equation

Where:

i_p = peak current (A)

n = number of moles of electrons

F = Faradays constant ($96485\ As \cdot mol^{-1}$)

A = surface area of the electrode (cm^2)

C = concentration of the Ox. or Red. species ($mol \cdot l^{-1}$)

D = diffusion coefficient of the Ox. or Red. species ($cm^2 \cdot s^{-1}$)

v = scan rate ($V \cdot s^{-1}$)

R = gas constant ($8.314\ J \cdot K^{-1}mol^{-1}$)

T = temperature (K)

The high degree of electrochemical reversibility seen for the EtV^{2+}/EtV^{+} redox couple is indicative of fast electron transfer kinetics. Using the diffusion coefficient shown above it is possible to probe the electron transfer kinetics using cyclic voltammetry simulation software. A comparison of the experimental and simulated data of ethyl viologen cycling in $100\ mM$ LiTFSI, $Pyr_{14}TFSI$ is shown in Figure 4.2. An electron transfer rate constant (k_s) of $> 0.1\ cm \cdot s^{-1}$ was used during the simulation as this is typical of fast electron transfer kinetics.
The simulated data shown in Figure 4.2 is a close fit to the experimental data collected for ethyl viologen cycling. This therefore supports the suggestion that ethyl viologen undergoes fast electron transfer.

The redox potential of the EtV^{2+}/EtV^{+} reaction is negative of that of the thermodynamic potential of lithium peroxide formation, $2.96\ V\ vs\ Li^{+}/Li$, this suggests that EtV^{+} maybe capable of satisfying the thermodynamic requirements for the chemical reduction of oxygen to lithium peroxide. This can be confirmed by determining the standard Gibbs free energy (ΔG^{0}) of the ethyl viologen mediated oxygen reduction reaction:

$$2EtV^{+} + O_2 + 2Li^{+} \rightarrow 2EtV^{2+} + Li_2O_2$$

$$\Delta G^{0} = (-nFE^{0})_{O_2/Li_2O_2} - 2(-nFE^{0})_{EtV^{2+}/EtV^{+}}$$

Where:

ΔG^{0} = Standard Gibbs free energy of reaction ($kJ \cdot mol^{-1}$)

n = number of moles of electrons

F = Faradays constant ($96485\ C \cdot mol^{-1}$)

E^{0} = Standard potential of the reaction ($V\ vs\ Li^{+}/Li$)

This gives a ΔG^{0} of $-109\ kJ \cdot mol^{-1}$ confirming that the mediated reduction of oxygen by ethyl viologen is thermodynamically favourable.

Having independently established the cycling behaviour of both oxygen and ethyl viologen in $100\ mM$ LiTFSI, $Pyr_{14}TFSI$ and established that there is a thermodynamic driving force for the mediation reaction the interaction between ethyl viologen and oxygen was then investigated through the use of cyclic voltammetry. The results of this investigation are shown in Figure 4.3.

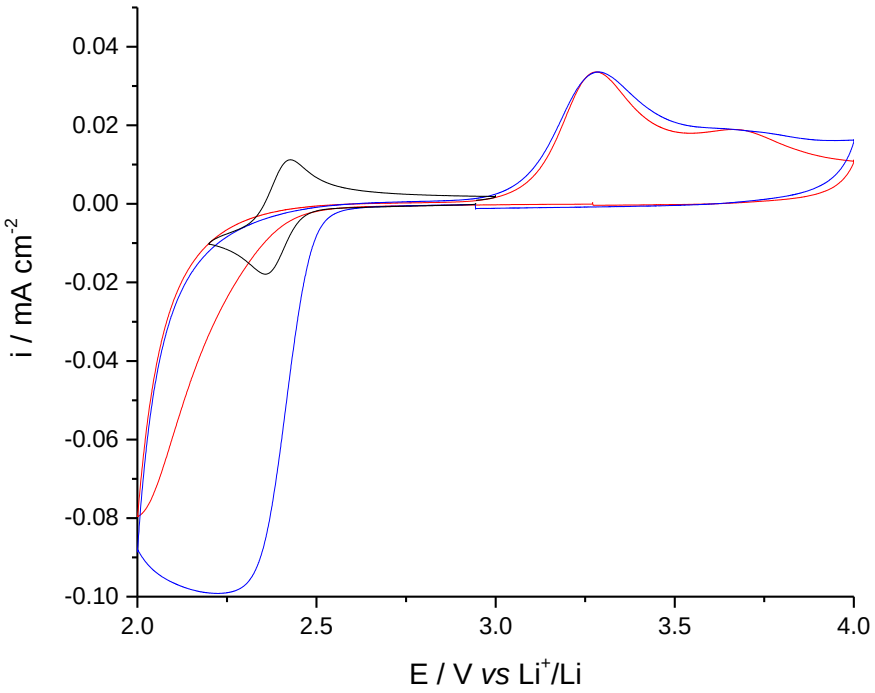

Figure 4.3. Cyclic voltammetry $\boldsymbol{100\ mM}$ LiTFSI, $Pyr_{14}TFSI$ on a GC working electrode with a lithium metal counter/reference electrode. A scan rate of $\boldsymbol{20\ mV\ s^{-1}}$ was used. (—) $\boldsymbol{2\ mM}$ $EtV(OTf)_2$ in argon. (—) $\boldsymbol{2\ mM}$ $EtV(OTf)_2$ in oxygen saturated electrolyte. (—) Oxygen saturated electrolyte.

In Figure 4.3 only the first redox process of EtV^{2+} is shown (black trace) as this is the process that is of most interest in the catalysis of the oxygen reduction reaction. The reason for this is that the standard potential of the second redox process of ethyl viologen, $1.99\ V\ vs\ Li^+/Li$, is significantly lower than the onset potential of oxygen reduction in $100\ mM$ LiTFSI, $Pyr_{14}TFSI$, ~$2.5\ V\ vs\ Li^+/Li$. Therefore, EtV^0 is not expected to be formed in significant amounts in a practical Li-O_2 cell. Furthermore, the EtV^0 molecule would be impractical for use as a catalyst as it would result in low round trip efficiencies in a practical cell. Further to this if EtV^+ is a good mediator of the oxygen reduction reaction the ethyl viologen molecule would not reach the EtV^0 state as the EtV^+ will be oxidised back to EtV^{2+} before it can undergo a second electron reduction (Diagram 4.7).

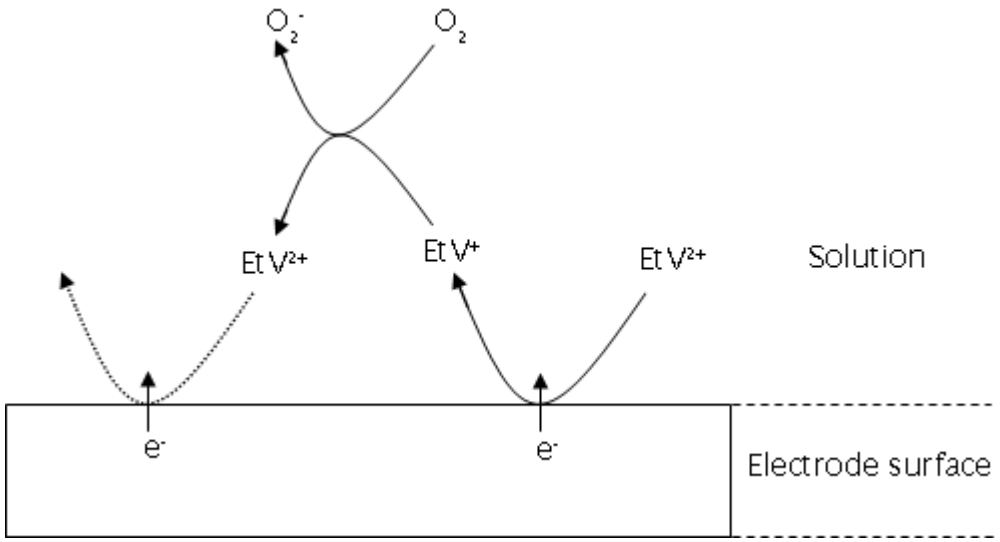

Diagram 4.7. Re-cycling of ethyl viologen at the electrode surface.

The effect of the addition of ethyl viologen to a cell with an oxygen saturated electrolyte (blue trace) is seen as an enhancement in the current density of the ethyl viologen reduction peak at $2.3\,V\ vs\ Li^+/Li$.

The increase in the reduction current density for the EtV^{2+}/EtV^{+} redox process can be explained by the mechanism shown in Diagram 4.7. EtV^{2+} is reduced at the electrode surface to EtV^{+} in a similar manner to that seen in argon. The newly formed EtV^{+} then goes on to reduce oxygen in the solution. At the same time this regenerates the EtV^{2+} close to the electrode surface. This EtV^{2+} can again be electrochemically reduced at the electrode surface. This cycle is repeated multiple times and results in the increase in the EtV^{2+} reduction current that is observed. The current seen during mediation is therefore proportional to the flux of mediator reacting at the surface of the electrode, as previously described by Albery *et al.*.[27] The increase in the peak current density of EtV^{2+} reduction therefore provides strong evidence that the oxygen reduction reaction is being mediated by EtV^{+}.

When scanning positive, between $2.0 - 2.75\ V\ vs\ Li^+/Li$, a peak pertaining to EtV^+ oxidation was not observed. The absence of this peak suggests that there was no EtV^+ present in the solution to be oxidised. It is suggested that this was a result of EtV^+ having been chemically oxidised through the reaction with oxygen. This provides further evidence that EtV^+ is catalysing the reduction of oxygen. The absence of a corresponding reduction/oxidation peak to the one that is mediating the reaction of interest is a well-documented phenomenon.[28] However, it should be noted that the absence of the oxidation peak could also result from electrode passivation, but it is not believed that this is the case as a reductive current was still seen when scanning from $2.0 - 2.5\ V\ vs\ Li^+/Li$.

As the potential of the working electrode was swept positive a large oxidative current was seen between $3.0 - 4.0\ V\ vs\ Li^+/Li$, with two associated oxidation peaks. These processes are seen at the same potential as those seen during oxidation in the absence of ethyl viologen (red trace), they are therefore associated with the oxidation of lithium peroxide. This in its self suggests that the end product of the ethyl viologen catalysed reduction of oxygen may be lithium peroxide.

It is interesting to note that the charge passed during oxidation in the presence of ethyl viologen was similar to that seen during oxidation in the absence of ethyl viologen, despite the large increase in charge during reduction. This suggests that the increased charge seen during reduction in the presence of ethyl viologen does not give rise to a significant increase in the quantity of lithium peroxide on the electrode surface. It is therefore suggested that through the use of a redox mediator the solution based formation of lithium peroxide was promoted according to Scheme 4.5 and Scheme 4.6, alongside the electrochemical reduction of oxygen to lithium peroxide. It has also recently been suggested that

the use of a soluble redox catalyst can help promote the formation of lithium oxide, Li_2O,[29] however based on the results shown here it was not possible to verify this.

$$EtV^{2+} + e^- \rightleftharpoons EtV^+ \qquad step\ 1$$

$$EtV^+ + O_2 + Li^+ \rightarrow EtV^{2+} + LiO_2 \qquad step\ 2$$

$$2LiO_2 \rightarrow Li_2O_2 \qquad Step\ 3$$

Scheme 4.5

$$EtV^{2+} + e^- \rightleftharpoons EtV^+ \qquad step\ 1$$

$$EtV^+ + O_2 + Li^+ \rightarrow EtV^{2+} + LiO_2 \qquad step\ 2$$

$$EtV^{2+} + e^- \rightleftharpoons EtV^+ \qquad step\ 3$$

$$EtV^+ + LiO_2 + Li^+ \rightarrow EtV^{2+} + Li_2O_2 \qquad step\ 4$$

Scheme 4.6

To help differentiate between the two reaction pathways shown in Scheme 4.5 and Scheme 4.6 UV-Vis spectroscopy was employed. Through the use of UV-Vis spectroscopy it was determined that ethyl viologen promotes the two electron reduction of O_2 to O_2^{2-} *via* O_2^- as shown in Scheme 4.6 (Figure 1, Appendix A). Further to this it was also shown that under certain conditions the pathway shown in Scheme 4.6 can be promoted over that shown in Scheme 4.5.[16]

4.3.2 Investigating the Stability of Ethyl Viologen Ditriflate

In the field of Li-O_2 cell research degradation reactions are a common problem.[30, 31] The possibility of irreversible reactions between ethyl viologen and superoxide should therefore not be ruled out. It could be suggested that the enhancement in

the current density seen during discharge in the presence of ethyl viologen, Figure 4.3, was the result of degradation reactions.

When investigating the interaction of ethyl viologen and the superoxide anion radical in non-aqueous media Sawyer *et al.* found that the superoxide anion can indeed react irreversibly with the ethyl viologen di-cation.[14]

To investigate the interaction between ethyl viologen and oxygen reduction products in $Pyr_{14}TFSI$ an electrolysing cell was employed. The cell consisted of a lithium metal negative electrode and a high surface area copper foam positive electrode in an electrolyte of $2\ mM$ $EtV(OTf)_2$ $Pyr_{14}TFSI$ with varying concentrations of lithium salt.

Reduction of EtV^{2+} to EtV^{+} was carried out by applying a constant potential of $2.2\ V\ vs\ Li^+/Li$ until $1/5^{th}$ of the ethyl viologen present had been reduced. The reduction of ethyl viologen resulted in a colour change of the solution from colourless (EtV^{2+}) to blue (EtV^{+}).

Two different lithium salt concentrations were used during these experiments. Under the first set of conditions the lithium concentration was kept extremely low ($0\ mM$ lithum salt was added). Under the second set of conditions a lithium salt concentration of $300\ mM$ was employed.

Following the electrochemical reduction of ethyl viologen a chemical oxidation step was carried out. The chemical step required oxygen to be bubbled through the cell. This resulted in the bleaching of the blue colour associated with the EtV^{+}. This was a result of the EtV^{+} reducing oxygen and in turn being oxidised back to EtV^{2+}.

Following this chemical step the electrolyte was purged of any remaining oxygen, by bubbling with argon. The procedure was then repeated.

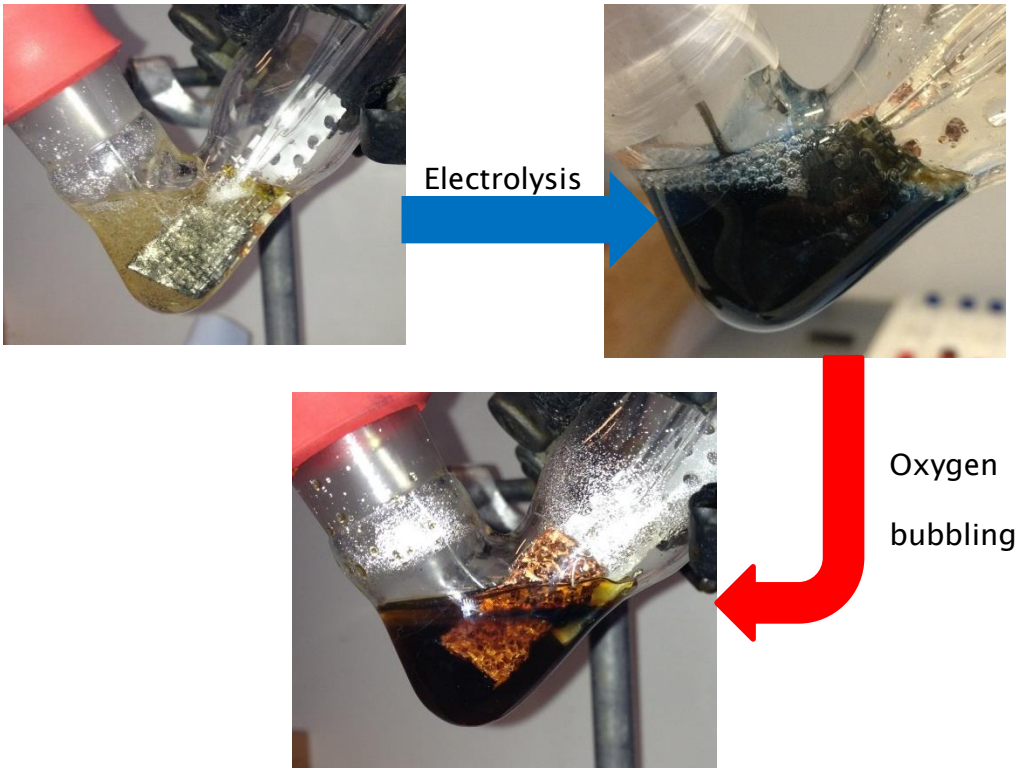

Figure 4.4. Images of the cycling behaviour of a solution of $2\,mM$ $EtV(OTf)_2$ in $Pyr_{14}TFSI$, with no added lithium salt, after electrochemical and chemical cycling. The blue arrow represents an electrolysis step while the red arrow represents a chemical step (bubbling with oxygen).

Figure 4.4 shows the results obtained when no lithium salt was added to the electrolyte. The initial electrochemical reduction of EtV^{2+} resulted in an intense blue solution that was associated with the production of EtV^{+}. This solution was then bubbled with oxygen resulting in the chemical oxidation of EtV^{+} by oxygen, which in turn resulted in the reduction of oxygen to superoxide.[16]

This chemical step resulted in a brown solution, rather than the colourless solution that was seen at the start of the experiment. When a further electrochemical reduction step was carried out the current obtained was less than $1/8^{th}$ the current seen during the initial electrochemical step (see Figure 3, in Appendix A). Further to the low current seen during the second electrochemical reduction the blue colour of the solution seen after the initial electrolysis step was not seen again. It is therefore believed that this brown solution was the result

of the degradation products from the reaction of the ethyl viologen di-cation, EtV^{2+}, with the superoxide anion according to Scheme 4.7.

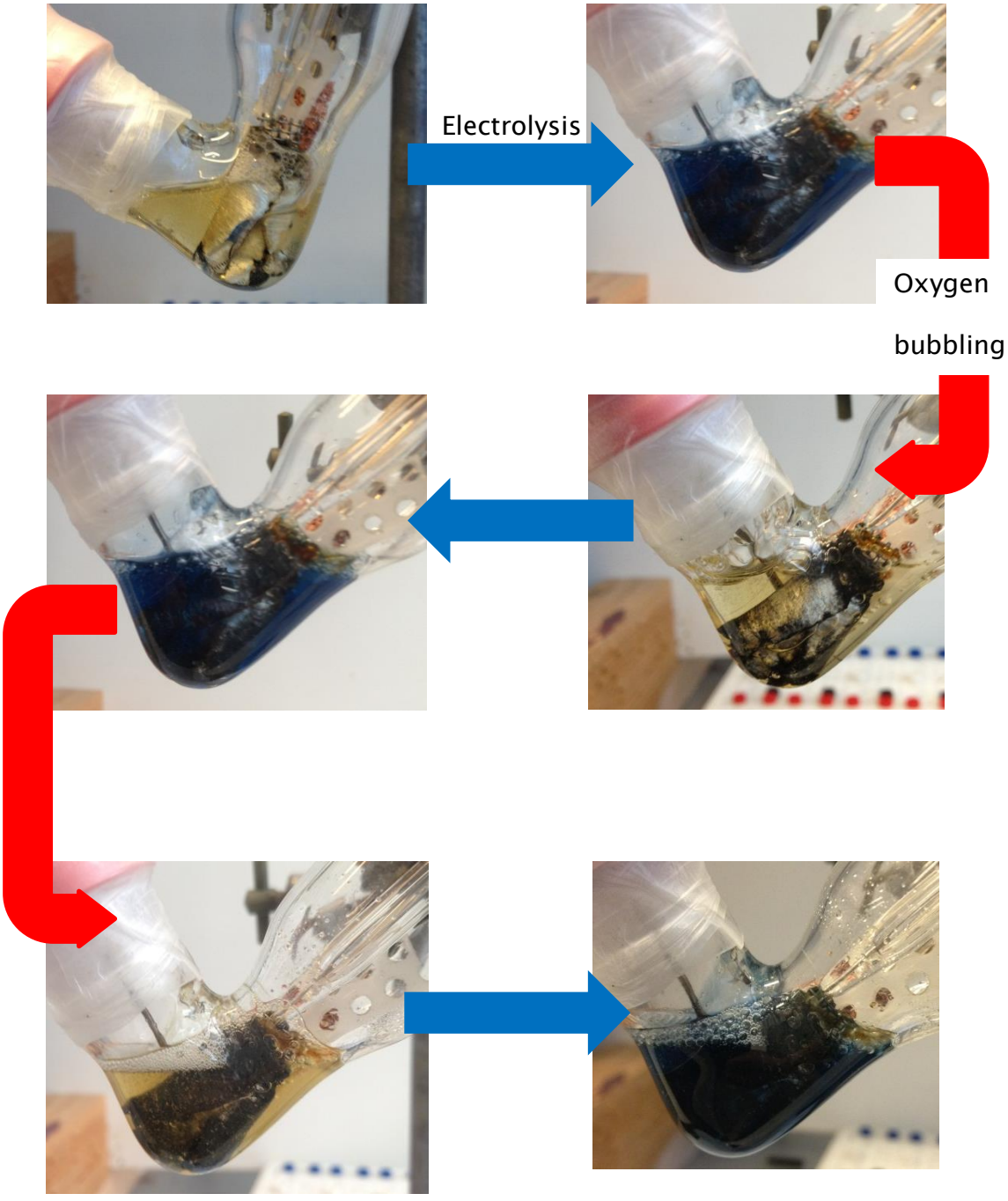

Figure 4.5. Images of the cycling behaviour of a solution of $\mathbf{2}\ \boldsymbol{mM}$ $EtV(OTf)_2$ in $\mathbf{300}\ \boldsymbol{mM}$ LiTFSI, $Pyr_{14}TFSI$ after electrochemical and chemical cycling. The blue arrows represents electrolysis steps while the red arrows represent chemical steps (bubbling with oxygen).

The electrochemical and chemical cycling behaviour of a cell containing a high lithium salt concentration of $300\,mM$ LiTFSI is shown in Figure 4.5. During the initial electrolysis step the cell behaved in a similar fashion to the cell shown in Figure 4.4, with ethyl viologen being reduced to give way to an intense blue solution associated with the production of EtV^{+}. After the first chemical oxidation step (by bubbling with oxygen) the blue colour was bleached resulting in a colourless solution. When this solution underwent a second electrochemical reduction step the blue colour of the reduced viologen was again observed along with a current of similar magnitude to that seen during the initial electrochemical step. This cycling behaviour was repeated over several cycles as shown in Figure 4.6.

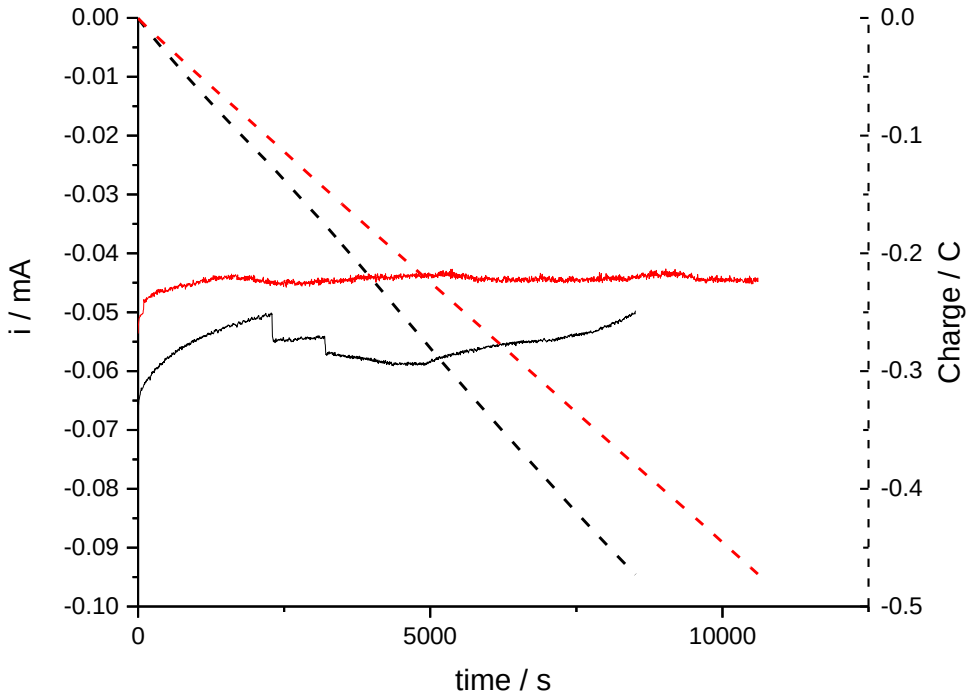

Figure 4.6. Results from constant potential experiments in a 'bleaching' cell with $\mathbf{2\,mM}$ $EtV(OTf)_2$, $\mathbf{300\,mM}$ LiTFSI, $Pyr_{14}TFSI$. Copper mesh was used as the working electrode and lithium metal was used as the counter/reference electrode. (—) Reduction cycle 1, (—) reduction cycle 3.

In Figure 4.6 it is apparent that there was a slight reduction in the magnitude of the current seen between the first and third cycle. When cycling in a solution with $0\ mM$ added lithium salt, Figure 4.4, this would indicate the breakdown of ethyl viologen through reaction with superoxide. However, in the case of the solution with $300\ mM$ added lithium salt, Figure 4.5, it is thought that this gradual reduction in the current was the result of a build of a passivating layer on the lithium metal electrode. It is thought that this layer was formed as a result of the viologen being in contact with the extremely reducing lithium metal, and also as a result of the lithium metal coming into contact with oxygen.

Based on the differences seen between the two cells shown in Figure 4.4 and Figure 4.5 it can be concluded that when low lithium salt concentration were used degradation reactions occurred which adversely affected the mediator action of ethyl viologen. In accordance with previously published results it is believed that these degradation reactions result from the generated superoxide attacking EtV^{2+} as shown in Scheme 4.7.[14] Further to this it has been shown that through the addition of lithium cations to the electrolyte these degradation reactions can be impaired. It is thought that the inclusion of lithium cations in the solution helps to stabilise the superoxide anions through the formation of lithium superoxide. This may then go on to form lithium peroxide *via* a disproportionation reaction or a second chemical reduction step as detailed in Scheme 4.7.

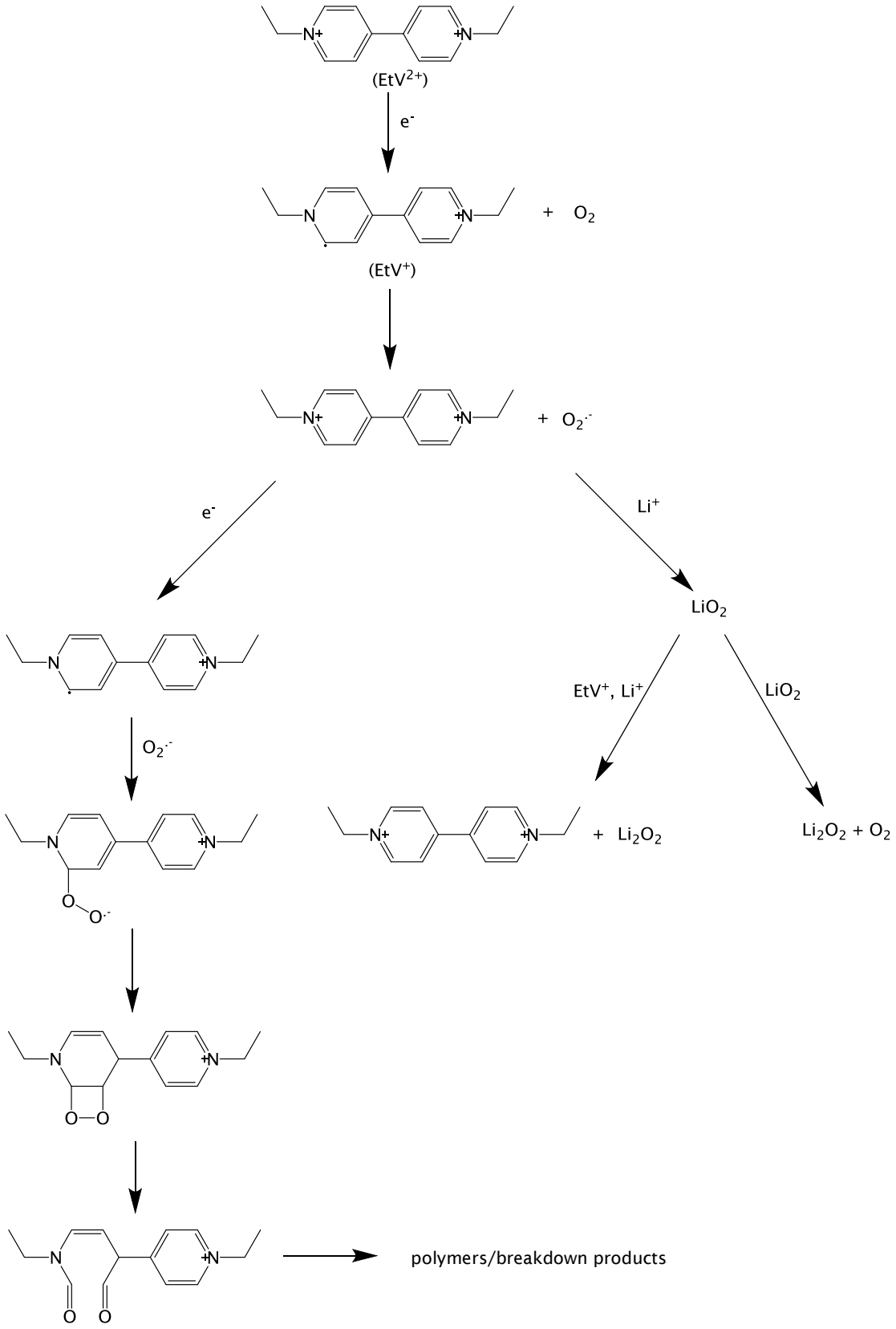

Scheme 4.7. Reaction pathways available in cells containing $EtV(OTf)_2$ and oxygen depending on the concentrations of lithium salt present. The degradation path shown has been adapted from that proposed by Sawyer *et al.*.[14]

This electrochemical/chemical cycling experiment was then repeated using a modified cell design with a $LiFePO_4$ counter electrode and a $Li_{0.5}FePO_4$ reference electrode as described in section 4.2.5. It was hoped that by using a negative electrode that was not lithium metal it would be possible to avoid the passivation of the counter electrode. This in turn would increase the number of cycles that could be achieved. Figure 4.7 shows the current response and associated charge data collected during potentiostatic experiments.

The changes in the current seen between cycles are as a result of the changes in the degree of agitation of the solution. However what is clear from this data is that it was possible to repeatedly perform electrochemical reduction of the ethyl viologen followed by chemical oxidation through exposure to oxygen for over 50 cycles. This shows that under the right conditions the degradation reactions between ethyl viologen and superoxide can be impeded.

It should be noted that in this cell, although there was little evidence of degradation reactions it was concluded that there were secondary reactions occurring between the $Li_{0.5}FePO_4$ reference electrode and the reduced form of ethyl viologen:

$$EtV^+ + 2Li_{0.5}FePO_4 + Li^+ \rightarrow EtV^{2+} + 2LiFePO_4$$

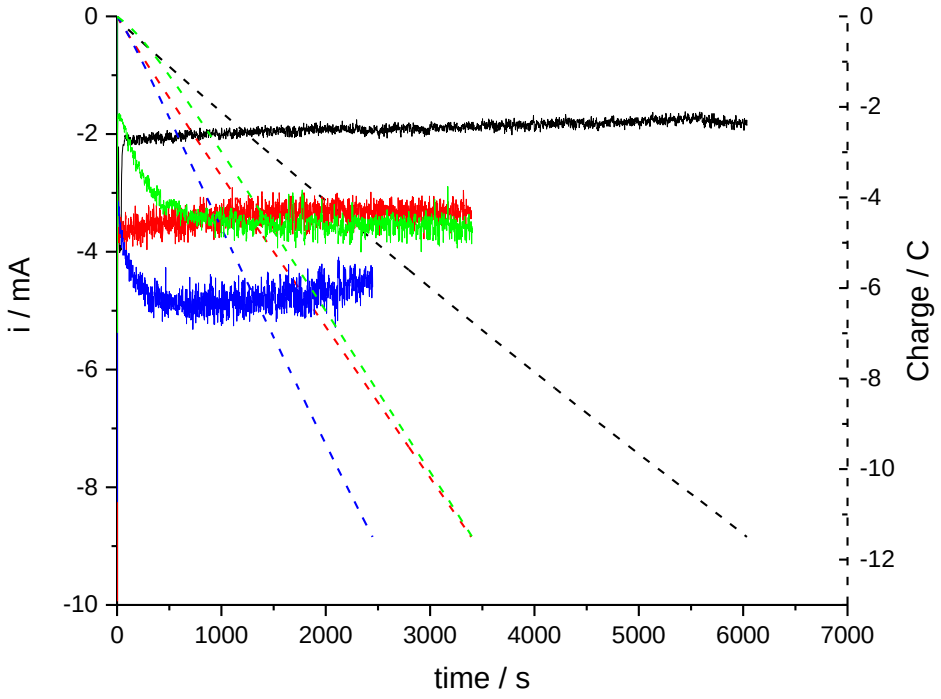

Figure 4.7. Results from constant potential experiments in a modified bleaching cell. Copper mesh was used as the working electrode, Li_1FePO_4 as the counter electrode and $Li_{0.5}FePO_4$ as the reference electrode. An electrolyte of $\boldsymbol{100\,mM}$ LiTFSI, acetonitrile was used containing $\boldsymbol{2\,mM}$ $EtV(OTf)_2$. (—) Reduction cycle 5, (—) reduction cycle 15 (—) reduction cycle 30 and (—) reduction cycle 54.

4.3.3 Investigations into the Galvanostatic Cycling Behaviour of Ethyl Viologen Ditriflate

Having identified conditions under which the reduction of oxygen by EtV^+ results in the desired oxygen reduction products, rather than breakdown products, the enhancement offered by ethyl viologen under practical battery operating conditions was investigated. To this end Galvanostatic cycling was used to investigate the effect of ethyl viologen mediation on the discharge capacity of a Li-O_2 cell.

During initial investigations a two compartment glass cell was used with a glassy carbon electrode working electrode and lithium metal as the counter/reference electrode. $100\ mM$ LiTFSI, $Pyr_{14}TFSI$ was used as the electrolyte.

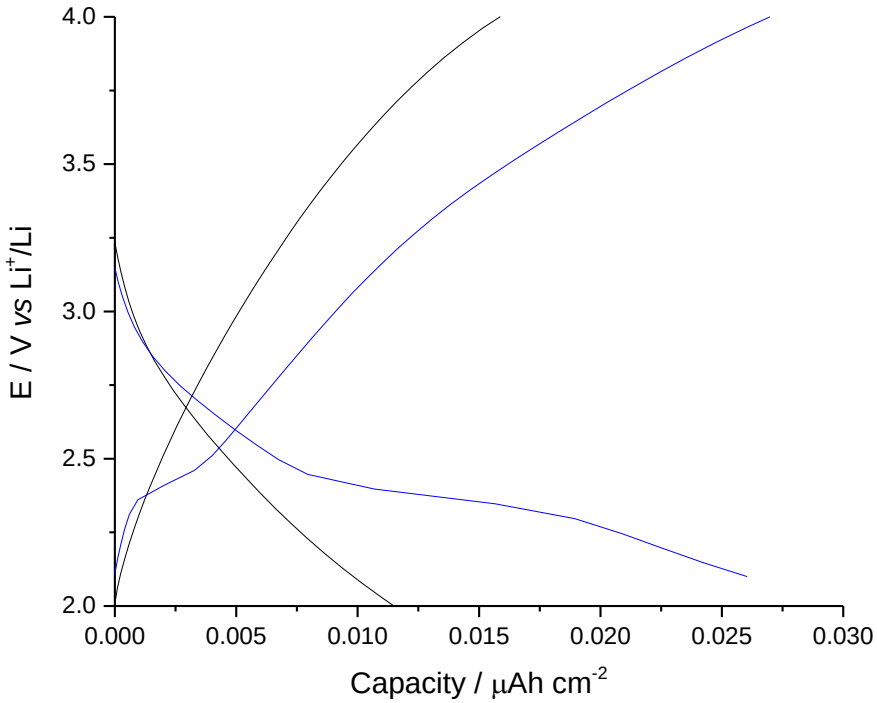

Figure 4.8. Galvanostatic measurments in $\mathbf{100}\ \boldsymbol{mM}$ LiTFSI, $Pyr_{14}TFSI$ under an argon atmosphere on a $\mathbf{3}\ \boldsymbol{mm}$ Ø GC working electrode in a two compartment cell. Lithium metal was used as a counter/reference electrode. The measurments were carried out at a current density of $\mathbf{20}\ \mu\boldsymbol{A} \cdot \boldsymbol{cm^{-2}}$. (—) $\mathbf{0}\ \boldsymbol{mM}$ $EtV(OTf)_2$, (—) $\mathbf{0.5}\ \boldsymbol{mM}$ $EtV(OTf)_2$.

Measurements were first carried out in an argon atmosphere at a current density of $20\ \mu A \cdot cm^{-2}$ and are shown in Figure 4.8. The cell that contained no ethyl viologen (black trace) exhibited only double layer charging ($1.1 \times 10^{-2}\ \mu Ah \cdot cm^{-2}$ during discharge), while the cell containing $0.5\ mM$ ethyl viologen (blue trace) exhibited a larger capacity, $2.6 \times 10^{-2}\ \mu Ah \cdot cm^{-2}$. This was due to the reduction of the ethyl viologen dication, during charge a corresponding capacity was seen due to the oxidation of EtV^{+}. Through the use of the Sand equation (Equation 4.2) it is possible to estimate a diffusion coefficient, D, for the EtV^{2+} cation.

$$j\tau^{1/2} = \frac{nFD^{1/2}C\pi^{1/2}}{2}$$

Equation 4.2. Sand equation

Where:

j = current density ($mA \cdot cm^{-2}$)

τ = transition time (s)

n = number of moles of electrons

F = Faradays constant (96487 $C \cdot mol^{-1}$)

D = diffusion coefficient ($cm^2 \cdot s^{-1}$)

C = concentration ($mol \cdot cm^{-3}$)

Using this equation a diffusion coefficient of $1.21 \times 10^{-7}\ cm^2 \cdot s^{-1}$ was estimated for the ethyl viologen di-cation in $100\ mM$ LiTFSI, $Pyr_{14}TFSI$. This is approximately one and a half times the diffusion coefficient estimated when using the Randles-Sevcik equation, $8.87 \times 10^{-8}\ cm^2 \cdot s^{-1}$. The discrepancy seen in the two calculated diffusion coefficients can be put down to several influencing factors; when preparing dilute solutions systematic errors in solution preparation are likely to have contributed to the observed discrepancy. While when carrying out galvanostatic cycling in argon the discharge and charge times were only several seconds, therefore a small change in the determined transition time could result in a relatively large change in the determined diffusion coefficient.

Compared to the diffusion coefficient for oxygen in pure $Pyr_{14}TFSI$ of $1.2 \times 10^{-5}\ cm^2 \cdot s^{-1}$ the diffusion coefficient of EtV^{2+} is relatively small.[20] Measuring the diffusion coefficient of oxygen in a solvent containing a lithium salt is of course challenging. This is due to the complications it entails, such as the formation of lithium peroxide on the electrode surface which results in a change in the active surface area over the course of the measurement. The diffusion coefficient of oxygen in $Pyr_{14}TFSI$ would be expected to decrease as the concentration of the

lithium salt is increased. This is a result of the increase in the viscosity with increasing lithium salt concentration. However, even in an electrolyte of $100\ mM$ LiTFSI, $Pyr_{14}TFSI$ the diffusion coefficient of oxygen would still be greater than that of ethyl viologen. This is of interest as the relationship of the two diffusion coefficients is likely to influence their interaction in a cell.

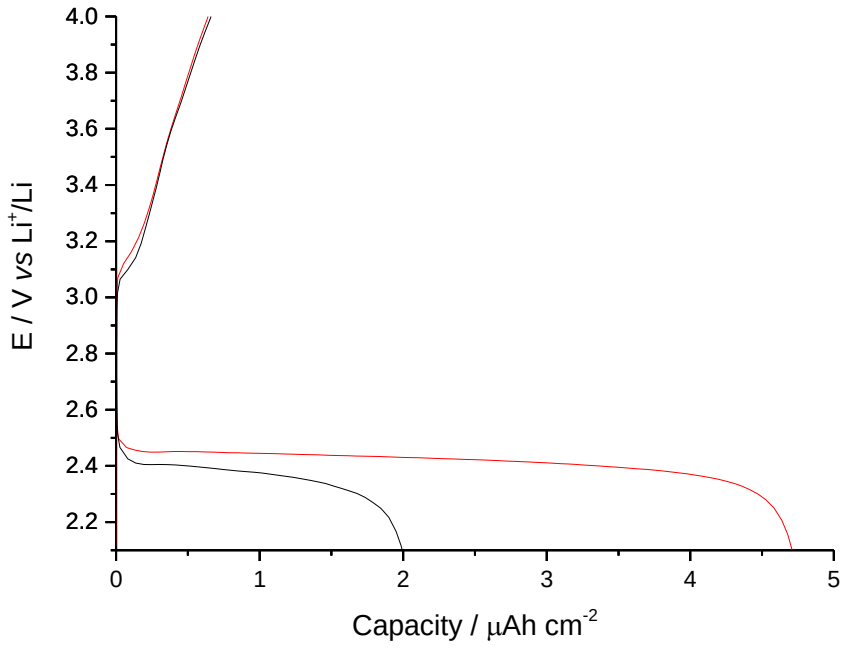

Figure 4.9. Galvanostatic measurments in oxygen saturated $\mathbf{100}\ \boldsymbol{mM}$ LiTFSI, $Pyr_{14}TFSI$ on a $\mathbf{3}\ \boldsymbol{mm}$ Ø GC working electrode in a two compartment cell. Lithium metal was used as a counter/reference electrode. The measurments were carried out at a current density of $\mathbf{20}\ \mu\boldsymbol{A} \cdot \boldsymbol{cm^{-2}}$. (—) $\mathbf{0}\ \boldsymbol{mM}$ $EtV(OTf)_2$, (—) $\mathbf{0.5}\ \boldsymbol{mM}$ $EtV(OTf)_2$.

When undergoing a galvanostatic discharge in an oxygen saturated electrolyte without a redox mediator (red trace) a capacity of $2.0\ \mu Ah \cdot cm^{-2}$ was achieved. This is in keeping with the findings of Johnson *et al.* when using glassy carbon electrodes.[32] When a galvanostatic discharge was repeated under the same conditions but with an oxygen saturated electrolyte containing $0.5\ mM$ $EtV(OTf)_2$ (blue trace) an almost two and a half fold increase in the capacity was observed, $4.7\ \mu Ah \cdot cm^{-2}$ (Figure 4.9). The observed increase in capacity cannot be accounted

for solely due to the increase in capacity as a result of EtV^{2+} reduction which would only increase the capacity by $2.6 \times 10^{-2}\ \mu Ah \cdot cm^{-2}$. It is therefore assumed that this increase in capacity was the result of the catalysis of the oxygen reduction reaction by EtV^{2+}, resulting in the final discharge product of lithium peroxide.

It is also of interest to note that the average discharge voltage seen in the cell containing $0.5\ mM$ $EtV(OTf)_2$ was ~$2.4\ V\ vs\ Li^+/Li$ compared to ~$2.3\ V\ vs\ Li^+/Li$ in the absence of ethyl viologen. This would be of use in a practical Li-O_2 cell where a higher discharge voltage would increase the round trip efficiency of the cell. When comparing the capacity seen during charging with and without a redox catalyst only a small fraction of the capacity seen on discharge was achieved in both cells. However for both cells the charging capacity was roughly the same, ~$0.7\ \mu Ah \cdot cm^{-2}$. This suggests that the majority of the lithium peroxide formed *via* the catalysed reduction of oxygen did so away from the electrode surface. It should also be noted that it is possible that the lithium peroxide was deposited on the electrode surface in a morphology that was not easily oxidised below $4.0\ V\ vs\ Li^+/Li$. The cycling behaviour seen in each cell can be used to examine this further.

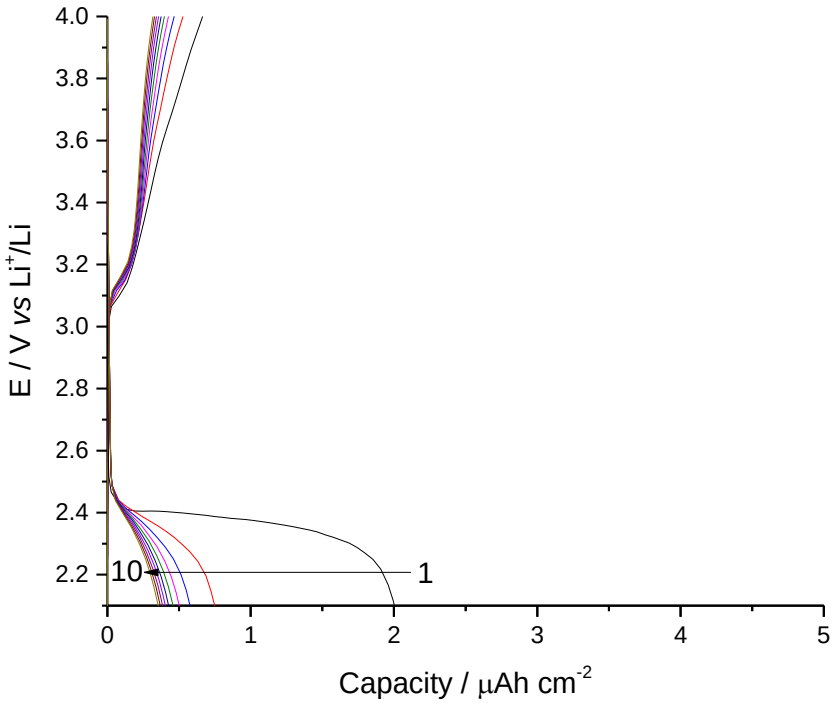

Figure 4.10. Galvanostatic measurments in oxygen saturated $\mathbf{0}\ \boldsymbol{mM}$ EtV^{2+}, $\mathbf{100}\ \boldsymbol{mM}$ LiTFSI, $Pyr_{14}TFSI$ on a $\mathbf{3}\ \boldsymbol{mm}$ Ø GC working electrode in a two compartment cell. Lithium metal was used as a counter/reference electrode. The measurments were carried out at a current density of $\mathbf{20}\ \mu\boldsymbol{A} \cdot \boldsymbol{cm}^{-2}$. The first 10 cycles are shown.

Figure 4.10 and Figure 4.11 show the data obtained during galvanostatic cycling over 10 cycles in $100\ mM$ LiTFSI, $Pyr_{14}TFSI$ with varying concentrations of $EtV(OTf)_2$. As is expected over multiple cycles of a Li-O_2 cell the capacity quickly fades. This is due to the build-up of lithium peroxide on the electrode surface.

The capacity seen on the second discharge in the cell containing $EtV(OTf)_2$ (Figure 4.11), $1.0\ \mu Ah \cdot cm^{-2}$, was larger than that seen in the absence of $EtV(OTf)_2$ (Figure 4.10), $0.7\ \mu Ah \cdot cm^{-2}$. This suggests that the passivation of the electrode surface after the first discharge did not vary significantly between the two cells. This therefore adds weight to the suggestion that the majority of the lithium peroxide formed *via* the catalysed reduction of oxygen did so away from the electrode surface.

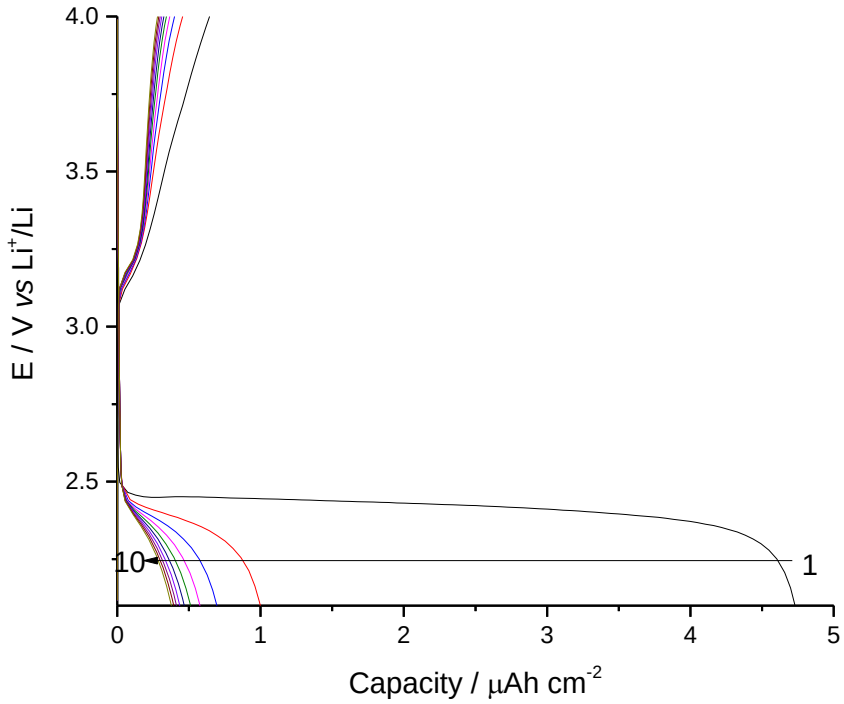

Figure 4.11. Galvanostatic measurments in oxygen saturated $\mathbf{0.5}\ \boldsymbol{mM}$ EtV^{2+}, $\mathbf{100}\ \boldsymbol{mM}$ LiTFSI, $Pyr_{14}TFSI$ on a $\mathbf{3}\ \boldsymbol{mm}$ Ø GC working electrode in a two compartment cell. Lithium metal was used as a counter/reference electrode. The measurments were carried out at a current density of $\mathbf{20}\ \mu\boldsymbol{A} \cdot \boldsymbol{cm}^{-2}$. The first 10 cycles are shown.

Having investigated the galvanostatic cycling behaviour of ethyl viologen in a two compartment glass cell it was important to see if this behaviour was still seen in a more practical cell design. To carry out this work a Swagelok cell utilizing an Ohara glass separator with valves allowing the cell to be flushed with oxygen was designed (see Chapter 2, section 2.2).

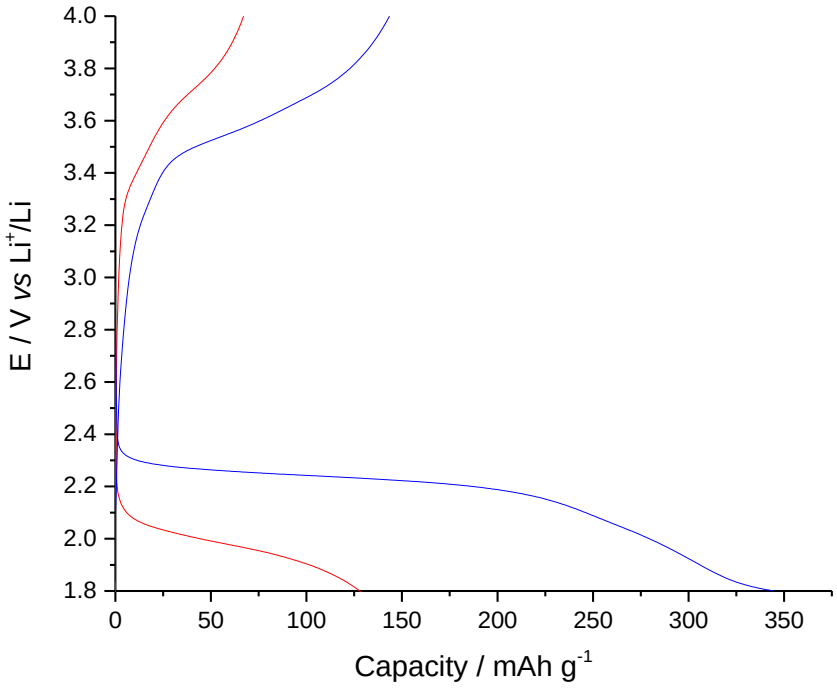

Figure 4.12. Galvanostatic cycling data collected using a current density of $\mathbf{100\ mA \cdot g_{CNT}^{-1}}$ in $\mathbf{100\ mM}$ LiTFSI, $Pyr_{14}TFSI$. Measurments were run in a 1 inch Swagelok® cell with a $\mathbf{13\ mm}$ Ø CNT positive electrode, $\mathbf{1}''$ Ohara glass separator and a lithium metal negative electrode. (—) $\mathbf{2\ mM}$ $EtV(OTf)_2$, oxygen saturated (—) oxygen saturated.

Data collected during galvanostatic discharge-charge experiments at $100\ mA \cdot g^{-1}$ in Swagelok cells with Ohara glass separators in $100\ mM$ LiTFSI, $Pyr_{14}TFSI$ with (blue trace) and without (red trace) $2\ mM$ $EtV(OTf)_2$ are shown in Figure 4.12. CNTs were used as the positive electrode material.

It is immediately clear that the use of ethyl viologen as a catalyst for the oxygen reduction reaction in $100\ mM$ LiTFSI, $Pyr_{14}TFSI$ resulted in an increase in the discharge capacity of the cell along with an increase of the discharge potential. The capacity in the presence of ethyl viologen was seen to increase to $344\ mAh \cdot g^{-1}$, from $134\ mAh \cdot g^{-1}$ in the absence of a catalyst. While the average discharge potential was ~$2.24\ V\ vs\ Li^+/Li$. The increase in the discharge capacity and average discharge potential in the presence of ethyl viologen, compared to in the absence

of a catalyst, is similar to what was seen when using a GC electrode in a glass cell Figure 4.11.

The average discharge potential seen in the Swagelok cell, for both uncatalysed and catalysed oxygen reduction, is however noticeably lower than the discharge potential seen in the glass cell. This is likely due to the increased Ohmic drop in the Swagelok cell as a result of the increased applied current and the inclusion of the Ohara glass as a separator.

During charge the capacity seen in the ethyl viologen catalysed cell, $143\,mAh \cdot g^{-1}$, was larger than that seen in the absence of a discharge catalyst, $69\,mAh \cdot g^{-1}$. The charge profile also varies with an oxidation process seen between $3.4 - 3.7$ $V\ vs\ Li^{+}/Li$. This would suggest that the morphology of the lithium peroxide deposit on the electrode surface varies significantly in the presence of a homogeneous discharge catalyst. The appearance of an oxidation process with a comparatively large capacity at a low potential could suggest that small lithium peroxide particles were formed rather than toroids.[33]

The morphology of the discharge product could be investigated further through the use of SEM. The use of OEMS or DEMS could also provide valuable knowledge with regards to quantifying the efficiency of the ORR and OER when using ethyl viologen as a homogeneous catalyst. The use of increasing concentrations of a catalyst may also provide further enhancement to the cell. At higher concentrations it may be possible to maintain high capacities while increasing the discharge current density. Up to a certain concentration the desirable small particle morphology of the product may also be promoted, however this requires further investigation

These results show a clear increase in the capacity when ethyl viologen is used as a homogeneous catalyst in both Swagelok and glass cells. However over multiple cycles capacity fading is seen. This is a common problem in lithium oxygen cells

and relates to the passivation of the electrode surface by lithium peroxide. It may be possible to overcome this passivation by selecting conditions under which oxygen reduction occurs solely *via* ethyl viologen catalysed reduction in solution. This would then cause lithium peroxide to form in solution. However problems will then arise when trying to oxidise lithium peroxide that is not on the electrode surface. Whether oxygen reduction is occurring in solution or at the electrode surface the efficiency of lithium peroxide oxidation can be greatly improved through the use of a homogeneous catalyst for the charge reaction. It is therefore suggested that ethyl viologen should be used in Li-O_2 cells in combination with a homogeneous catalyst for the charge reaction.

4.4 Conclusions and Further Work

A thorough investigation into the electrochemistry of ethyl viologen di-triflate was carried out using various techniques. The results obtained showed that the electron transfer kinetics of ethyl viologen are fast in the ionic liquid $Pyr_{14}TFSI$, this was confirmed through the use of digital fitting software, where a rate constant of $10{,}000\ cm \cdot s^{-1}$ was used to fit the experimental data. The standard potential of the EtV^{2+}/EtV^{+} redox process, $2.39\ V\ vs\ Li^{+}/Li$, was deemed to satisfy the thermodynamic conditions required for the reduction of oxygen to lithium peroxide. Through the use of cyclic voltammetry and galvanostatic cycling it was then shown experimentally that ethyl viologen can indeed catalyse the reduction of oxygen in Li-O_2 cells. The catalysis of the oxygen reduction reaction by ethyl viologen results in increased cell capacities as a large proportion of oxygen reduction occurs away from the electrode surface. Further to this if the right conditions are employed lithium peroxide can be promoted as the dominant discharge product.[16, 26] The discharge potential in $100\ mM$ LiTFSI, $Pyr_{14}TFSI$ with $2\ mM$ $EtV(OTf)_2$ was shown to be $100\ mV$ positive of that seen without a catalyst. This promises better round trip efficiencies, although it should be pointed out that the geometry of the cell used was not similar to what would be seen in a practical battery.

The use of ethyl viologen does not significantly improve the cycling behaviour of a Li-O_2 cell under galvanostatic conditions. This was believed to be due to the electrochemical reduction of oxygen on the electrode surface occurring in tandem with the catalysed reduction of oxygen. It is suggested that through the combination of ethyl viologen as a discharge catalyst with soluble catalyst for the charge reaction the cycle life could be improved.

It is also recommended that in future work the use of ethyl viologen in alternative solvents should be investigated. It is expected that ethyl viologen will result in

increased capacities in solvents other than $Pyr_{14}TFSI$. The use of less viscous solvents would also allow cells to be cycled at higher current densities. The identification of the discharge products resulting from the use of ethyl viologen should also be prioritised.

4.5 References

[1] K. U. Schwenke, M. Metzger, T. Restle, M. Piana, and H. A. Gasteiger, *J. Electrochem. Soc.*, **162**, A2605–A2622, (2015).

[2] K. Xue, E. Mcturk, L. Johnson, P. G. Bruce, and A. A. Franco, *J. Electrochem. Soc.*, **162**, 614–621, (2015).

[3] H. Wang, X. Liao, Q. Jiang, X. Yang, Y. He, and Z. Ma, *Chinese Sci. Bull.*, **57**, 1959–1963, (2012).

[4] T. Meng, M. Ara, L. Wang, R. Naik, and K. Y. S. Ng, *J. Mater. Sci.*, **49**, 4058–4066, (2014).

[5] S. S. Zhang, X. Ren, and J. Read, *Electrochim. Acta*, **56**, 4544–4548, (2011).

[6] C. Selvaraj, N. Munichandraiah, and L. G. Scanlon, *J. Porphyr. Phthalocya.*, **16**, 255–259, (2012).

[7] L. Yu, Y. Shen, and Y. Huang, *J. Alloys Compd.*, **595**, 185–191, (2014).

[8] A. Débart, A. J. Paterson, J. Bao, and P. G. Bruce, *Angew. Chem. Int. Ed.*, **47**, 4521–4524, (2008).

[9] M. Lefèvre, E. Proietti, F. Jaouen, and J.-P. Dodelet, *Science*, **324**, 71–4, (2009).

[10] Z. Jian, P. Liu, F. Li, P. He, X. Guo, M. Chen, and H. Zhou, *Angew. Chem. Int. Ed. Engl.*, **53**, 442–6, (2014).

[11] C. L. Bird and A. T. Kuhn, *Chem. Soc. Rev.*, **10**, 49–82, (1981).

[12] D. T. Sawyer, *Oxygen Chemistry*, Oxford University Press, 1991.

[13] J. S. Bus, S. D. Aust, and J. E. Gibson, *Biochem. Biophys. Res. Commun.*, **58**, 749–755, (1974).

[14] E. J. Nanni, C. T. Angelis, J. Dickson, and D. T. Sawyer, *J. Am. Chem. Soc.*, **387**, 4268–4270, (1981).

[15] K. P. Reis, V. K. Joshi, and M. E. Thompson, *J. Catal.*, **67**, 62–67, (1996).

[16] L. Yang, J. T. Frith, N. Garcia-Araez, and J. R. Owen, *Chem. Commun.*, **51**, 1705–8, (2014).

[17] S. Monaco, A. M. Arangio, F. Soavi, M. Mastragostino, E. Paillard, and S. Passerini, *Electrochim. Acta*, **83**, 94–104, (2012).

[18] J. T. Frith, A. E. Russell, N. Garcia-Araez, and J. R. Owen, *Electrochem. Commun.*, **46**, 33–35, (2014).

[19] F. Soavi and M. Mastragostino, *J. Power Sources*, **224**, 115–119, (2013).

[20] A. W. Lodge, M. J. Lacey, M. Fitt, N. Garcia-Araez, and J. R. Owen, *Electrochim. Acta*, **140**, 168–173 (2014).

[21] Z. Peng, S. A. Freunberger, L. J. Hardwick, Y. Chen, V. Giordani, F. Bardé, P. Novák, D. Graham, J.-M. Tarascon, and P. G. Bruce, *Angew. Chem. Int. Ed. Engl.*, **50**, 6351–5, (2011).

[22] C. J. Allen, S. Mukerjee, E. J. Plichta, M. A. Hendrickson, and K. M. Abraham, *J. Phys. Chem. Lett.*, **2**, 2420–2424, (2011).

[23] B. M. Gallant, D. G. Kwabi, R. R. Mitchell, J. Zhou, C. V Thompson, and Y. Shao-Horn, *Energy Environ. Sci.*, **6**, 2518–28, (2013).

[24] M. D. Radin, J. F. Rodriguez, F. Tian, and D. J. Siegel, *J. Am. Chem. Soc.*, **134**, 1093–103, (2012).

[25] W. Xu, J. Hu, M. H. Engelhard, S. A. Towne, J. S. Hardy, J. Xiao, J. Feng, M. Y. Hu, J. Zhang, F. Ding, M. E. Gross, and J.-G. Zhang, *J. Power Sources*, **215**, 240–247, (2012).

[26] M. J. Lacey, J. T. Frith, and J. R. Owen, *Electrochem. Commun.*, **26**, 74–76, (2013).

[27] W. J. Albery, P. N. Bartlett, B. J. Driscoll, and R. B. Lennox, *J. Electroanal. Chem.*, **323**, 77–102, (1992).

[28] A. E. G. Cass, G. Davis, G. D. Francis, H. A. O. Hill, W. J. Aston, I. J. Higgins, E. V Plotkin, L. D. L. Scott, and A. P. F. Turner, *Anal. Chem*, **56**, 667–671, (1984).

[29] V. S. Dilimon, D.-G. Lee, S.-D. Yim, and H.-K. Song, *J. Phys. Chem. C*, **119**, 3472–3480, (2015).

[30] F. Mizuno, S. Nakanishi, Y. Kotani, S. Yokoishi, and H. Iba, *Electrochemistry*, **78**, 403–405, (2010).

[31] M. M. Ottakam Thotiyl, S. A. Freunberger, Z. Peng, and P. G. Bruce, *J. Am. Chem. Soc.*, **135**, 494–500, (2013).

[32] L. Johnson, C. Li, Z. Liu, Y. Chen, S. A. Freunberger, and P. G. Bruce, in *ECS 226th Meeting - Cancun*, 2014.

[33] B. M. Gallant, D. G. Kwabi, R. R. Mitchell, J. Zhou, C. V. Thompson, and Y. Shao-Horn, *Energy Environ. Sci.*, **6**, 2518, (2013).

4.6 Related Publications

M. J. Lacey, J. T. Frith, and J. R. Owen, *Electrochem. Commun.*, **26**, 74–76, (2013).

L. Yang, J. T. Frith, N. Garcia-Araez, and J. R. Owen, *Chem. Commun.*, **51**, 1705–8, (2014).

Chapter 5:
The Electrochemcial Behaviour of the Cobalt Bis(Terpyridine) Complex

5.1 Introduction

The use of homogeneous catalysts in Li-O_2 cells to aid the discharge reaction, or oxygen reduction reaction (ORR), has been investigated in Chapter 4. In this chapter the use of a redox molecule that may also interact with lithium peroxide oxidation, or the oxygen evolution reaction (OER), during cell charging will be explored.

As mentioned in the introduction (Chapter 1) the vast majority of the literature related to the catalysis of the OER in Li-O_2 cells focuses on the use of heterogeneous catalysts. The problem associated with the use of heterogeneous catalysts during the OER relates primarily to their immobility which limits their effectiveness.

On the surface of an electrode where the cell has been fully discharged under extremely dry conditions, and in a solvent with a low donor number,[1,2] it is expected that an even deposit of Li_2O_2 would form over the electrode surface.[3] On charging the electrode bound catalyst would then only be able to catalyse the oxidation of peroxide deposits within a few monolayers distance (Diagram 5.1). Therefore unless an extremely high and even distribution of the catalyst on the electrode surface can be achieved it would not be possible to catalyse the oxidation of all the lithium peroxide.

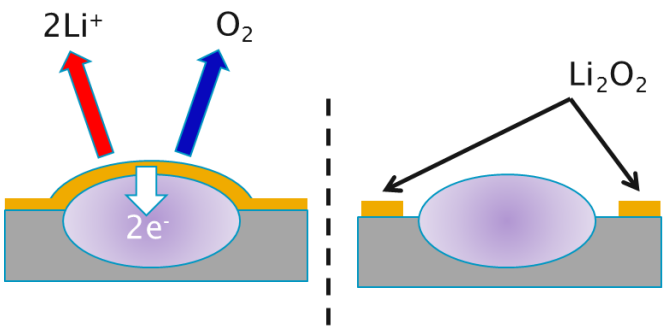

Diagram 5.1. Action of a heterogeneous catalyst during charging. (●) Catalyst particles. (●) Electrode surface. (●) Lithium peroxide deposit.

Based on this a more suitable approach to the catalysis of the OER in Li-O_2 cells is the use of soluble catalysts (homogeneous catalysts), this is an idea that was proposed by Liox and subsequently demonstrated by the Bruce group.[4, 5]
Solution based catalysts are by their very nature dissolved in the electrolyte, this is extremely beneficial in the Li-O_2 cell as it allows them freedom to move around the cell. As a result a solution based catalyst can shuttle electrons from the electrode surface to lithium peroxide deposits that may not be in electrical contact with the electrode (Diagram 5.2).

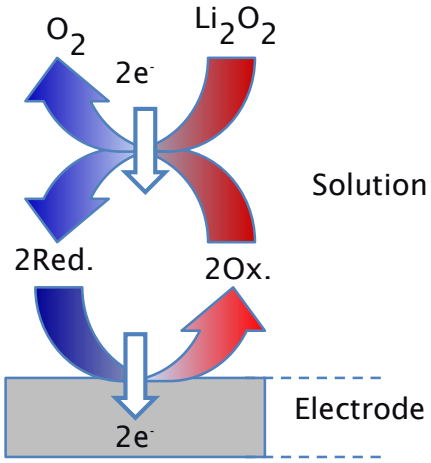

Diagram 5.2

The use of homogeneous catalysts in Li-O_2 cells has gained wide spread attention over a very short time frame,[6-10] this reflects the huge benefits that result from their use. In this chapter a complex, Cobalt (II) bis(2,2':6,2"-terpyridine) (CoTerpy, Diagram 5.3), that satisfies the thermodynamic conditions required to catalyse the ORR as well as the OER has been investigated.
When investigating molecules for use as homogeneous catalysts of the OER in Li-O_2 cells it is important that the redox potential of the molecule is such that it results in favourable thermodynamics for the mediated OER. If this criteria is to be met the redox potential must be greater than the standard potential, E^0, of

lithium peroxide oxidation, $2.96\,V\ vs\ Li^+/Li$.[11] However for the operation of the cell to be practical a redox potential as close to ~$3\,V\ vs\ Li^+/Li$ is desirable. If the redox potential of the homogeneous catalyst was to be much higher than $3\,V\ vs\ Li^+/Li$ the round trip efficiency of the cell would be poor. The excess energy required during charging would also need to be dissipated as heat. On top of this the molecule must be reasonably soluble, $>\ 2\,mM$, in the desired solvent.

CoTerpy was identified as a suitable candidate following a comprehensive literature search. Complexes based on cobalt have been in use in dye-sensitized solar cells (DSSC) for several years,[12–16] the $Co^{II/III}$ oxidation occurs between $3 - 4\,V$ in various solvents. A potential in this region results in favourable thermodynamics, while at the same time the potential is not so high as to result in low round trip efficiencies.

Identification of a suitable ligand was based on previous work (not shown here) that found that bipyridine (2,2'-bipyridine) was extremely soluble in $Pyr_{14}TFSI$. As a bidentate ligand the complex would be stable, however, it was hoped that the use of a tridentate ligand would afford further stability, therefore the tridentate ligand terpyridine (2,2':6,2"-terpyridine, Terpy) was investigated. Ligands such as phthalocyanine were ruled out due to *pi* stacking reducing the solubility of the complex in certain solvents.

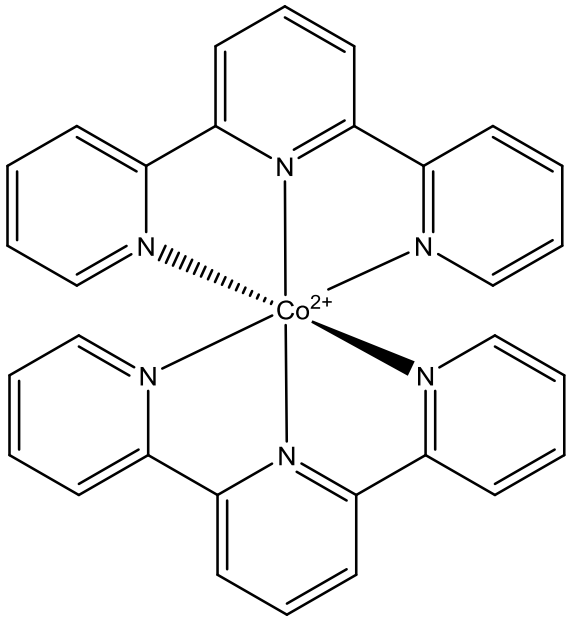

Diagram 5.3. Cobalt (II) bis(2,2':6,2"-terpyridine)

5.2 Experimental

5.2.1 Electrochemical Techniques

Cyclic voltammetry and galvanostatic cycling have been used in this chapter. These techniques are explained in detail in Chapter 2, section 2.3.

5.2.2 Scanning Electron Microscopy and Energy-Dispersive X-Ray Spectroscopy

A scanning electron microscope (SEM) uses electrons to image a sample, in a similar way to how an optical microscope uses photons to image a sample. The use of an SEM, however, provides greater resolution than what is seen with an optical microscope.

Topographical images are created through detection of secondary electrons. These secondary electrons are electrons that are emitted from the inner electron shell, K shell, of atoms that have been excited by the electron beam.

To produce an image electrons are accelerated in a vacuum between 1-200 kV, a magnetic lens is then used to focus the beam. The beam is then scanned across the specimen to build up an image (Diagram 5.4).

Due to the nature of the process samples must be electronically conducting. The use of non-conducting materials can result in a build-up of electrons on the surface of the sample. This causes a blurring of the image due to the interaction with the beam.

When an electron is ejected from the K shell of an atom an electron from a higher energy outer shell fills the electron hole. The energy difference between the inner and outer shell means that the electron must release some energy. This energy is released in the form of an X-ray. The energy of the X-ray is characteristic of the elemental atomic structure of the atom. These X-rays can therefore be used to

identify the different atoms present in a sample. This forms the basis of electron dispersive X-ray (EDX) spectroscopy.

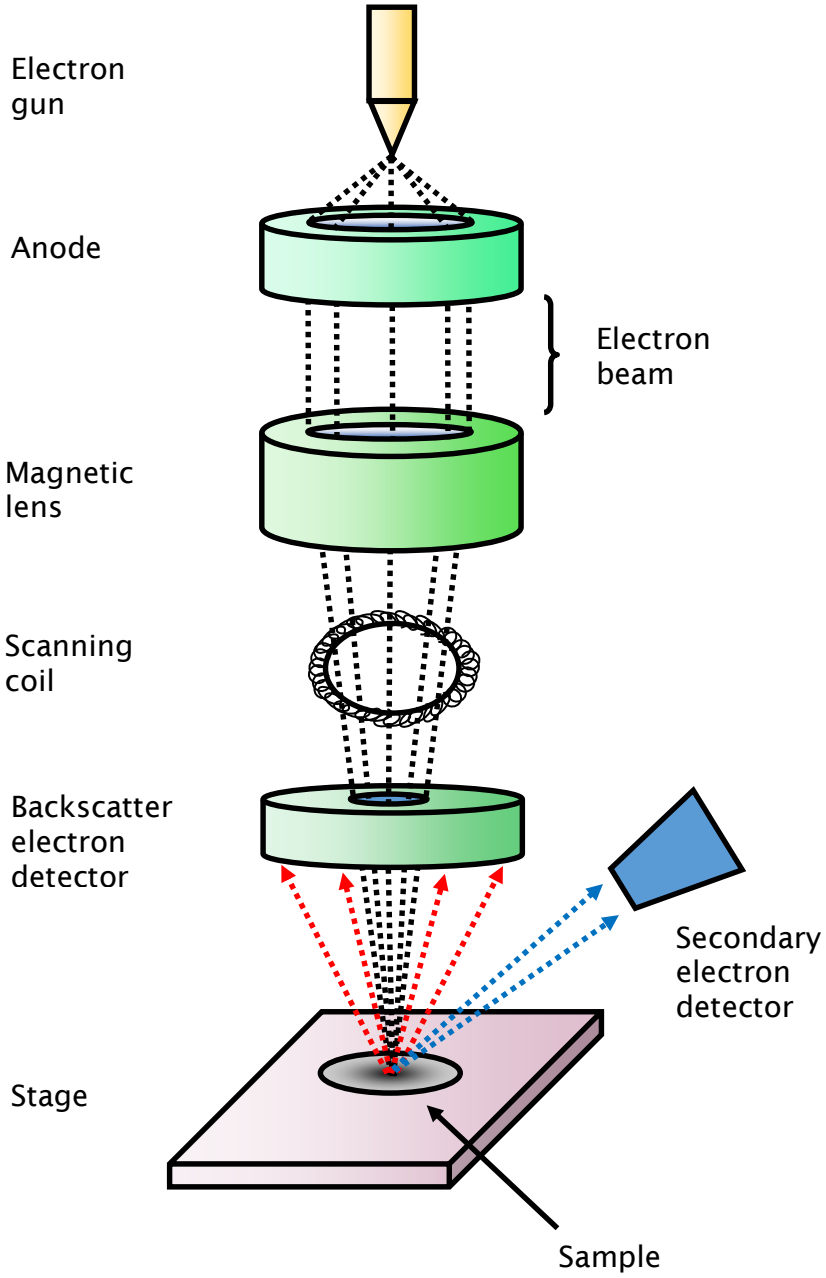

Diagram 5.4. SEM microscope

When using scanning electron microscopy to investigate electrodes that had been cycled the electrodes were washed twice in fresh anhydrous diglyme to remove any lithium salt from the electrode surface.

5.2.3 Chemical Reagents

Electrolytes were prepared as detailed in Chapter 2, section 2.1.

5.2.4 Synthesis of Chemical Reagents

Cobalt (II) bis(terpyridine) bis(trifluoromethane)sulfonylimide was synthesised according to the literature.[17] An aqueous solution of cobalt (II) chloride ($CoCl_2$, Puriss $\geq$ 98.5 %, Fluka) was added drop-wise to a solution of 2,2':6',2"-terpyridine (Terpy, 98 %, Sigma-Aldrich) in the molar ratio 1:2. This produced a yellow solution. Excess Lithium bis(trifluoromethane)sulfonylimide (LiTFSI, 99.95 %, Sigma-Aldrich) in water was then added, causing a red/brown product to crash out of solution. The product was washed with water and dried overnight under vacuum at $80\,^{\circ}C$ before being transferred to a dry glovebox ($< 1\,ppm$ H_2O, $< 10\,ppm$ O_2).

5.2.5 Instrumentation

Electrochemical experiments were carried out using a Bio-Logic VMP2 (Variable Multi-channel Potentiostat).

SEM and EDX were carried out on a JSM 6500 scanning electron microscope.

5.3 Results and Discussion

5.3.1 Understanding the Effect of Electrolyte Composition on Soluble Catalysts

The initial literature search into the use of cobalt complexes in DSSC revealed a shift in the potential of the $Co^{II/III}$ redox process as the solvent was varied. Different solvents have therefore been investigated to develop an understanding of the potential shift. Figure 5.1 shows cyclic voltammetry data of $2\ mM$ CoTerpy in three different solvents; Diglyme, $Pyr_{14}TFSI$ and $Pyr_{14}TFSI$:diglyme.

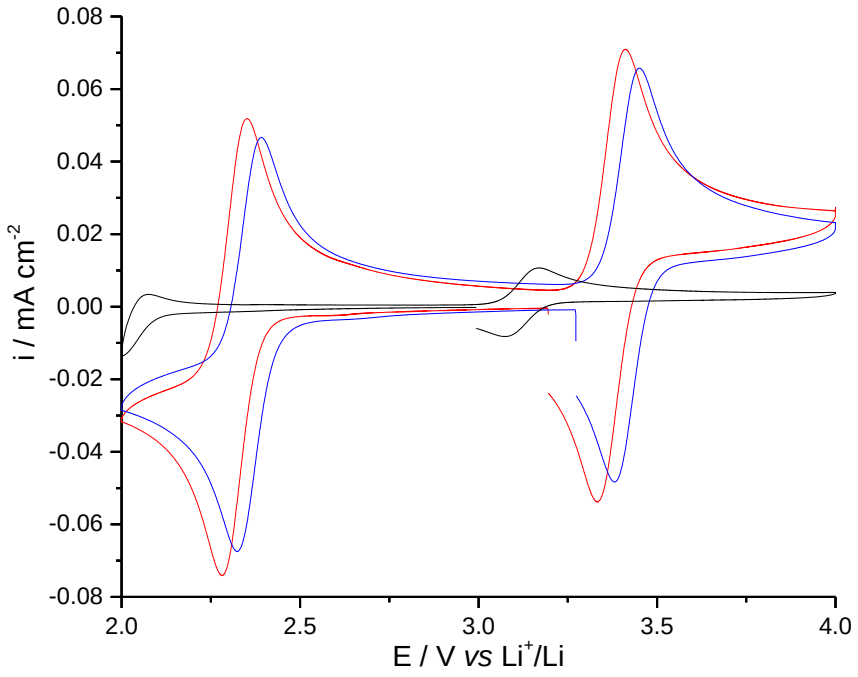

Figure 5.1. Cyclic voltammetry data of $\mathbf{2}\ \boldsymbol{mM}$ CoTerpy under argon in different electrolytes collected at $\mathbf{20}\ \boldsymbol{mV\ s^{-1}}$ on a $\mathbf{3}\ \boldsymbol{mm}$ Ø glassy carbon (GC) electrode. (—) $\mathbf{100}\ \boldsymbol{mM}$ LiTFSI, $Pyr_{14}TFSI$. (—) $\mathbf{100}\ \boldsymbol{mM}$ LiTFSI, $Pyr_{14}TFSI$:Diglyme. (—) $\mathbf{1}\ \boldsymbol{M}$ LiTFSI, Diglyme.

In Figure 5.1 the potential window has been limited to $2 - 4\ V$ as this is the region within which a practical Li-O_2 battery should operate. It is immediately obvious

that the cobalt (II) ion undergoes two redox reactions within the potential window being investigated.

The first process, at potentials lower than $2.5\ V\ vs\ Li^+/Li$, was a reversible 1 electron reduction from Co^{II} to Co^{I} according to Scheme 5.1. When scanning positive, at potentials higher than $3\ V\ vs\ Li^+/Li$, a reversible 1 electron oxidation from Co^{II} to Co^{III} was seen, according to Scheme 5.2.

$$Co^{2+}(Terpy)_2 + e^- \rightleftharpoons Co^{+}(Terpy)_2$$

Scheme 5.1

$$Co^{2+}(Terpy)_2 \rightleftharpoons Co^{3+}(Terpy)_2 + e^-$$

Scheme 5.2

In diglyme and Pyr_{14}TFSI:diglyme both redox processes appear to be extremely reversible. In Pyr_{14}TFSI it appears that the reduction of Cobalt (II) to Cobalt (I) was irreversible, however this is in fact just a result of the potential window used cutting off the process. A full CV showing the reversible nature of the process is shown in the appendix (Figure 1, Appendix B).

When moving between electrolytees a clear shift in the potential of the redox processes was observed. In the case of both the reduction and oxidation of Co^{II}Terpy the potential of the redox process moved positive in the order Pyr_{14}TFSI→diglyme→Pyr_{14}TFSI:diglyme. This shift in the potential as you move between electrolytes could be attributed to the ease with which electrons can be removed from the cobalt ion which in turn would be related to the solvation of the complex and how this affects the electron density around the central cobalt atom.

However, it is known that the standard potential of metal complexes is almost completely independent of the solvent used. The magnitude of this potential shift

is therefore more likely to be due to a variation in the potential of the lithium C_e/R_e, $E^0_{(Li+/Li)}$, in the various solvents. This change in the potential is as a result of the difference in the solvation of the Li^+ ions in solution.[18] The redox potentials of the cobalt ion are $\sim 200\ mV$ lower in $Pyr_{14}TFSI$ than the diglyme and $Pyr_{14}TFSI$:diglyme. This suggest that the lithium ions are least solvated in the ionic liquid. While the extent of solvation is greater in the diglyme containing solvents, this results in a lower $E^0_{(Li/Li+)}$ relative to the measured $E^0_{(Li+/Li)}$ in the ionic liquid. This in turn means that the corresponding measured potential of the cobalt redox reactions are higher (Diagram 5.5). This effect was also seen when the ferrocene/ferrocinium redox couple was investigated in the solvents mentioned above (Figure 2, Appendix B).

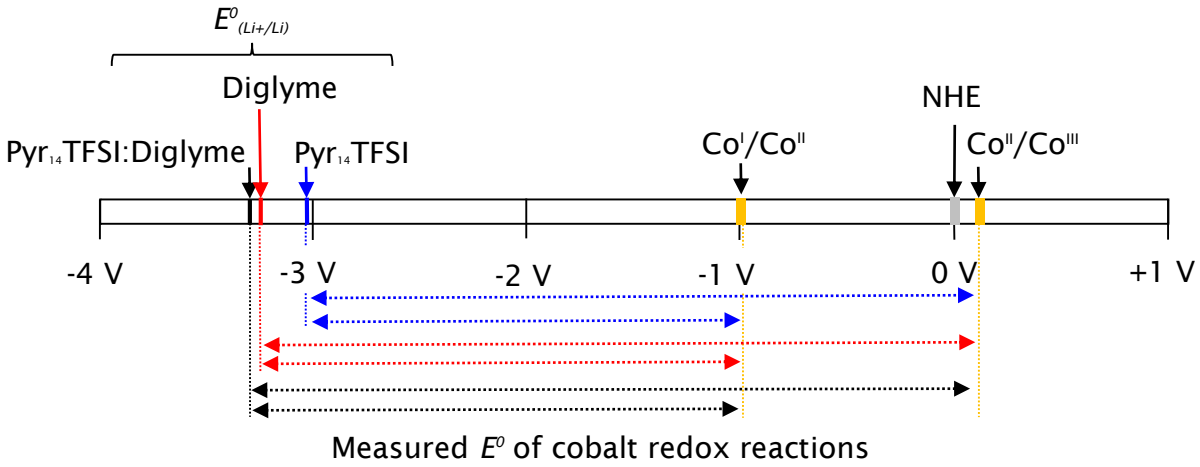

Diagram 5.5. Visual representation of potential shift in different solvents

This explanation holds true for the redox potentials of cobalt seen in the ionic liquid and diglyme electrolytes. The potential seen in the $Pyr_{14}TFSI$:diglyme electrolyte would be expected to be between the potentials of the other two electrolytes. Instead the potential of the redox processes in the mixed electrolyte was $48\ mV$ higher than that seen in diglyme. The explanation for this lies in the Nernst equation (Equation 5.1) which predicts a change in the potential of $59\ mV$ when moving from a $1\ M$ Li^+ solution to a $100\ mM$ Li^+ solution (considering that the

activity coefficients of lithium ions do not change and that the activities of all other ions remain constant).

$$E = E^0 + \frac{RT}{nF} \ln a_{Li^+}$$

Equation 5.1

Where:

E = Potential ($V\ vs\ Li^+/Li$)
E^o = standard potential ($V\ vs\ Li^+/Li$)
R = gas constant ($8.314\ kJ \cdot mol^{-1}K^{-1}$)
T = temperature (K)
n = number of moles of electrons
F = Faradays constant ($96485\ kJ \cdot mol^{-1}$)
a_{Li^+} = activity of Li^+

The lower lithium concentration in the mixed solvent results in a negative shift in the $E^0_{(Li+/Li)}$ and a corresponding positive shift in the measured redox potentials of the cobalt complex. This effect is clearly seen when comparing CVs recorded in diglyme with $100\ mM$ and $1\ M$ LiTFSI (Figure 5.2), where the potential was seen to shift by 65 mV.

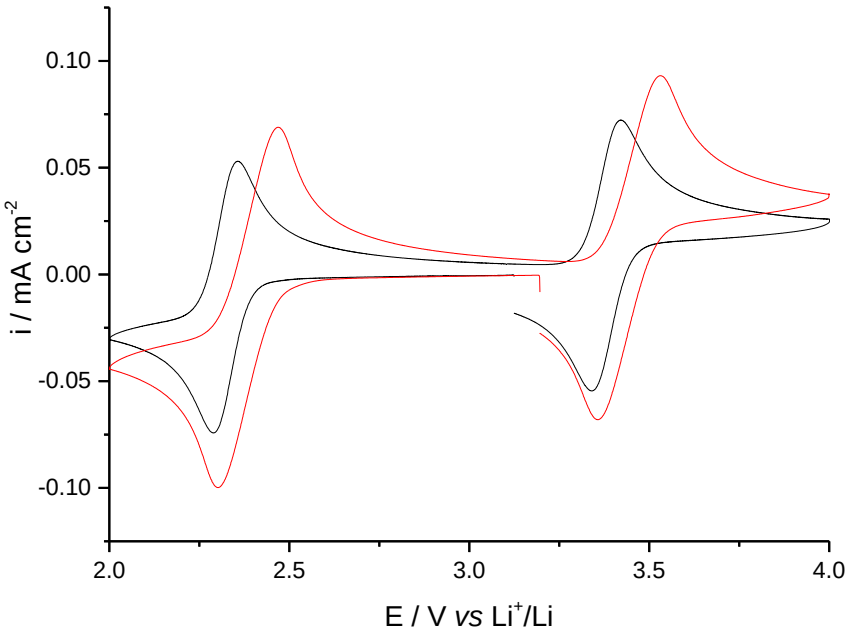

Figure 5.2. Cyclic voltammetry data of $\mathbf{2}\ \boldsymbol{mM}$ CoTerpy in argon saturated diglyme, with varying [LiTFSI], recorded on a $\mathbf{3}\ \boldsymbol{mm}$ Ø GC electrode at a scan rate of $\mathbf{20}\ \boldsymbol{mV \cdot s^{-1}}$. (—) $\mathbf{1}\boldsymbol{M}$ LiTFSI. (—) $\mathbf{100}\ \boldsymbol{mM}$ LiTFSI.

Along with the change in the redox potentials of the cobalt complex between solvents there was also a notable change in the peak current densities observed for the redox processes. This can be explained by the change in the viscosity of the solvents and the resulting change in the diffusion coefficient of the CoTerpy. It is possible to estimate the diffusion coefficient of Co^{II}Terpy in each solvent based upon the peak current value for the Co^{II} to Co^{I} reduction, or the Co^{II} to Co^{III} oxidation processes. This was done through the use of the Randles-Sevcik equation (Equation 5.2).

$$i_p = (2.68 \times 10^6) n^{\frac{3}{2}} A D^{\frac{1}{2}} C v^{\frac{1}{2}}$$

Equation 5.2. Randles-Sevcik equation at $\mathbf{298}\ \boldsymbol{K}$

Where:

i_p = peak current (A)

n = number of moles of electrons

F = Faradays constant $(96485\ As \cdot mol^{-1})$

A = surface area of the electrode (cm^2)
C = concentration of the Ox. or Red. species ($mol \cdot ml^{-1}$)
D = diffusion coefficient of the Ox. or Red. species ($cm^2 \cdot s^{-1}$)
v = scan rate ($V \cdot s^{-1}$)

Based on the diffusion coefficients for Co^{II}Terpy in each electrolyte it is also possible to approximate the viscosity of the solvent by rearranging the Stokes-Einstein equation (Equation 5.3).

$$D = \frac{k_B T}{6\pi\eta r}$$

Equation 5.3

Where:

D = diffusion coefficient of the Ox. or Red. species ($cm^2 \cdot s^{-1}$)
k_B = Boltzmann constant ($1.38 \times 10^{-23}\ m^2 kg \cdot s^{-2} K^{-1}$)
T = temperature (K)
η = kinematic viscosity ($m^2 \cdot s^{-1}$)
r = radius of molecule (m)

It should be noted that when applying this equation to ionic liquids it has previously been shown to only apply to the diffusion of certain molecules in ionic liquids.[19] In particular it holds true for molecules that are of a similar size to the solvent molecules such as ferrocene and cobaltocenium.[20] It is therefore assumed that this holds true for the Co^{II}Terpy complex in the Pyr_{14}TFSI ionic liquid and the mixed solvent of 1:1 Pyr_{14}TFSI:diglyme. The calculated diffusion coefficients of Co^{II}Terpy in each solvent and the viscosities of the solvents are shown in Table 5.1. To calculate the viscosity of each of the electrolytes the radius of CoTerpy must first be determined. To do this the diffusion coefficient of Co^{II}Terpy in Pyr_{14}TFSI in the absence of a supporting salt was determined. This was calculated from the peak current density of Co^{II}Terpy oxidation as shown in Figure 5.3.

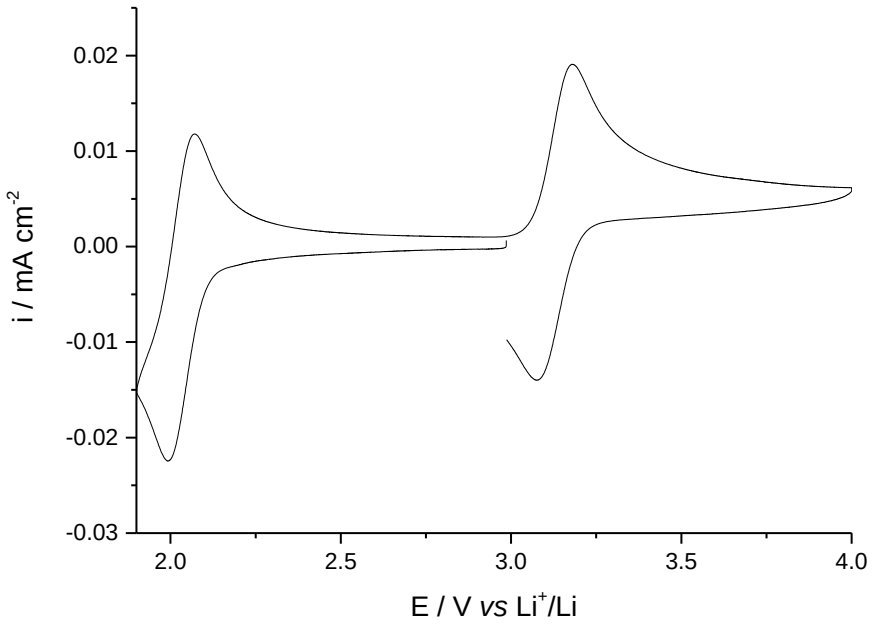

Figure 5.3. Cyclic voltammetry for $\mathbf{2}\ \boldsymbol{mM}$ CoTerpy in $Pyr_{14}TFSI$ on a GC electrode. There was no added lithium salt in the working electrode compartment. The counter/reference electrode was lithium metal in an electrolyte of $\mathbf{100}\ \boldsymbol{mM}$ LiTFSI at a scan rate of $\mathbf{20}\ \boldsymbol{mV \cdot s^{-1}}$.

From the data shown in Figure 5.3 a diffusion coefficient of $6.3 \times 10^{-8}\ cm^2 \cdot s^{-1}$ was calculated for Co^{II}Terpy in $Pyr_{14}TFSI$. This was then used to calculate a value for the radius of CoTerpy, of $4\ \text{Å}$, according to Equation 5.3.

Solvent	[LiTFSI] $(\boldsymbol{mol \cdot l^{-1}})$	Diffusion coefficient $(\boldsymbol{cm^2 \cdot s^{-1}})$	Viscosity $(\boldsymbol{kg \cdot s^{-1} m^{-1}})$
$Pyr_{14}TFSI$	0.1	2.09×10^{-8}	0.26
	1	1.99×10^{-9}	2.69
Diglyme	0.1	1.51×10^{-6}	3.6×10^{-3}
	1	8.66×10^{-7}	6.2×10^{-3}
$Pyr_{14}TFSI$:diglyme	0.1	7.66×10^{-7}	7.1×10^{-3}
	1	1.38×10^{-7}	3.9×10^{-2}

Table 5.1. A comparison of the diffusion coefficient of Co^{II}Terpy, in various solvents with different supporting salt concentrations, and the viscosity of the electrolyte.

The viscosity of the electrolytes examined was shown to increase with increasing lithium salt concentration, as expected. The order of the viscosity of the solvents used also increased in the expected order $Pyr_{14}TFSI$ < $Pyr_{14}TFSI$:diglyme < diglyme.

Solvent	[LiTFSI] $(mol \cdot l^{-1})$	$E^0_{Co^{II}/Co^{I}}$ $(V\ vs\ Li^+/Li)$	$E^0_{Co^{III}/Co^{II}}$ $(V\ vs\ Li^+/Li)$
$Pyr_{14}TFSI$	0.1	2.03	3.14
	1	-	3.05
Diglyme	0.1	2.38	3.44
	1	2.31	3.37
$Pyr_{14}TFSI$:diglyme	0.1	2.35	3.41
	1	2.27	3.33

Table 5.2. Standard potential of Co^{II} oxidation and reduction in various electrolytes

Based on the standard potentials of the Co^{II}/Co^{I} redox process it can be concluded that Co^{I}Terpy fulfils the thermodynamic requirements to mediate the reduction of oxygen in all the solvents investigated. It can also be concluded that Co^{III}Terpy satisfies the thermodynamic conditions required to oxidise lithium peroxide in all of the solvents investigated.

5.3.2 Voltammetric Characterisation of Cobalt bis-Terpyridine in Li-O_2 Cells

Having investigated how the cobalt complex behaves in various solvents under an argon atmosphere the interaction between the complexes and lithium peroxide/oxygen was explored.

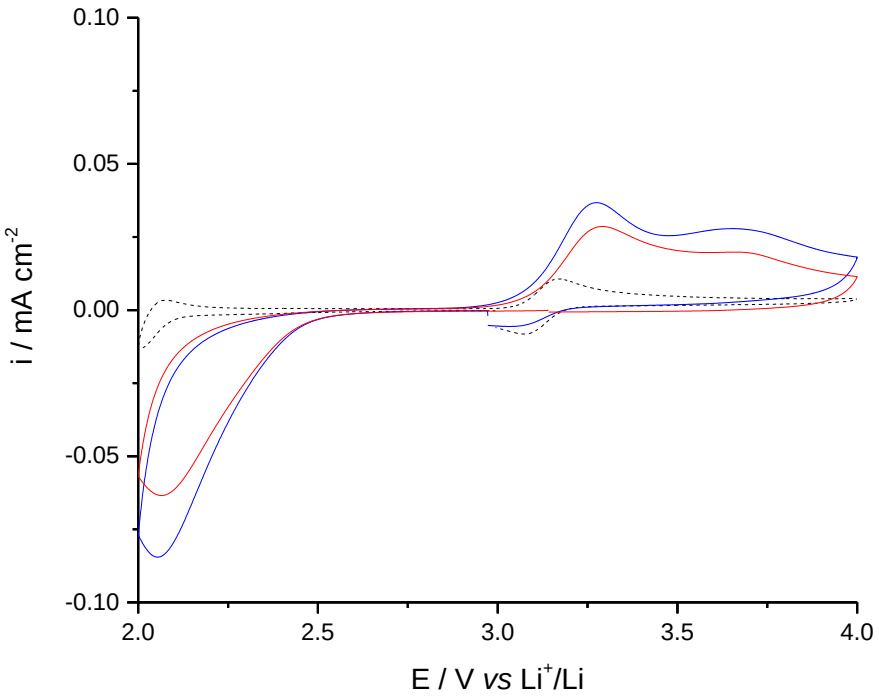

Figure 5.4. Cyclic voltammetry data collected in $\mathbf{100\ mM}$ LiTFSI, $Pyr_{14}TFSI$ at a scan rate of $\mathbf{20\ mV \cdot s^{-1}}$ on a $\mathbf{3\ mm}$ Ø GC electrode. (···) $\mathbf{2\ mM}$ CoTerpy, argon saturated. (—) $\mathbf{2\ mM}$ CoTerpy, oxygen saturated. (—) Oxygen saturated.

Figure 5.4 shows the data collected when investigating the cycling behaviour of $2\ mM$ CoTerpy in $100\ mM$ LiTFSI, $Pyr_{14}TFSI$, oxygen. To allow for easy comparison traces showing the cycling beahviour of $2\ mM$ Co^{II}Terpy in argon (black) and of oxygen cycling in the absence of a CoTerpy (red) have been included.

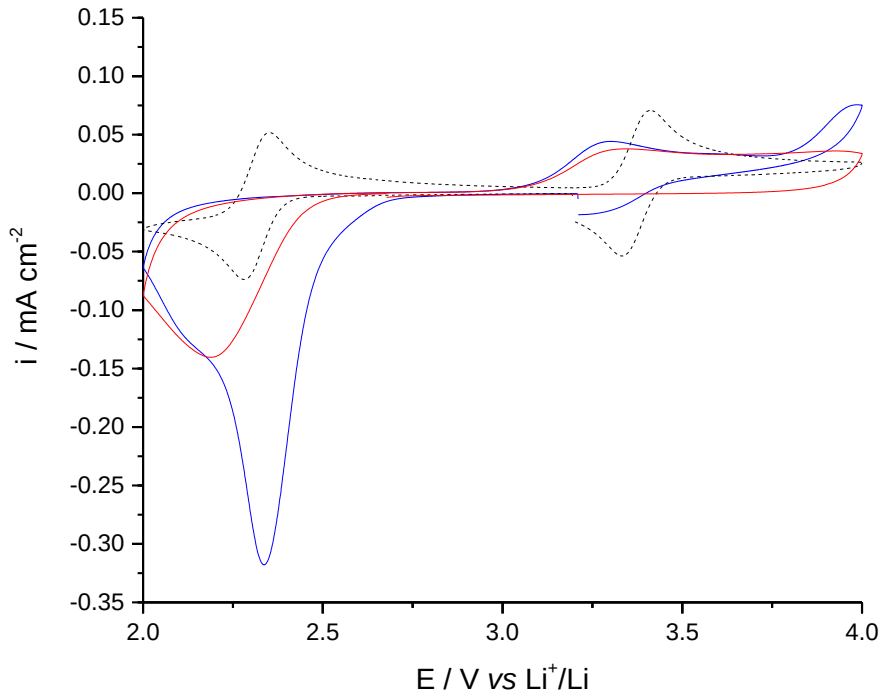

Figure 5.5. Cyclic Voltammetry data collected in $\mathbf{1}\,\boldsymbol{M}$ LiTFSI, Diglyme at a scan rate of $\mathbf{20}\,\boldsymbol{mV \cdot s^{-1}}$ on a $\mathbf{3}\,\boldsymbol{mm}$ Ø GC electrode. (···) $\mathbf{2}\,\boldsymbol{mM}$ CoTerpy, argon saturated. (—) $\mathbf{2}\,\boldsymbol{mM}$ CoTerpy, oxygen saturated. (—) Oxygen saturated.

Figure 5.5 shows the data collected during cyclic voltammetry experiments in an oxygen saturated solution of $1\,M$ LiTFSI, Diglyme with $2\,mM$ Co^{II}Terpy. To allow easy comparison traces of Co^{II}Terpy in argon (black) and of oxygen cycling in the absence of CoTerpy (red) have also been included.

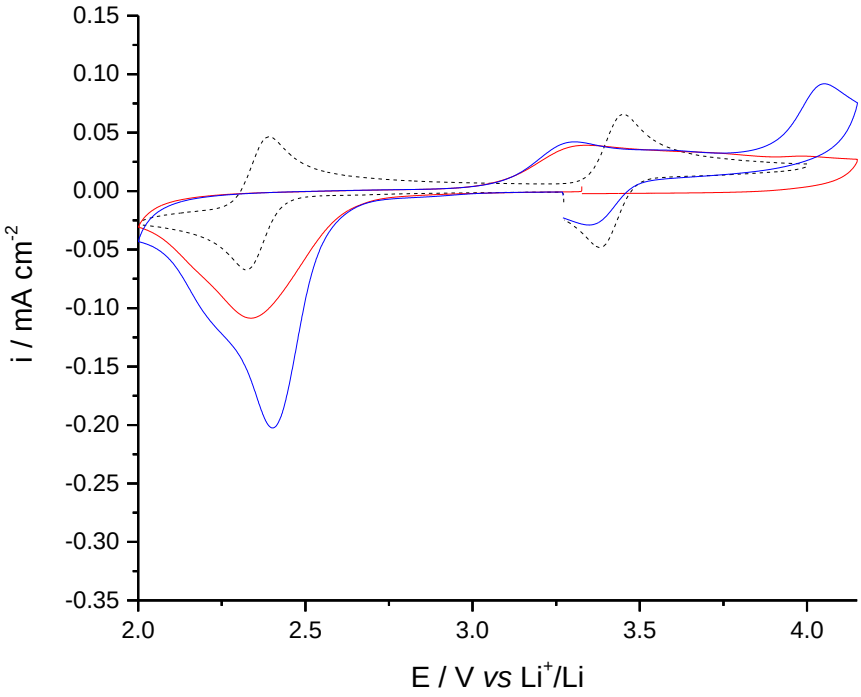

Figure 5.6. Cyclic voltammetry data collected in $\mathbf{100}\ \boldsymbol{mM}$ LiTFSI, Pyr_{14}TFSI:Diglyme at a scan rate of $\mathbf{20}\ \boldsymbol{mV \cdot s^{-1}}$ on a $\mathbf{3}\ \boldsymbol{mm}$ Ø GC electrode. (···) $\mathbf{2}\ \boldsymbol{mM}$ CoTerpy, argon saturated. (—) $\mathbf{2}\ \boldsymbol{mM}$ CoTerpy, oxygen saturated. (—) Oxygen saturated.

The data shown in Figure 5.6 is for CoTerpy cycling in the mixed solvent electrolyte Pyr_{14}TFSI:diglyme with $100\ mM$ LiTFSI as a supporting electrolyte salt. Cycling data was collected under an argon atmosphere (black trace) as well as with an oxygen saturated electrolyte (blue trace). Cycling data of oxygen in the absence of CoTerpy is also shown (red trace). A voltage range of $2.0 - 4.15\ V\ vs\ Li^+/Li$ was used in this case so as to not cut off the CoTerpy oxidation processes when cycling in an oxygen saturated electrolyte with $2\ mM$ CoTerpy.

Electrolyte		Onset potential of reduction processes ($V\ vs\ Li^+/Li$)		
Solvent	[LiTFSI] ($mol \cdot l^{-1}$)	O_2	CoTerpy argon	CoTerpy/O_2
Pyr_{14}TFSI	0.1	2.52	2.12	2.52
Diglyme	1	2.55	2.45	2.72
Pyr_{14}TFSI:diglyme	0.1	2.70	2.50	2.70

Table 5.3. Comparison of onset potentials of the reduction processes seen in the electrolytes investigated.

When cycling in an oxygen saturated electrolyte of Pyr_{14}TFSI and of diglyme the oxygen reduction behaviour was similar to what has previously been reported in the literature.[21, 22] Based on the viscosity of the mixed solvent, along with the change in the measured potentials seen when changing between solvents (Figure 5.1), it can be concluded that the cycling behaviour of oxygen in Pyr_{14}TFSI:diglyme is as would be expected.

During the positive scan the oxidation of lithium peroxide was seen above $3.0\ V$ in all of the electrolytes investigated. In fact in all three electrolytes the initial oxidation peak was seen at ~$3.30\ V$. The absence of a shift in the potential of this process is due to the oxidation of Li_2O_2 generating Li^+ ions. The global reaction of the cell, with a lithium counter and reference electrode, therefore does not depend on the activity of Li^+ since:

$$Li_2O_2 \rightarrow O_2 + 2Li$$

The similarity in the oxidation process also suggests that the morphology of the discharge product in each solvent is similar when performing cyclic voltammetry experiments.

Electrolyte		Charge relating to reduction (mC)		
Solvent	[LiTFSI] ($mol \cdot l^{-1}$)	O_2 red.	CoTerpy argon	CoTerpy/O_2
$Pyr_{14}TFSI$	0.1	-0.078	-0.0044	-0.098
Diglyme	1	-0.19	-0.084	-0.33
$Pyr_{14}TFSI$:diglyme	0.1	-0.15	-0.082	-0.24

Table 5.4. Comparison of the charge for the reduction processes seen in the electrolytes investigated.

When cycling in an oxygen saturated electrolyte in the presence of CoTerpy the reduction process varied significantly in both the diglyme based electrolyte and the mixed solvent, $Pyr_{14}TFSI$:diglyme, based electrolyte. In both of these systems a new reduction peak was seen slightly positive of both the oxygen reduction peak, seen in the absence of CoTerpy, and the CoTerpy reduction peak, seen in argon. In diglyme the onset potential of the reduction process was also seen to shift positive (Table 5.3). Further to this the charge seen when cycling in the presence of CoTerpy and oxygen was larger than the combined charge of the two individual processes (Table 5.4). This suggests that there was an interaction between oxygen/superoxide and Co^{II}Terpy/Co^{I}Terpy. It is suggested that this maybe an indicator that Co^{I}Terpy was mediating the reduction of oxygen. However, it should also be considered that this may be an indicator of degradation reactions between CoTerpy and superoxide.

Alternatively this effect may also arise as a result of the cobalt complex transporting oxygen to the electrode surface without undergoing a redox reaction itself, in a similar way to iron in haemoglobin and to the method recently proposed by Sun *et al.* when using iron phthalocyanine.[7]

When cycling CoTerpy in an oxygen saturated electrolyte of $Pyr_{14}TFSI$ although there was no shift in the onset potential, the charge of the reduction process was

greater than the combined charge of the two individual processes. This again suggests an interaction between some of the species present.

Electrolyte		Charge relating to oxidation (mC)			
Solvent	[LiTFSI] ($mol \cdot l^{-1}$)	O_2 red.	CoTerpy argon	CoTerpy/O_2	Theoretical CoTerpy/O_2
Pyr_{14}TFSI	0.1	0.064	0.023	0.091	0.10
Diglyme	1	0.11	0.12	0.18	0.31
Pyr_{14}TFSI:diglyme	0.1	0.12	0.11	0.21	0.26

Table 5.5. Comparison of the charge relating to the oxidation processes seen in the electrolytes under investigation.

Table 5.5 shows a comparison of the total charge seen for the oxidation process in each electrolyte under the various conditions investigated. The theoretical CoTerpy/O_2 charge relates to the combined charge of oxygen reduction in each solvent in the absence of CoTerpy (Table 5.4) and the charge seen for CoTerpy oxidation in argon. This therefore assumes that the additional charge seen during reduction when both CoTerpy and oxygen are present in solution does not result in the formation of lithium peroxide on the electrode surface.

From the data shown in the cyclic voltammograms and the charges determined in Table 5.5 it does not appear that Co^{III}Terpy has an effect on the oxidation of lithium peroxide. Instead it appears that the increase in the charge observed is simply a result of the two oxidation processes being overlaid on top of each other.

In Figure 5.5 and Figure 5.6 the position of the Co^{II}Terpy oxidation peak was seen to shift positive by up to $600\,mV$ in cells where lithium peroxide had been formed on the surface of the electrode. The cause of this effect was thought to be the insulating property of the lithium peroxide deposit on the surface. To investigate this further the potential window of cells, containing $2\,mM$ CoTerpy in oxygen

saturated $1\,M$ LiTFSI, diglyme, was varied. The lower potential limit was varied between $2.4\,V$, $2.2\,V$ and $2.0\,V$ while the upper limit was maintained at $4.0\,V$.

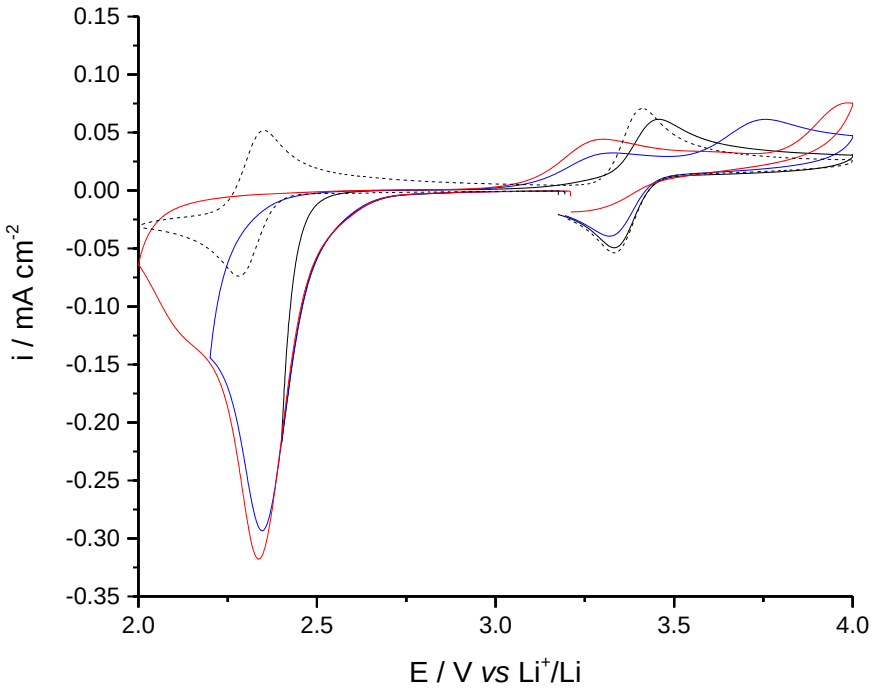

Figure 5.7. Cyclic voltammetry data of $\mathbf{2}\,\boldsymbol{mM}$ CoTerpy in $\mathbf{100}\,\boldsymbol{mM}$ LiTFSI, diglyme with a varying voltage window on a $\mathbf{3}\,\boldsymbol{mm}$ Ø GC electrode. A scan rate of $\mathbf{20}\,\boldsymbol{mV \cdot s^{-1}}$ was used in all cases and the electrolyte was oxygen saturated unless specified. (—) $\mathbf{2.4 - 4.0}\,\boldsymbol{V\ vs\ Li^{+}/Li}$. (—) $\mathbf{2.2 - 4.0}\,\boldsymbol{V\ vs\ Li^{+}/Li}$. (—) $\mathbf{2.0 - 4.0}\,\boldsymbol{V\ vs\ Li^{+}/Li}$. (···) $\mathbf{2.0 - 4.0}\,\boldsymbol{V\ vs\ Li^{+}/Li}$ under an argon atmosphere.

Figure 5.7 shows the results of the set of experiments in which the lower potential limit of cells was varied. As the lower potenital limit was changed from $\mathbf{2.4}$ to $\mathbf{2.0}\,\boldsymbol{V}$, and therefore the amount of lithium peroxide on the surface increased, there was a clear change in the potential of the oxidation peak of Co^{II}Terpy. As the potential window was extended and the electrode surface became more passivated the Co^{II}Terpy oxidation peak potential was seen to shift positive.

The data shown in Figure 5.7 provides evidence that the positive shift in the Co^{II}Terpy oxidation peak seen in Figure 5.5 and Figure 5.6 was a direct result of the passivation of the electrode surface by lithium peroxide. This result also offers further insight into the optimal performance of Li-O_2 cells that utilise mediators. It can be concluded that if mediators are being used to lower the overpotential needed to oxidise lithium peroxide it is necessary to prevent the full passivation of the electrode surface. In not doing so the working potential of the mediator may be greater than that seen in argon. This was demonstrated by Chen *et al.* when investigating the use of TTF as a mediator, where to obtain optimal performance the discharge capacity of the cell was limited.[5]

5.3.3 Galvanostatic Cycling of CoTerpy in Swagelok Cells

Cyclic voltammetry is a useful technique for assessing the behaviour of CoTerpy in different solvents and in the presence of oxygen/lithium peroxide. However the technique is limited as it doesn't provide information on how a catalyst performs under conditions used in commercial cells, where constant currents are used for both the discharge and charge reactions.

Galvanostatic cycling experiments have therefore been carried out to investigate how CoTerpy behaves under constant current conditions. The work shown here was carried out using a 1 inch Swagelok cell as described in Chapter 2, section 2.2. The working electrode used was a celgard separator coated with a CNT ink. A 1 inch Ohara glass separator was used to prevent reactions between CoTerpy and the lithium negative electrode.

The galvanostatic cycling behaviour of CoTerpy in three different electrolytes was investigated, the results of which are show in Figure 5.8 – Figure 5.10. As It was believed that Co^{I}Terpy may mediate the reduction of oxygen the capacity was not limited.

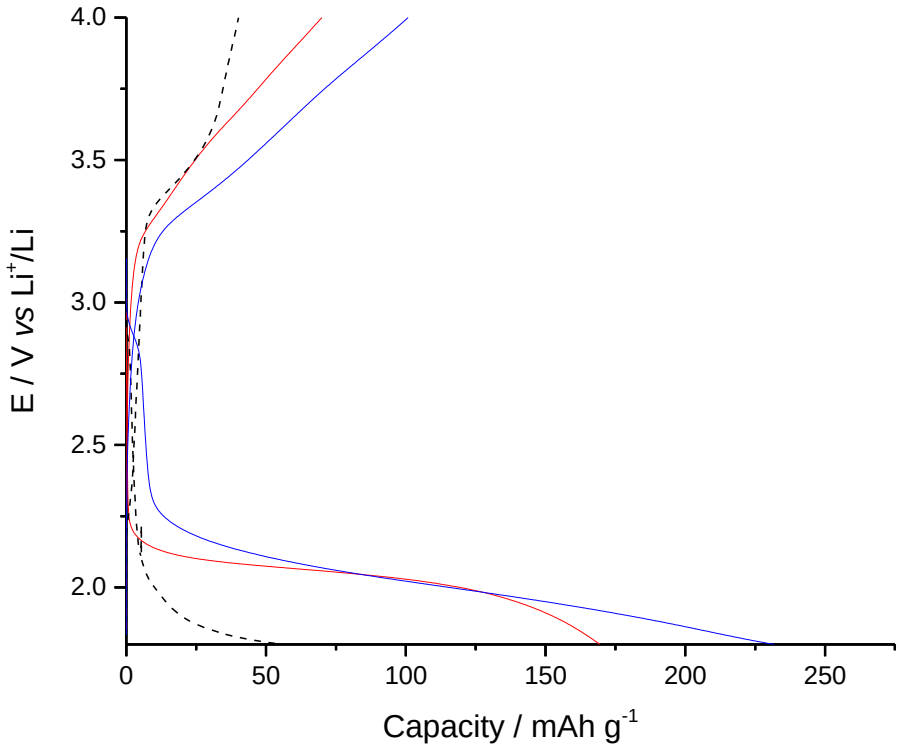

Figure 5.8. Galvanostatic cycling data collected in $\mathbf{100}\ \boldsymbol{mM}$ LiTFSI, Pyr_{14}TFSI on a CNT electrode at a rate of $\mathbf{100}\ \boldsymbol{mA \cdot g_{CNT}^{-1}}$. (┈┈) $\mathbf{50}\ \boldsymbol{mM}$ CoTerpy, argon, (—) $\mathbf{50}\ \boldsymbol{mM}$ CoTerpy, oxygen saturated electrolyte, (—) oxygen saturated.

Figure 5.8 shows a comparison of the capacity seen during discharge and charge in a Swagelok cell with an oxygen saturated electrolyte of $100\ mM$ LiTFSI, Pyr_{14}TFSI with (blue trace) and without (red trace) $50\ mM$ CoTerpy. The cycling data of CoTerpy in argon is also included (black dashed trace). A current density of $100\ mA \cdot g^{-1}$, rather than $200\ mA \cdot g^{-1}$, was used when cycling in $100\ mM$ LiTFSI, Pyr_{14}TFSI as the Ohmic drop seen across the cell when using higher current densities resulted in high overpotentials and low capacities within the voltage range investigated, an example is shown in Figure 3, Appendix C.

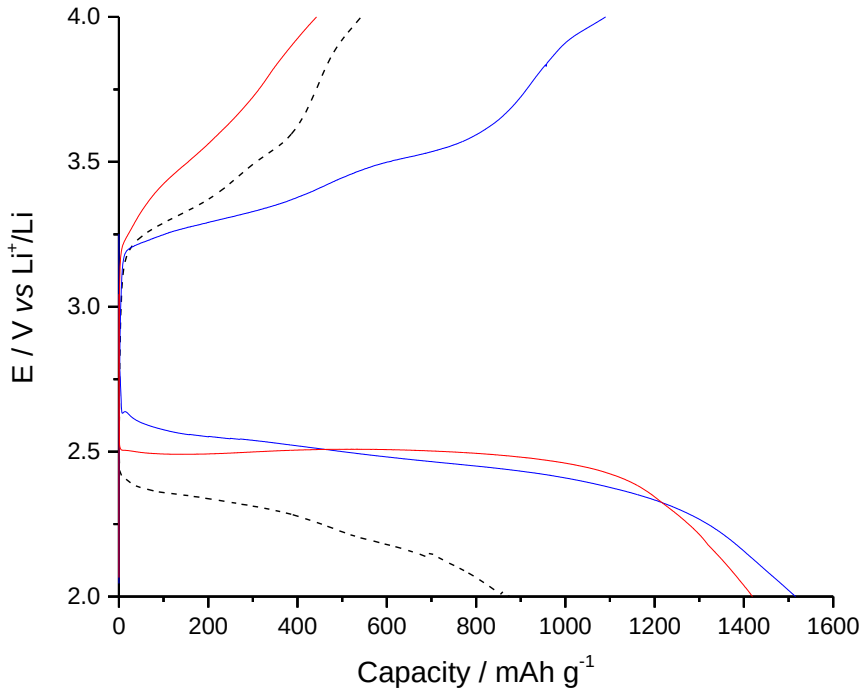

Figure 5.9. Galvanostatic cycling data collected in $\boldsymbol{100\,mM}$ LiTFSI, diglyme on a CNT electrode at a rate of $\boldsymbol{200\,mA \cdot g^{-1}}$. (┈┈) $\boldsymbol{50\,mM}$ CoTerpy, argon, (—) $\boldsymbol{50\,mM}$ CoTerpy, oxygen saturated electrolyte, (—) oxygen saturated.

The data shown in Figure 5.9 was collected in an oxygen saturated electrolyte of $100\,mM$ LiTFSI, Diglyme. The red trace was collected in the absence of CoTerpy while the blue trace was recorded with $50\,mM$ CoTerpy. The cycling behaviour of $50\,mM$ CoTerpy in argon has also been included. The data shown was collected when cycling with a current density of $200\,mA \cdot g^{-1}$ on CNT electrodes.

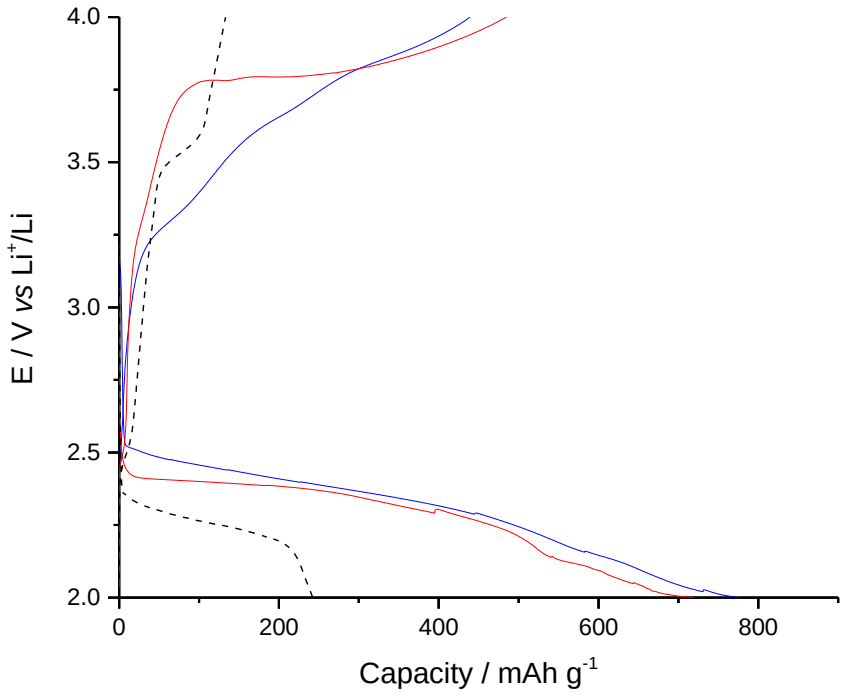

Figure 5.10. Galvanostatic cycling data collected in $\mathbf{100}\ \boldsymbol{mM}$ LiTFSI, Pyr_{14}TFSI:diglyme on a CNT electrode at a rate of $\mathbf{200}\ \boldsymbol{mA \cdot g_{CNT}^{-1}}$. (·····) $\mathbf{50}\ \boldsymbol{mM}$ CoTerpy, argon, (—) $\mathbf{50}\ \boldsymbol{mM}$ CoTerpy, oxygen saturated electrolyte, (—) oxygen saturated.

The cycling behaviour in a mixed solvent of 1:1 Pyr_{14}TFSI:diglyme, $100\ mM$ LiTFSI was investigated. The results of this investigation are shown in Figure 5.10. The cycling behaviour of $50\ mM$ CoTerpy in oxygen (red trace) and an oxygen saturated electrolyte without CoTerpy (blue trace) was also investigated. The results of galvanostatic cycling in an argon saturated electrolyte with $50\ mM$ CoTerpy are also shown (black trace).

Electrolyte solvent	Experimental capacity $(mAh \cdot g^{-1})$	Transition time (s)	Theoretical capacity $(mAh \cdot g^{-1})$	Diffusion coefficient $(cm^2 \cdot s^{-1})$
Pyr_{14}TFSI	50	1682	46	2.09×10^{-8}
Diglyme	850	14,455	800	1.51×10^{-6}
Pyr_{14}TFSI:diglyme	240	6852	380	7.66×10^{-7}

Table 5.6. Comparison of experimentally obtained capacities and the transition time calculated from the sand equation for the electrolytes investigated.

When cycling in argon in diglyme and $Pyr_{14}TFSI$ the capacities seen for the reduction of Co^{II} to Co^{I} were slightly in excess of those that had been estimated using the Sand equation (Equation 5.4). While when cycling in the mixed solvent electrolyte, $Pyr_{14}TFSI$:diglyme, the capacity seen for the reduction of Co^{II}Terpy deviated from the expected value to a greater extent.

$$j\tau^{1/2} = \frac{nFD^{1/2}C\pi^{1/2}}{2}$$

Equation 5.4. Sand equation

Where:

j = current density ($mA \cdot cm^{-2}$)
τ = transition time (s)
n = number of moles of electrons
F = Faradays constant (96487 $C \cdot mol^{-1}$)
D = diffusion coefficient ($cm^2 \cdot s^{-1}$)
C = concentration ($mol \cdot cm^{-3}$)

When cycling in oxygen in the absence of CoTerpy (red traces) the capacities seen for oxygen reduction increased as the viscosity of the solvent decreased. This was as expected and was in-line with what was seen during cyclic voltammetry.[23] The end point of the discharge in oxygen is thought to be a result of a passivating layer of lithium peroxide forming on the electrode surface.

When charging in an oxygen saturated electrolyte in the absence of CoTerpy (red trace) the capacities seen were smaller than those seen during discharge. This is commonly seen in Li-O_2 cells, and is due to the insulating nature of lithium peroxide. The shape of the charge curve was notably different when cycling in the mixed solvent electrolyte compared to the two individual electrolytes. This may be indicative of a change in the morphology of the deposit.[24]

When cycling $50\,mM$ CoTerpy in an oxygen saturated electrolyte (blue traces) the capacities seen during discharge did not vary significantly from what was seen when cycling in the presence of oxygen alone. If Co^{I}Terpy was acting as a

mediator of the oxygen reduction reaction increases in the discharge capacities would have been expected, as seen when using ethyl viologen as a mediator (Chapter 4).[25] Therefore the result shown here provide no evidence of Co^{I}Terpy mediating the oxygen reduction reaction in this system.

During charging in the presence of $50\,mM$ CoTerpy the capacities seen were larger than those seen when cycling CoTerpy in argon and when cycling in oxygen in the absence of CoTerpy. However, this does not necessarily provide conclusive evidence for the mediated oxidation of lithium peroxide by Co^{III}Terpy. As demonstrated in Table 5.7 if Co^{III}Terpy were to successfully mediate the oxidation of lithium peroxide the capacity seen in each system would be expected to be equal to $Q_{O_2+CoTerpy}^{Theoretical}$, where $Q_{O_2+CoTerpy}^{Theoretical}$ is the combined capacity seen for oxygen reduction in the absence of CoTerpy and the capacity seen for the oxidation of Co^{II} to Co^{III} in argon. If mediation of lithium peroxide were to occur in these systems, a capacity equal to this combined capacity would be expected as this would indicate complete oxidation of any lithium peroxide formed during discharge.

Electrolyte solvent	$Q_{O_2\ Red.}^{exp}$ $(mAh \cdot g^{-1})$	$Q_{CoTerpy\ Ox.}^{exp}$ $(mAh \cdot g^{-1})$	$Q_{O_2+CoTepry}^{exp}$ $(mAh \cdot g^{-1})$	$Q_{O_2+CoTerpy}^{Theoretical}$ $(mAh \cdot g^{-1})$
Pyr_{14}TFSI	168	39	101	207
Diglyme	1410	560	1090	1970
Pyr_{14}TFSI:diglyme	700	56	546	756

Table 5.7. Comparison of the experimentally observed capacities seen during charging in an oxygen saturated electrolyte in the presence of 50 mM CoTerpy and the Theoretical expected capacity.

Comparison of the experimentally obtained capacities, $Q_{O_2+CoTepry}^{exp}$, and the expected capacities shows little correlation. Instead the experimentally observed capacities seen were similar to the combined capacities of lithium peroxide oxidation in the absence of CoTerpy and Co^{II} to Co^{III} oxidation in argon. This

suggests that in these systems lithium peroxide oxidation occurs in a similar manner to what was seen in the absence of CoTerpy. Further to this it can also be presumed that CoTerpy oxidation occurs in a similar manner to that seen in argon. It can therefore be said that in this system there appears to be no interaction between the CoTerpy oxidation process and lithium peroxide oxidation.

The performance of Swagelok cells cycled in the presence of CoTerpy varied from what was expected based on the observed cycling behaviour during cyclic voltammetry experiments (Figure 5.4 - Figure 5.6). Principally during cyclic voltammetry an enhancement in the reduction current seen when cycling in an oxygen saturated electrolyte in the presence of CoTerpy was thought to represent an interaction between CoTerpy and oxygen/superoxide, possibly the catalysed reduction of oxygen by Co^{I}Terpy. However, this was not seen during galvanostatic cycling. Furthermore during galvanostatic cycling in the electrolytes investigated there was not clear evidence of an interaction between Co^{III}Terpy and the oxidation of lithium peroxide.

5.3.4 SEM and EDX Analysis of Galvanostatically Cycled Electrodes

To further investigate the results seen during galvanostatic cycling SEM images of the electrodes after cycling in an electrolyte of $100\ mM$ LiTFSI, diglyme were collected. This was combined with EDX spectroscopy to try to understand the composition of any material seen on the electrode surface.

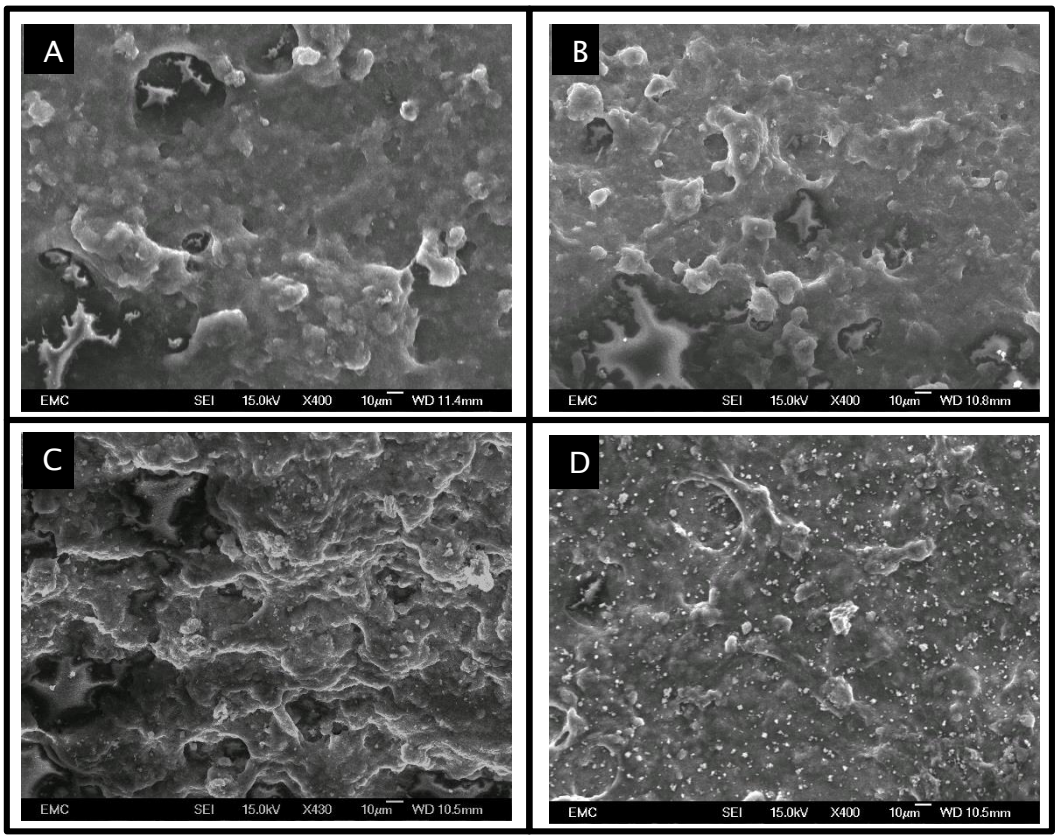

Figure 5.11. SEM images of CNT electrodes cycled under different conditions. **A)** As prepared electrode prior to cycling. **B)** Electrode discharged and charged in $\mathbf{50}\,\boldsymbol{mM}$ Coterpy, $\mathbf{100}\,\boldsymbol{mM}$ LiTFSI, diglyme, argon at $\mathbf{200}\,\boldsymbol{mAh}\cdot\boldsymbol{g^{-1}}$. **C)** Electrode discharged and charged in $\mathbf{50}\,\boldsymbol{mM}$ CoTerpy, $\mathbf{100}\,\boldsymbol{mM}$ LiTFSI, diglyme, oxygen at $\mathbf{200}\,\boldsymbol{mAh}\cdot\boldsymbol{g^{-1}}$. **D)** Electrode discharged and charged in $\mathbf{100}\,\boldsymbol{mM}$ LiTFSI, diglyme, oxygen at $\mathbf{200}\,\boldsymbol{mAh}\cdot\boldsymbol{g^{-1}}$.

The SEM images shown in Figure 5.11 are for CNT electrodes cycled under various conditions. The electrode cycled in $2\,mM$ CoTerpy in argon shows little difference from the pristine electrode. This was as to be expected.

When cycling in both $2\,mM$ CoTerpy in oxygen and in oxygen without CoTerpy it was clear that, after discharging and charging the cell, there was still a deposit on the electrode surface. This is in agreement with what was seen electrochemically, where the capacity seen during charging does not represent complete oxidation of the discharge product.

The composition of the deposit on the electrode surface was then investigated using EDX spectroscopy. The results of this study are shown in Figure 5.12 and Table 5.8.

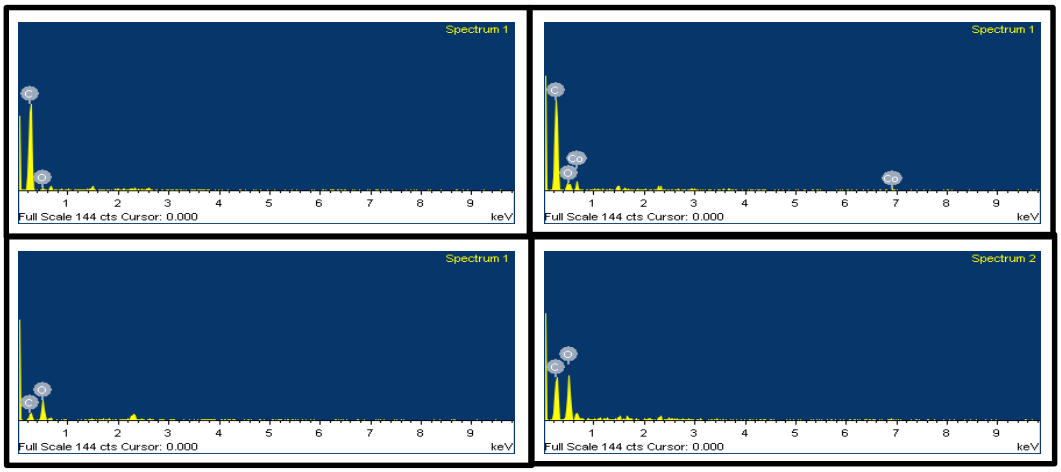

Figure 5.12. EDX spectra of CNT electrodes. **A)** As prepared electrode prior to cycling. **B)** Electrode discharged and charged in $\mathbf{50}\ \boldsymbol{mM}$ CoTerpy, $\mathbf{100}\ \boldsymbol{mM}$ LiTFSI, diglyme, argon at $\mathbf{200}\ \boldsymbol{mAh \cdot g^{-1}}$. **C)** Electrode discharged and charged in $\mathbf{50}\ \boldsymbol{mM}$ CoTerpy, $\mathbf{100}\ \boldsymbol{mM}$ LiTFSI, diglyme, oxygen at $\mathbf{200}\ \boldsymbol{mAh \cdot g^{-1}}$. **D)** Electrode discharged and charged in $\mathbf{100}\ \boldsymbol{mM}$ LiTFSI, diglyme, oxygen at $\mathbf{200}\ \boldsymbol{mAh \cdot g^{-1}}$.

Figure 5.12 shows the EDX spectra for CNT electrodes discharged and charged under various conditions as well as an as prepared, or pristine, CNT electrode. The elemental analysis of these spectra are also show in Table 5.8. The spectrum of the pristine electrode and its corresponding elemental analysis reveals that the electrode surface is almost completely formed of carbon. This is as would be expected as only CNTs and PvDF are present in the electrode. There was however some oxygen present. The source of this oxygen is likely to be a result of the acid treatment of the CNTs, as it has previously been shown that acid treatment results in CO groups on the CNT surface.[26, 27]

When cycling a CNT electrode in an electrolyte of $50\ mM$ CoTerpy in argon the elemental analysis was similar to what was seen for the pristine electrode. There was however a slight increase in the percentage of oxygen detected. This may be an indication of electrolyte breakdown. A small percentage of cobalt was also

detected. As any of the soluble cobalt complex would have been removed when the electrodes were washed after cycling, the cobalt detected may be an indication of a small amount of breakdown of the complex.

The electrodes cycled in an oxygen saturated electrolyte in the presence of CoTerpy and in its absence both exhibit similar percentages of both oxygen and carbon. In both these cases the majority of the oxygen present is believed to be due to oxygen reduction products, primarily lithium peroxide (it is not possible to detect lithium using EDX). The similarity in the percentage of oxygen present on the electrodes suggests that the degree of oxidation of lithium peroxide during charging was similar. This therefore provides further evidence that CoTerpy does not have an effect on the charge reaction in a lithium oxygen cell.

Element	Pristine ($At\%$)	CoTerpy/Argon ($At\%$)	CoTerpy/Oxygen ($At\%$)	Oxygen ($At\%$)
C	91.52	83.60	45.75	41.62
O	8.48	15.64	54.25	58.38
Co	-	0.76	-	-
Total	100	100	100	100

Table 5.8. EDX elemental analysis of a pristine CNT electrode and electrodes discharged and charged under various conditions in $100\ mM$ LiTFSI, diglyme. CoTerpy/Argon was cycled with $50\ mM$ CoTerpy in argon, CoTerpy/Oxygen was cycled with $50\ mM$ CoTerpy in oxygen and Oxygen was cycled in oxygen without CoTerpy.

5.4 Conclusions

In this chapter the electrochemistry of CoTerpy in several solvents with varying supporting salt concentrations was investigated. It was hoped that due to the standard potential of the Co^{II}/Co^{III} process in this complex that the Co^{III} ion would be able to mediate the oxidation of lithium peroxide, the principal discharge product in lithium-oxygen batteries.[28] At the same time the standard potential of the Co^{II}/Co^{I} process was such that the mediated reduction of oxygen may have been possible.

Initially the effect of solvent on the measured potential of the two redox processes was investigated using cyclic voltammetry. It was found that the measured potential changes in different solvent. However, this was due to a change in the measured potential of the Li^{+}/Li equilibrium in different solvents, which is related to the solvation of lithium ions in solution.[18] This means that the effectiveness of a molecule as a soluble mediator is dependent on the electrolyte in use.

Based on cyclic voltammetry experiments in various solvents in the presence of oxygen Co^{I}Terpy showed promise as a mediator of the oxygen reduction reaction. However, Co^{III}Terpy appeared to show little activity towards mediating lithium peroxide oxidation, although this was harder to judge based on cyclic voltammetry experiments alone.

The performance of lithium-oxygen cells with a more practical cell design was then investigated. Cells with a stacked geometry are generally used in commercial batteries, the use of Swagelok cells therefore results in performance that is more reminiscent of commercial cells.

Through the use of galvanostatic cycling it was found that in this system Co^{I}Terpy had little effect on the oxygen reduction reaction, as evidenced by the absence of any capacity enhancement. During charging in the presence of CoTerpy an

increase in the capacity compared to charging in oxygen alone was observed. However, through the use of SEM and EDX spectroscopy it was shown that this increase in the charge was not related to the mediated oxidation of lithium peroxide but was simply an effect of the combined capacity of lithium peroxide oxidation and Co^{II}Terpy oxidation.

5.5 References

[1] C. O. Laoire, S. Mukerjee, K. M. Abraham, E. J. Plichta, and M. A. Hendrickson, *J. Phys. Chem. C*, **114**, 9178–9186, (2010).

[2] K. Xue, E. Mcturk, L. Johnson, P. G. Bruce, and A. A. Franco, *J. Electrochem. Soc.*, **162**, 614–621, (2015).

[3] K. U. Schwenke, M. Metzger, T. Restle, M. Piana, and H. A. Gasteiger, *J. Electrochem. Soc.*, **162**, A2605–A2622 (2015).

[4] G. V. Chase, S. Zecevic, W. Walker, J. Uddin, K. Sasaki, V. Giordani, V. S. Bryantsev, M. Blanco, and D. Addison, G. V. Chase, S. Zecevic, W. Walker, J. Uddin, K. Sasaki, V. Giordani, V. S. Bryantsev, M. Blanco, and D. Addison, **US 20120028137 A1**, 2011.

[5] Y. Chen, S. A. Freunberger, Z. Peng, O. Fontaine, and P. G. Bruce, *Nat. Chem.*, **5**, 489–94, (2013).

[6] B. J. Bergner, A. Schürmann, K. Peppler, A. Garsuch, and J. Janek, *J. Am. Chem. Soc.*, **136**, 15054–15064, (2014).

[7] D. Sun, Y. Shen, W. Zhang, L. Yu, Z. Yi, W. Yin, D. Wang, Y. Huang, J. Wang, D. Wang, and J. B. Goodenough, *J. Am. Chem. Soc.*, **136**, 8941–6, (2014).

[8] H.-D. Lim, H. Song, J. Kim, H. Gwon, Y. Bae, K.-Y. Park, J. Hong, H. Kim, T. Kim, Y. H. Kim, X. Lepró, R. Ovalle-Robles, R. H. Baughman, and K. Kang, *Angew. Chem. Int. Ed. Engl.*, **53**, 3926–31, (2014).

[9] M. Yu, X. Ren, L. Ma, and Y. Wu, *Nat. Commun.*, **5**, 5111, (2014).

[10] D. S. Kim and Y. J. Park, *J. Alloys Compd.*, **591**, 164–169, (2014).

[11] Y.-C. Lu, Z. Xu, H. A. Gasteiger, S. Chen, K. Hamad-Schifferli, and Y. Shao-Horn, *J. Am. Chem. Soc.*, **132**, 12170–12171, (2010).

[12] K. Ben Aribia, T. Moehl, S. M. Zakeeruddin, and M. Grätzel, *Chem. Sci.*, **4**, 454 – 459, (2013).

[13] D. Xue, L. N. Ashbrook, R. S. Gaddie, and C. Michael Elliott, *J. Electrochem. Soc.*, **160**, H355–H359, (2013).

[14] J. J. Nelson, T. J. Amick, and C. M. Elliott, *J. Phys. Chem. C.,* **112**, 18255–18263, (2008).

[15] R. S. Gaddie, C. B. Moss, and C. M. Elliott, *Langmuir*, **29**, 825–31, (2013).

[16] T. W. Hamann, *Dalton Trans.*, **41**, 3111–5, (2012).

[17] K. Ben Aribia, T. Moehl, and S. M. Zakeeruddin, *Chem. Sci.*, **4**, 454–459, (2012).

[18] H. Schneider, C. Gollub, T. Weiss, J. Kulisch, K. Leitner, R. Schmidt, M. M. Safont-Sempere, Y. Mikhaylik, T. Kelley, C. Scordilis-Kelley, M. Laramie, and H. Du, *J. Electrochem. Soc.*, **161**, A1399–A1406, (2014).

[19] L. E. Barrosse-Antle, A. M. Bond, R. G. Compton, A. M. O'Mahony, E. I. Rogers, and D. S. Silvester, *Chem. Asian J.*, **5**, 202–30, (2010).

[20] E. I. Rogers, D. S. Silvester, D. L. Poole, L. Aldous, C. Hardacre, and R. G. Compton, *J. Phys. Chem. C*, **112**, 2729–2735, (2008).

[21] F. Soavi and M. Mastragostino, *J. Power Sources*, **224**, 115–119, (2013).

[22] E. J. Nemanick, *J. Power Sources*, **247**, 26–31, (2014).

[23] J. Read, K. Mutolo, M. Ervin, W. Behl, J. Wolfenstine, A. Driedger, and D. Foster, *J. Electrochem. Soc.*, **150**, A1351, (2003).

[24] B. M. Gallant, D. G. Kwabi, R. R. Mitchell, J. Zhou, C. V. Thompson, and Y. Shao-Horn, *Energ. Environ. Sci.*, **6**, 2518–2528, (2013).

[25] L. Yang, J. T. Frith, N. Garcia-Araez, and J. R. Owen, *Chem. Commun.*, **51**, 1705–1708, (2014).

[26] M. a M. Motchelaho, H. Xiong, M. Moyo, L. L. Jewell, and N. J. Coville, *J. Mol. Catal. A Chem.*, **335**, 189–198, (2011).

[27] J. Y. Kwon and H. D. Kim, *J. App. Poly. Sci.*, **96**, 595–604, (2005).

[28] J. T. Frith, A. E. Russell, N. Garcia-Araez, and J. R. Owen, *Electrochem. Commun.*, **46**, 33–35, (2014).

Appendix A

The graphs shown in Appendix A provide some background/further information to support the experiments described in Chapter 4.

UV-Vis spectroscopy – Titration of reduced ethyl viologen by oxygen

In this simple proof of concept experiment aliquots of a solvent saturated with oxygen were titrated against a solution of $2\ mM$ ethyl viologen. As both the concentration of oxygen and volume of solvent in each aliquot was known it was possible to determine the number of moles of oxygen added to the viologen. The results shown in Figure A.1.A. and Figure A.1.B. are for the addition of one aliquot of oxygen saturated solvent to a solution of ethyl viologen. The change in the absorbance of the EtV^+ band at $600\ nm$ was then monitored with time. Application of the Beer-Lambert law allowed the number of moles of EtV^+ that were oxidised by oxygen to be calculated (Figure A.1.B.). This revealed that the stoichiometric reaction ratio EtV^+:O_2 was greater than 1:1, in fact in this experiment the ratio was found to be ~1.6:1. This suggested that Etv^+ could reduce oxygen past superoxide towards peroxide.

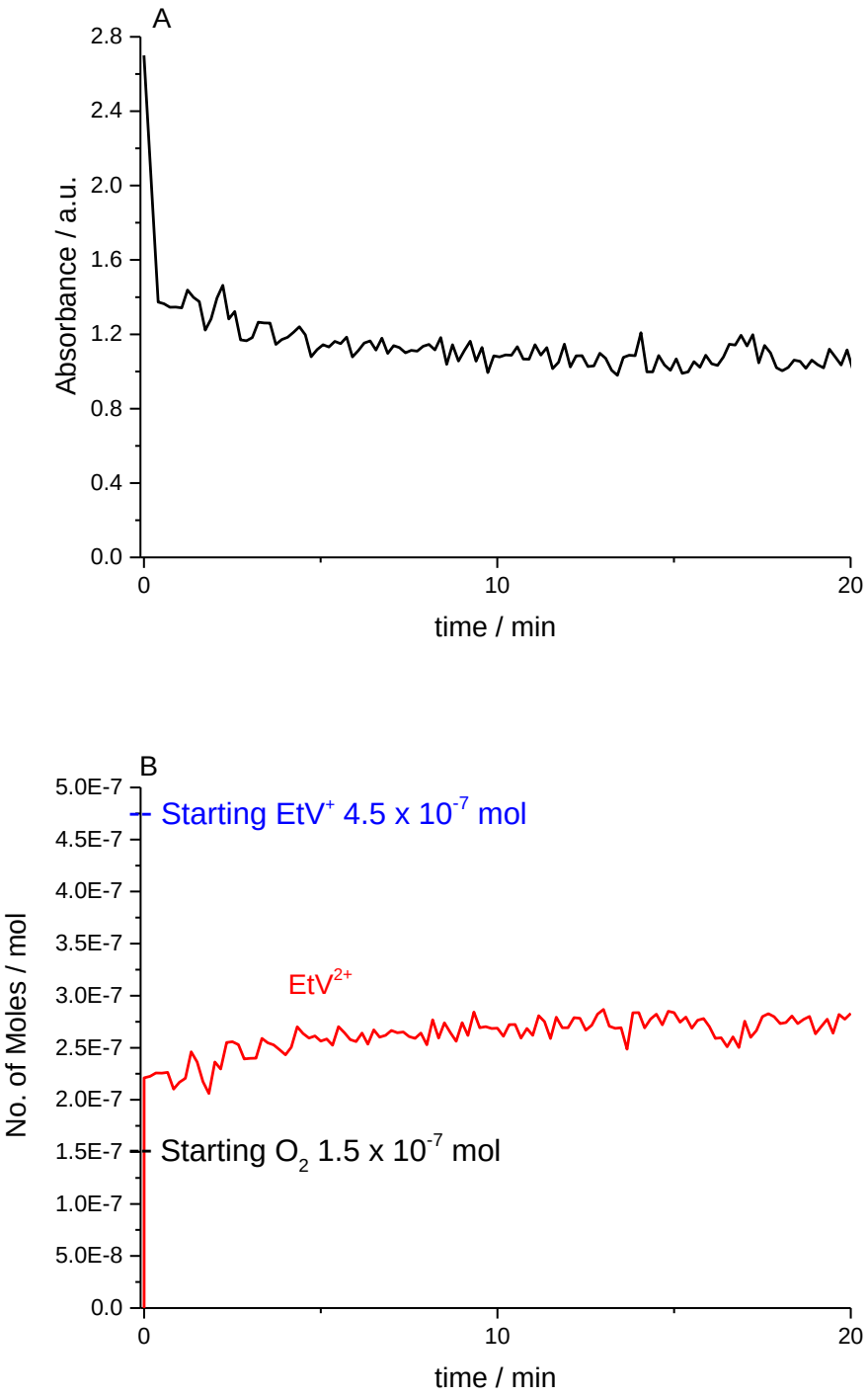

Figure A.1.A) Absorbance plot at $600\ nm$ for a solution of *2 mM* EtV^+, $100\ mM$ LiTFIS, $Pyr_{14}TFSI$ after the addition of an aliquot of oxygen saturated solvent. **B)** Change in the number of moles of EtV^{2+} present in solution after the addition of oxygen to a solution of containing *2 mM* EtV^+.

The cycling behaviour of a lithium-oxygen cell

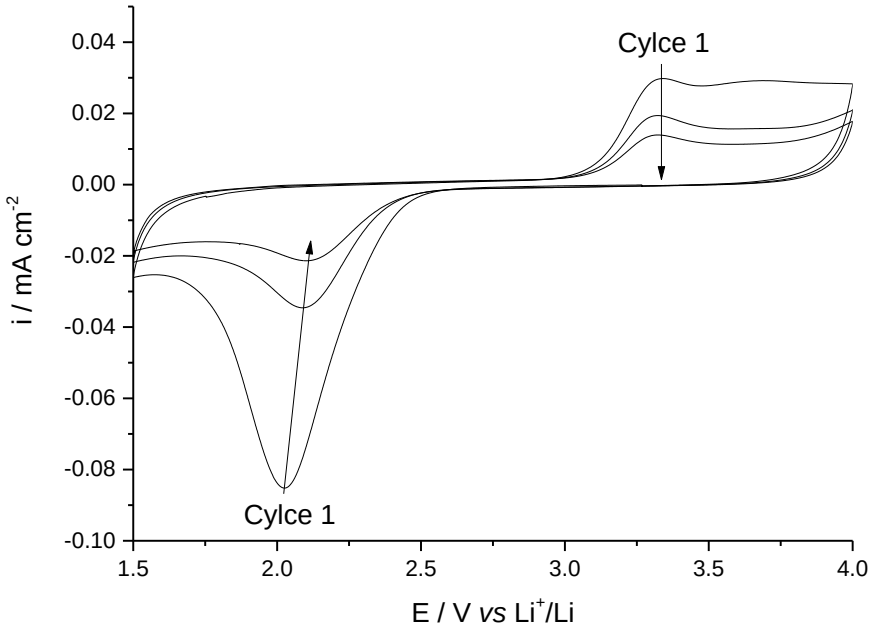

Figure A.2. Cyclic voltammetry data recorded in $\boldsymbol{100\ mM}$ LiTFSI, $Pyr_{14}TFSI$ on a $\boldsymbol{3\ mm}$ Ø glassy carbon (GC) electrode. The scans were recorded at a scan rate of $\boldsymbol{20\ mV\ s^{-1}}$ under an argon atmosphere. The first three scans are shown.

This figure illustrates the capacity fading upon multiple cycles in a lithium-oxygen cell. This is generally agreed to be a result of the formation of lithium peroxide on the electrode surface.

The effect of not adding a lithium salt on the cycling behaviour of ethyl viologen

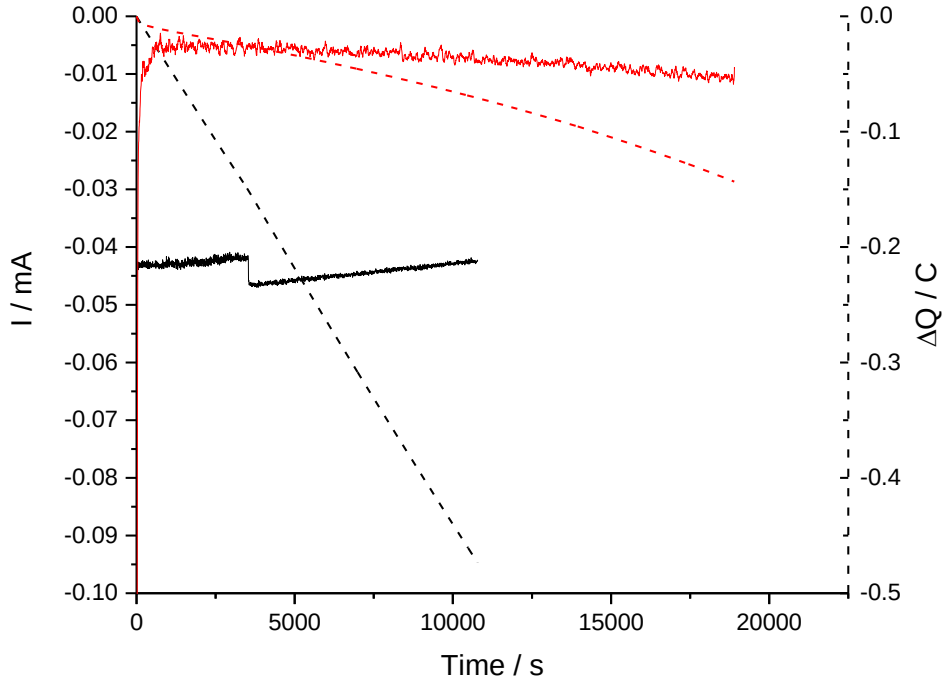

Figure A.3. Results from constant potential experiments in a 'bleaching' cell with $\mathbf{0}\,\boldsymbol{mM}$ LiTFSI. Copper mesh was used as the working electrode and lithium metal was used as the counter/reference electrode. (—) Reduction cycle 1, (—) reduction cycle 2.

This figure illustrates the drop in current seen upon successive cycles when chemically reducing oxygen using reduced ethyl viologen in the absence of large quantities of a lithium salt.

Appendix B

The graphs shown in Appendix B provide some background/further information to support the experiments described in Chapter 5.

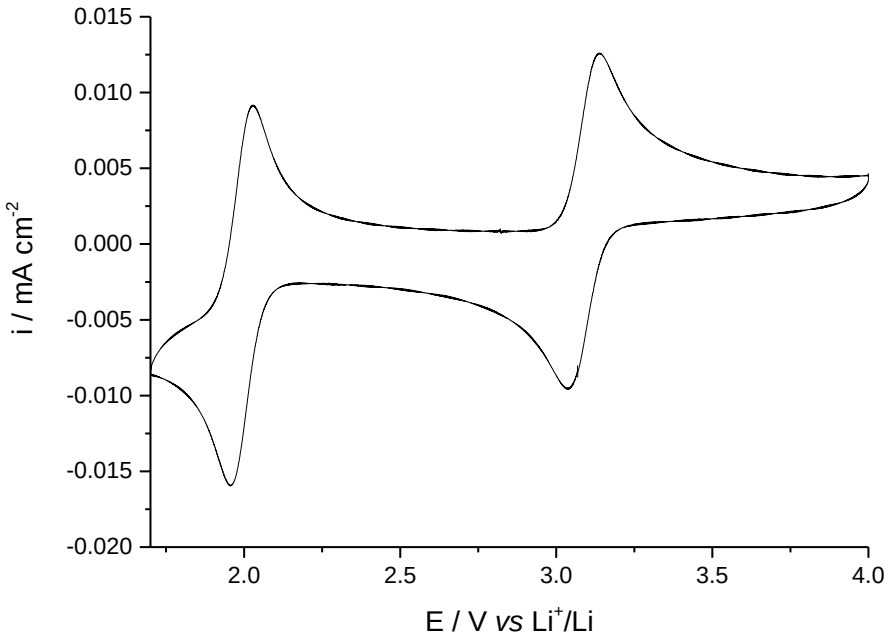

Figure B.1. CV of $2\ mM$ CoTerpy in $100\ mM$ LiTFSI, $Pyr_{14}TFSI$, Ar. Both the Co^{II} reduction and oxidation are shown in full. The data was collected at $20\ mV \cdot s^{-1}$ on a $3\ mm$ Ø GC electrode. The second scan is shown here.

This figure shows the reduction of Co^{II}Terpy in full in $100\ mM$ LiTFSI, $Pyr_{14}TFSI$, something that is not seen when the potential window is limited to $2\ V$.

The effect of electrolyte on the standard potential of Fc/Fc^+

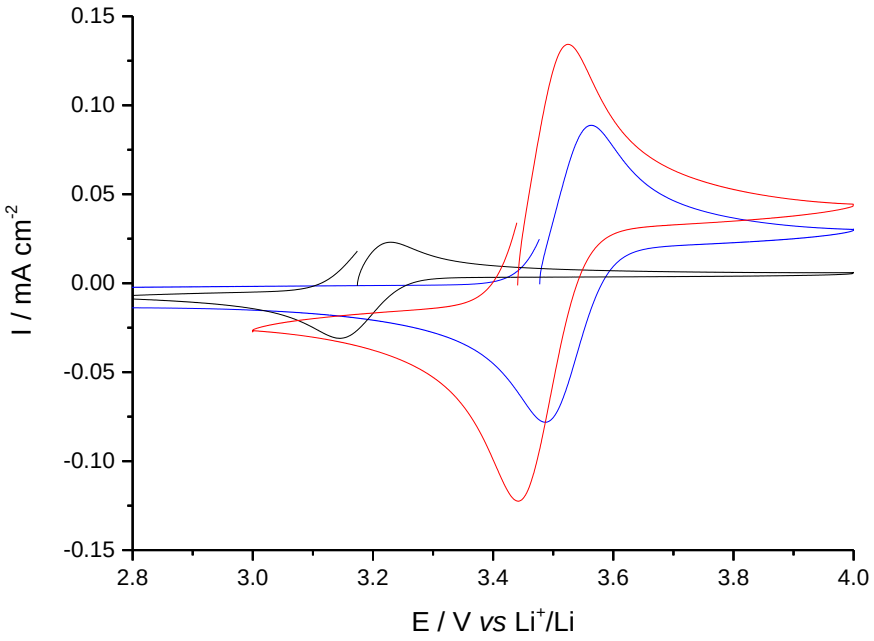

Figure B.2. Cyclic voltammetry data of $\mathbf{2}\ \boldsymbol{mM}$ Ferrocene under argon in different electrolytes collected at $\mathbf{20}\ \boldsymbol{mV\ s^{-1}}$ on a $\mathbf{3}\ \boldsymbol{mm}$ Ø glassy carbon electrode (GC). (—) $\mathbf{100}\ \boldsymbol{mM}$ LiTFSI, $Pyr_{14}TFSI$. (—) $\mathbf{100}\ \boldsymbol{mM}$ LiTFSI, $Pyr_{14}TFSI$:Diglyme. (—) $\mathbf{1}\ \boldsymbol{M}$ LiTFSI, Diglyme.

This figure illustrates that the potential shift of the standard potentials of CoTerpy seen between various solvents was also seen when using the well-defined redox molecule, ferrocene.

The effect of high current densities when cycling in ionic liquids

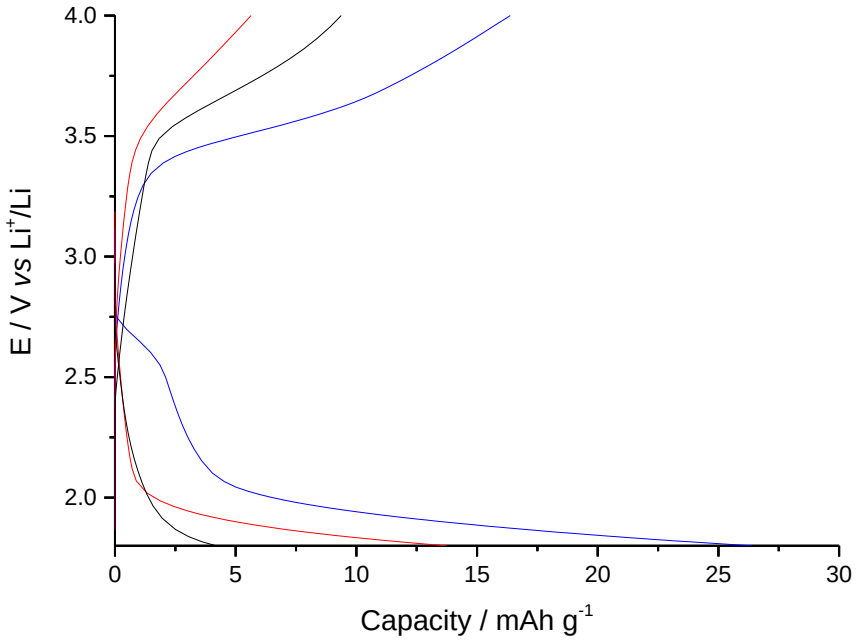

Figure B.3. Galvanostatic cycling data in $100\ mM$ LiTFSI, $Pyr_{14}TFSI$ on a CNT electrode at a rate of $\boldsymbol{200\ mA \cdot g_{CNT}^{-1}}$. (┈┈) $\boldsymbol{50\ mM}$ CoTerpy, argon, (—) $\boldsymbol{50\ mM}$ CoTerpy, oxygen saturated electrolyte, (—) oxygen saturated.

This figure illustrates how the use of higher current densities affects the capacity and discharge potential of a lithium-oxygen cell using an ionic liquid electrolyte. Compared to when cycling at $100\ mAh \cdot g^{-1}$ the capacity seen is less and the overpotential seen increased.